Astronomy & Astrophysics manuscript no. aa56942-25-arXiv
October 7, 2025

Ten new, ultracompact triply eclipsing triple star systems

T. Borkovits[1,2,3], S. A. Rappaport[1,4], T. Mitnyan[1,5], R. Gagliano[6], T. Jacobs[7], B. Powell[8], V. Kostov[8,9], M. Omohundro[10], M. H. Kristiansen[11,12], I. Terentev[13], H.M. Schwengeler[10], D. LaCourse[13], Z. Garai[14,15], T. Pribulla[14], I. B. Bíró[1,2], I. Csányi[2], Z. Dencs[3,15], and A. Pál[3]

1 HUN–REN–SZTE Stellar Astrophysics Research Group, H-6500 Baja, Szegedi út, Kt. 766, Hungary
2 Baja Astronomical Observatory of University of Szeged, H-6500 Baja, Szegedi út, Kt. 766, Hungary.
e-mail: borko@bajaobs.hu
3 Konkoly Observatory, Research Centre for Astronomy and Earth Sciences, H-1121 Budapest, Konkoly Thege Miklós út 15-17, Hungary
4 Department of Physics, Kavli Institute for Astrophysics and Space Research, M.I.T., Cambridge, MA 02139, USA
e-mail: sar@mit.edu
5 Department of Experimental Physics, University of Szeged, H-6720, Szeged, Dóm tér 9, Hungary
6 Amateur Astronomer, Glendale, AZ 85308
7 Amateur Astronomer, Missouri City, Texas 77459 USA
8 NASA Goddard Space Flight Center, 8800 Greenbelt Road, Greenbelt, MD 20771, USA
9 SETI Institute, 189 Bernardo Avenue, Suite 200, Mountain View, CA 94043, USA
10 Citizen Scientist, c/o Zooniverse, Dept, of Physics, University of Oxford, Denys Wilkinson Building, Keble Road, Oxford, OX1 3RH, UK
11 Brorfelde Observatory, Observator Gyldenkernes Vej 7, DK-4340 Tølløse, Denmark
12 National Space Institute, Technical University of Denmark, Elektrovej 327, DK-2800 Lyngby, Denmark
13 Amateur Astronomer, 7507 52nd Place NE Marysville, WA 98270, USA
14 Astronomical Institute, Slovak Academy of Sciences, 05960 Tatranská Lomnica, Slovakia
15 ELTE Gothard Astrophysical Observatory, Szent Imre herceg u. 112, H-9700 Szombathely, Hungary

Received .., 2025; accepted ... , ...

ABSTRACT

Aims. We have identified more than a hundred close triply eclipsing hierarchical triple star systems from data taken with the space telescope TESS. Many of them have outer periods less than or, close to 100 days, hence, we call them 'ultracompact hierarchical triples'. These systems are noteworthy in that we can potentially determine their dynamical and astrophysical parameters with a high precision, in many cases even without radial velocity data. In the present paper we report the comprehensive study of ten new ultracompact triply eclipsing triple star systems, located in the northern ecliptic hemisphere, taken from this larger sample: TICs 198581208, 265274458, 283846096, 337993842, 351404069, 378270875, 403792414, 403916758, 405789362, 461500036.

Methods. Most of the data for this study come from TESS observations, but we obtained supplemental ground-based photometric measurements for two of the systems. The eclipse timing variation curves extracted from the TESS and the ground-based follow up data, the photometric light curves, and the spectral energy distribution are combined in a complex photodynamical analysis to yield the stellar and orbital parameters of all ten systems.

Results. The outer periods are in the range of 46.8-101.4 days. We found third-body forced, rapid apsidal motion in four systems. Moreover, TIC 403916758 was found to be a double twin triple (i.e. both the inner and the outer mass ratios are close to unity). All of the systems are substantially flat, with mutual inclination angles of $\lesssim 5°$. Finally, we have taken the results for the ten systems in the present paper, and combined them with the system parameters for more than 30 other compact triples that we have reported on in previous work, in order to examine some of the global properties of these systems on a statistical basis.

Key words. (Stars:) binaries (including multiple): close – (Stars:) binaries: eclipsing – (Stars:) binaries: general – Stars: fundamental parameters – Stars: individual: TICs 198581208, 265274458, 283846096, 3337993842, 51404069, 378270875, 403792414, 403916758, 405789362, 461500036

1. Introduction

Triple and multiple stellar systems are quite frequent. Their fractional abundance grows quickly with the mass of the primary component. For example, according to the recent review of Offner et al. (2023), the bias corrected triple/high-order faction of brown dwarfs and main-sequence (MS) stars exceeds 10% for solar-type stars, and may reach even 60-70% for multiple systems that consist of at least one O-type component. Restricting ourselves only to triple stars (or, at least the innermost triple subsystems of higher-order hierarchies), the characteristic sizes of such systems may span several magnitudes from the regime of some tens of millions of kilometers (that is, scalesizes smaller than the orbit of Mercury or, at least, Venus) to some parsecs. These correspond to outer periods, $P_{\rm out}$, of just a few weeks to billions of years.

The astrophysical, dynamical, as well as evolutionary significances of binary and multiple systems which belong to different size scales are discussed in several works, (e.g. Kisseleva-Eggleton & Eggleton 2010; Grishin & Perets 2022; Offner et al. 2023; Saglia et al. 2025). The various observing techniques which may be best for one or the other kinds of multiple stellar systems (or, even, different subsystems within the same multiple star system) are also discussed in a number of papers (see, e.g. the chart of Tokovinin 2014).

In this paper we concentrate on triple systems that have the smallest physical sizes (or, what is practically the same, which have the shortest outer periods). These are referred to as 'compact' or even 'ultracompact' triples, depending on the outer period. Before the advent of the recent planet-hunter space-telescopes, e.g., Kepler (see Borucki et al. 2010) and TESS (see Ricker et al. 2015) which produce(d) nearly uninterrupted high-precision photometric observations (from months to years) for millions of stars, it was exceedingly rare to serendipitously identify such triple star systems where the period of the outer, third star did not exceed a number of years.

In contrast to this, the *K*epler spacecraft identified many compact triple systems, including more than a dozen such systems where the distant third star periodically eclipses, or is eclipsed by, the inner binary members (see Carter et al. 2011, for the discovery of the first such object, KOI-126). Naturally, the presence and discovery of such 'triply eclipsing triple stars' are only a matter of purely geometric effects (that is, the outer orbit should be seen almost exactly edge-on by an observer), and the chances of observing third-body eclipses are roughly proportional to $P_{\rm out}^{-2/3}$. The relatively easy detection of such systems opens up a new window for the discovery of compact triple star systems.

Besides, or more precisely after, these *K*epler discoveries, a number of other triply eclipsing triples were also reported (see the compilation of Borkovits 2022). The real breakthrough, however, came with the regular operation of the TESS spacecraft in 2018. Since the beginning of the survey observations with this instrument, the number of known triply eclipsing triple stars started to grow quickly and, by now, our group has identified more than a hundred such new systems. (Of course, one should keep in mind, that this number of the identified or, at least suspected, triply eclipsing triple systems continues to be very low compared to the total number of known or, at least hypothesized, multiple stars; but, this is now quite sufficient to carry out detailed studies of a substantial number of individual triples, as well as to carry out statistical investigations of the group.) Formerly, in a series of earlier papers, we have carried out homogeneous photodynamical analysis of 32 TESS-discovered triply eclipsing triple systems (Borkovits et al. 2020b, 2022a; Mitnyan et al. 2020; Rappaport et al. 2022, 2023, 2024; Czavalinga et al. 2023; Kostov et al. 2024). In the current paper we introduce a similar investigation of ten additional newly discovered triply eclipsing triple stellar systems.

In Section 2 we describe the collection of 10 ultra-compact triply eclipsing triple systems that we have selected for this detailed study. We explain briefly how these sources were discovered. In Section 3, the light curves exhibiting third body eclipses are introduced along with model fits, and briefly discussed. The eclipse timing variation curves (ETVs) are introduced and discussed in general in Section 4. The photodynamical code, with which the system parameters are extracted, is briefly reviewed in Section 5. In Section 6 we summarize the system parameters in a set of comprehensive tables, and the results for each individual system are presented.

2. The ten triply eclipsing triples

In this compilation we select ten potentially interesting, formerly unanalysed, triply eclipsing triples from the northern ecliptic hemispheres. We focused our attention on those systems with outer periods of $\lesssim 100$ days.[1] The main catalogue parameters for these ten triples can be found in Tables A.1 and A.2. We refer to these systems as 'ultra compact hierarchical triple' (UCHT) star systems. Choosing northern ecliptic systems has two purely practical aspects. First, according to the currently available observing schedule of the TESS mission, the spacecraft will not observe any northern ecliptic sectors until at least the end of Cycle 8 (September 7th, 2026). Therefore, we cannot expect any newer TESS observations in the forthcoming year. Second, objects in the northern ecliptic hemisphere are easily available for follow up ground-based observations (at least in some parts of the year) with telescopes in Central Europe.

The discoveries of the triply eclipsing nature of the currently investigated ten triples were made in three different ways. Six of the ten systems were found by our 'Visual Survey Group' (VSG; Kristiansen et al. 2022) in the manner described in detail, e.g., in Rappaport et al. (2024). Moreover, two triples, TICs 265274458 and 351404069, were first identified as doubly eclipsing 2+2 quadruples, and the former was even catalogued as such by Kostov et al. (2021). Finally, the presence of likely third-body eclipses in the early TESS light curves of the previously known eclipsing binaries (EBs) (TIC 198581208 = CSS J170425.5+463533 and TIC 461500036 = ASASSN-V J221919.64+850413.4) were first reported by Zasche et al. (2022).

The analysis of UCHT objects has both theoretical and practical aspects. Regarding the theoretical aspects, (i) these systems have small characteristic sizes, e.g., they would typically fit within Venus' orbit around the Sun. Therefore, we may expect, that the components of such systems formed in a different way than is the case for wider triples (see, e.g., Tokovinin 2021), and perhaps the orbital and dynamical configurations of such systems retained some relics of these formation mechanism(s). Moreover (ii), in these systems we may expect some rare and extreme stellar evolutionary end states (such as multiple common envelope stages, solo or multiple stellar mergers, etc.), which might help to explain the origin of some extreme stellar systems or phenomena. Finally, (iii) the vast majority of such systems are not only compact or, ultra compact, but also 'tight' enough for the continuous occurrence and detection of gravitational perturbations (even higher order ones, see, e.g. Borkovits & Mitnyan 2023), which are not only interesting in themselves, but may also lead to more accurate dynamical determinations of the stellar and orbital parameters. In this regard, note that formerly, tight triples were defined as outer-to-inner period ratios less than 100 (i.e., $P_{\rm out}/P_{\rm in} \lesssim 100$) (see, e.g. Borkovits et al. 2022b), but in the newer works a value of $P_{\rm out}/P_{\rm in} \lesssim 50$) is considered 'tight'. In such triples, the third-body perturbations substantially affect the orbit of the inner binary, and, at least in the case of compact systems, such dynamical effects are observable within months or years (Borkovits et al. 2025). Regarding these definitions, one can see that the former definition for tightness is naturally satisfied in all ten of our selected UCHT systems, as the inner EB period in all these triples is longer than 1 day. Considering the newer, and more strict definition, the ratio of the outer and the inner periods is less than 50 for all but one system amongst our ten UCHTs. And, as will be shown below in Sect. 4, the ETVs in

[1] Originally we had intended to use the exact value of $P_{\rm out} \leq 100$ days as the upper limit on the outer periods of the triple systems considered in this paper. Finally, however, we decided not to exclude TIC 337993842 for which the outer period is longer than this by only $\sim 1.4\%$.

these nine systems are clearly dominated by the short-timescale third-body perturbations.

The practical aspects of the very short outer periods also manifest themselves in at least two ways. First, (i) the shorter the outer orbital period (and, hence, the separation of the third star from the members of the inner binary), the larger the chance for third-body eclipses (see, quantitatively, e.g. in Borkovits et al. 2022b). Second, (ii) TESS has revisited the northern ecliptic hemisphere several times since 2019. Despite the fact that the nominal duration of each sector is only ~27.5 days (and, practically, even less), there is a good chance, at least for the shortest outer period systems, that the total outer orbital phase has been covered with observations (even several times). Therefore, numerous third-body eclipse events have been observed. In this context we refer to Table A.3 where one can see that all of our targets were measured during 4–15 sectors and, moreover, at least four third-body eclipsing events were observed for all but one of our targets. (The sole exception is, our longest period triple, TIC 337993842, for which only two third-body eclipse events were detected with TESS and, moreover, both of them belong to the superior conjunction of the third star.) In the case of the shortest outer period system, TIC 405789362, 15 such outer eclipsing events were detected (see examples in Figs. 1 and, C.1–C.2).

Adding to the important third-body eclipses are the multiply covered ETV curves (Figs. 2 and D.1). It is not surprising that, for all systems, we were able to determine the outer orbital period (which is a key parameter to start the complex, photodynamical analysis) with the TESS ETV observations alone. This is valid even in the case of TIC 337993842 where, despite the lack of any observed third-body events at the inferior conjunction of the outer orbit, due to the well-covered, dynamically dominated ETV curve, we were able to determine the orbital parameters exclusively from the available TESS data.) Therefore, for the current analysis, the importance of the ground-based archival data was less important than in our previous studies of triples. On the other hand, however, these statements are valid only a posteriori, i.e., after collecting several cycles of TESS data. When we first discovered this newest set of triples, however, we followed the same steps of the preliminary period determinations as before (that is, we used the archival data to find reliable input periods for the first, analytic ETV studies, as it was described e.g., in Rappaport et al. 2022).

3. Light curve and model fits

TESS observed 70 third-body eclipsing events from the currently investigated group of ten triples, of which we have selected three such events for TIC 2838846096, in Fig. 1, to illustrate the main properties of the different third-body eclipses. Moreover, we present 26 additional third-body events in Figs. C.1–C.2 for the remaining nine systems. The blue points represent the TESS measurements. For the light curve analysis and modelling we used 30-min cadence data. For those sectors where shorter cadence data were available, we binned them to 30-min cadence. Therefore, all the blue points are at the same 30-min cadence. In the vicinity of the third-body, or 'extra", eclipses, naturally, several regular binary eclipses are also shown. These latter eclipses are generally self-evident, while the 'extra' eclipses are, for the most part, all the dips in flux that cannot be ascribed to the regular EB eclipses. In some cases, especially, when the third-body eclipses (or eclipsed by) the members of the inner binary system during a regular two-body eclipse (that is, when the three stars, from the point of view of the observer are aligned), the third-body eclipses are quite irregular and anomalous looking (see the left panel of Fig. 1), while in other cases, in general, around the quadratures of the inner binary, the eclipses look almost 'normal' but occur in rapid succession and/or are clearly out of place. This latter situation is illustrated in the middle and right panels of Fig. 1. (The difference in the depths of the extra dips between the two panels, is due to the fact that in the middle panel the cooler inner binary members occulted the third star, separately, while in the right panel, this latter, hottest star eclipsed the two cooler EB members, one by one.)

We also plot the light curve solution taken from the joint photodynamical analysis, as a smooth red curve. These solutions will be discussed below, in Sect. 5.

These third-body eclipses, especially their shapes, durations, as well as their occurrence times, contain crucial information about both the orbits and the properties of the stars themselves (e.g., the relative sizes and effective temperatures).

4. ETV curves

In addition to the light curves of the third-body eclipses discussed above, as well as the regular eclipses, another very important input for the comprehensive photodynamical analysis (to be discussed in Sect. 5) comes from the ETV curves. These are based on the mid-times of both kinds of eclipses (primary and secondary) of the inner EB in each triple. These mid-eclipse times are extracted in the manner discussed previously in Borkovits et al. (2015, 2016). As one can see in Fig. 2 for TIC 351404069 and, in Fig. D.1 for the other nine triples, well characterised non-linear behavior can be seen all but one of these ETV curves. These features come predominantly from three basic effects, as follows. First is the classical light-travel-time effect (LTTE; Roemer 1677) due to the changing distance to the EB as it is pulled around in its outer orbit by the tertiary star. The amplitude of this effect is proportional to $P_{\rm out}^{2/3}$ (see, e.g. Borkovits et al. 2016) and, therefore, due to the short outer periods of the current systems, this effect is generally the least significant in these particular systems as can nicely be seen in Fig. 2, where the cyclic, sinusoidal nature of the black horizontal LTTE curve is almost unnoticeable).

Second are the 'dynamical' delays which, in nearly coplanar orbits, are caused largely by the lengthening of the EB orbit due to the presence of the tertiary star (see, e.g., Rappaport et al. 2013; Borkovits et al. 2015). This effect manifests itself in Fig. 2 as the $P_{\rm out}$-period wobbles. The magnitude of this effect depends on the instantaneous separation between the EB and the more distant third star, and hence, it varies with the phase of the outer orbit (at least when it is eccentric). (3) Finally, there is the so-called apsidal motion (AM), which may occur in eccentric binaries. This is a longer timescale effect which has three main types: (i) the classical, tidal AM, caused by the non-spherical mass distributions of the tidally distorted binary components; (ii) the general relativistic AM and; (iii) the dynamically driven one, forced by the perturbations of the tertiary star. The timescale of the dynamically driven AM is on the order of $P_{\rm out}^2/P_{\rm in}$ (see, e.g. Söderhjelm 1975). The dominant driver of AM in the currently investigated systems is the third-body forced AM; however, in a minority of these ten systems, the mutual tidal deformations of the two EB stars are also significant. The largest amplitude, longer period anti-correlated nature of the primary and secondary ETV curves in Fig. 2 is due to this, dynamically driven AM.

As was mentioned above, the ETV curves themselves are shown in Figs. 2 and D.1, while the mid-eclipse times used for the derivation of these ETV curves are tabulated in Appendix F.

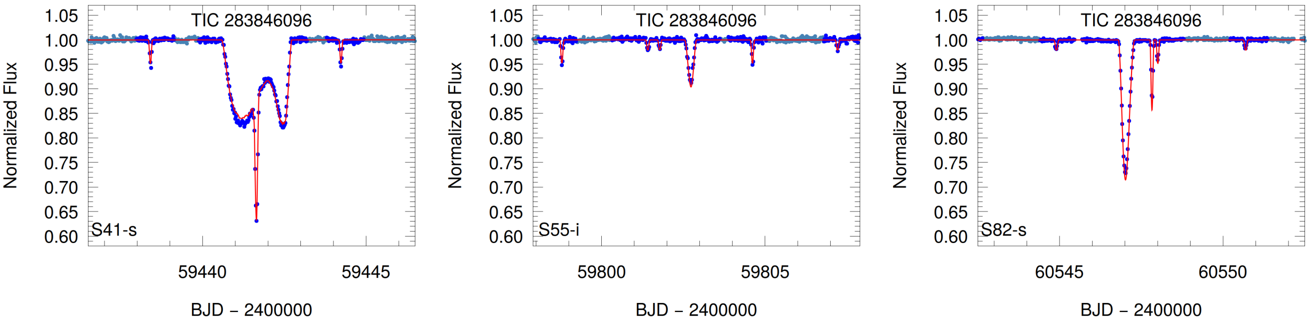

Fig. 1. Light curves (blue points) and model fits (smooth red curves) near three illustrative third-body eclipses of TIC 283846096. Dark/pale blue points are for those light curve sections which were used/not-used for the photodynamical solution. The sector numbers are indicated in the lower left corner of each panel. Letters 'i' or 's' after the sector numbers refer to the inferior or superior conjunction of the third star, respectively.

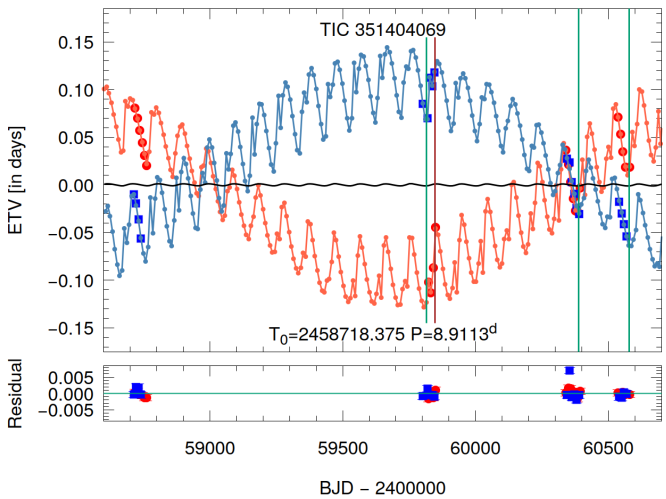

Fig. 2. Primary and secondary ETV curves (red and blue circles, respectively) formed from the TESS observations with the best-fit photodynamical solution for TIC 351404069 (see Sect. 5). The dynamically forced, rapid apsidal motion of the inner, eccentric EB is nicely visible. (Be aware of the huge amplitude of the ETV!) The horizontally centred black curve represents the pure LTTE contribution. Vertical lines mark the times of the observed outer eclipses (green – the binary occulting the tertiary star and, brown – vica versa).

5. Photodynamical models

Similar to our former works on triply eclipsing triples, the ten multiple systems considered in this work have been subjected to a detailed photodynamical analysis with the use of our own developed software package LIGHTCURVEFACTORY. The details as well as the input data sets and the input/output parameters have been explained in several of our earlier papers (see, e.g. Borkovits et al. 2018, 2019a,b, 2020a,b, 2021; Mitnyan et al. 2020). Therefore, here we note only that the code contains four basic features. First, there are emulators for multi-passband light curve(s), the ETVs, and radial velocity (RV) curve(s) (the latter feature was unused in the current work due to the absence of any RV data). Second, the main astrophysical parameters of the stars are calculated with the use of built-in, tabulated PARSEC isochrones (Bressan et al. 2012) and, therefore, we are able to produce theoretical combined spectral energy distributions (SED) for the given system under investigation (this feature is optional). Third, there is a built-in numerical integrator (a seventh-order Runge-Kutta-Nyström algorithm) to calculate the instantaneous (Jacobian) coordinates and velocities of the stars along their perturbed three-, or multiple-body orbits. Finally, there a Markov Chain Monte Carlo (MCMC)-based search routine for determining the best-fit system parameters, as well as the statistical uncertainties. The latter feature uses our own implementation of the generic Metropolis-Hastings algorithm (see, e.g., Ford 2005).

Note also that all the essential details of how this code was used to analyse compact triply eclipsing triple systems, especially those which were found with the TESS spacecraft, were described in Rappaport et al. (2022). Here we provide only a very concise overview of the inputs to the code and the parameters that are either fitted or constrained by the MCMC fit. Altogether, for a hierarchical triple configuration, there are 25 – 27 system parameters that result directly from the analysis. These are nine stellar parameters (masses, radii, and effective temperatures of all the three stars), all 12 of the elements of the inner and outer orbits (or, some equivalents of the classic orbital elements, e.g. orbital periods instead of semi-major axes), as well as the 4 system parameters: distance to the source and the interstellar extinction, as well as the system metallicity and age.

In Fig. 3 we illustrate schematically the process of the entire photodynamical analysis, denoting all the initially adjusted, constrained and fixed input parameters. Another, more detailed flow chart can be found in Fig. 5 of Borkovits et al. (2020a). Finally, one may optionally adjust the amount of any passband-dependent contaminated (extra) light ℓ_x if it is necessary. We note that, in the case of TESS observations, due to the large pixel sizes, the contamination might come from other nearby stars, which may affect the eclipse depths of the investigated source. And, even in the absence of other nearby stars, due to the unavoidable stray light, some extra flux can be expected in the light curve and, therefore, it is useful to allow the extra flux parameter to vary. (And, moreover, note that another source of such contaminated flux might be an unknown, unresolved, more distant bound stellar component.) Hence, in all ten of our sources, we set and adjust the extra light ratio in the TESS band, as the 26th input parameter. Moreover, note that for two of our ten targets (TICs 405789362 and 461500036) we used a second light curve, compiled from ground-based observations in Sloan r'-band, too. In these two systems, though there was no a priori information about any contaminating sources in the aperture of the CCD photometry, for homogeneity in the analysis we also allowed (and adjusted) a second extra light parameter and, therefore, for these two triples we used 27 input parameters. (Note, these latter one or two optionally used and adjustable parameters are not shown in Fig. 3.)

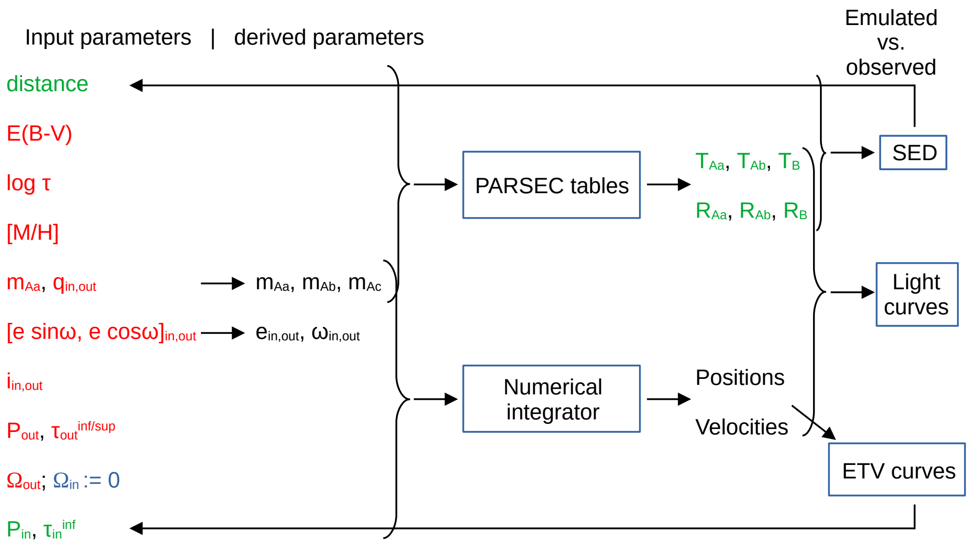

Fig. 3. Schematic flow chart of the entire photodynamical fitting process. Parameters marked in red font give those input parameters that are allowed to adjust during each MCMC trial step. Green symbols stand for the constrained quantities, while the black symbols denote quantities derived directly from the (adjustable, red) input parameters just at the beginning of each trial step and used during the subsequent part of the given step. The other quantities, not shown in the chart, but listed in the result tables below are computed a posteriori, at the end of the entire photodynamical analysis process. Note also, the only parameter with fixed input value ($\Omega_{\rm in} = 0$) is given in blue font. (For the meaning of each symbol, see Table B.1.)

The TESS light curves which primarily determine the EB and third-body eclipse profiles, as well as the ETV curves via the timing data used in our analysis, were taken from the TESS full-frame images ('FFI'). For eight of the ten systems, the photometry of the FFIs up to Sector 77 was done with András Pál's FITSH package (Pál 2012). The two exceptions are TICs 337993842 and 351404069 for which all-sector photometry was processed with the publicly available software LIGHTKURVE (Lightkurve Collaboration 2018). For technical reasons, the most recent sectors (from 78 to 86) in the case of all ten triples were processed with this latter software package. Note that changing to another photometry pipeline for the last set of sectors might introduce smaller inhomogeneities into the TESS light curves. Therefore, we made some steps to 'validate', or synchronize, the FITSH and LIGHTKURVE processed light curves to each other. For this reason we processed with the LIGHTKURVE pipeline some of those earlier sectors as well, which had been made with the FITSH pipeline. In the process, we tested the parameters to be used for the LIGHTKURVE-processed light curves to obtain outputs which are close to the FITSH light curves (especially in eclipse depths) of the same sectors.

Again, similar to our previous works, in order to save on computational time, we binned the 200-sec and 10-min cadence data to 30-min cadence[2], and dropped the out-of-eclipse regions of these light curves, keeping only the $\pm 0\overset{p}{.}15$ phase-domain regions around the EB eclipses themselves. This latter process of dropping the out-of-eclipse regions was not applied in the vicinities of any third-body eclipses, where we keep the data for an entire binary period before and after the first and last contacts of that particular third-body eclipse. Keeping the out-of-eclipse light curve points for at least two binary periods around each expected third-body eclipse was done for two reasons. First, due to the continuously varying configurations of the three stars, the occurrence times of the outer eclipses are not strictly periodic. Some small shifts in the outer eclipse features may occur which would be taken into account in such a manner. Second, complete omission of the out-of-eclipse light variations would result in the suppression of such lower amplitude effects, as ellipsoidal variations, reflection effects, and Doppler-boosting, which would arise from the binarity, and would introduce some smaller bias in our results. With such a decision, we retained the signals of these possible effects in our investigated light curves, but rendered smaller weights to them with respect to the most important eclipsing patterns.

We also note, that in the case of two targets, TICs 405789362 and 461500036, ground-based photometric follow-up observations were carried out with the two identical 80-cm RC telescopes of Gothard Astrophysical Observatory (GAO80) Szombathely, Hungary and Baja Observatory of Szeged University (BAO80), Baja, Hungary. The details of these instruments, the methods of observation, and the data processing were described in detail in Borkovits et al. (2022a). The sloan r'-band light curves that were obtained were also included in our complex analysis, though with half the weight as that of the TESS photometry.

Regarding the mass determination of the investigated stars, we should make some additional comments. In the absence of RV data, the question naturally arises: how are we able to derive absolute stellar masses, temperatures, and radii? This was done with the use of the above mentioned PARSEC isochrones as proxies. The details of this process, together with its limits were described in Borkovits et al. (2022a). Moreover, we also discussed this question in Rappaport et al. (2024). Therefore, we suggest that the interested reader might consult these two earlier papers.

6. System parameters

6.1. Tables of fitted parameters

In what follows, we discuss the astrophysically and/or dynamically most interesting findings regarding the currently investi-

[2] We note, however, that this binning was applied only to the light curve analysis. The mid-eclipse times for the ETV curves were calculated from the original shorter cadence data sets.

gated ten UCHT systems. In addition to these discussions, similar to our former works, we also give our results in tabulated form. These tables do not contain all the directly fitted (i.e. adjusted, constrained) parameters but, in several cases, they instead give parameters that are calculated from those directly derived parameters. Naturally, we include all the basic stellar parameters in our results but, regarding the orbital elements, for example, instead of the adjusted parameters $e\sin\omega$ and $e\cos\omega$, we give directly the eccentricities (e) and arguments of periastron (ω) for each orbit. We also put into our tables such additional calculated or derived geometrical parameters as the relative orientations of the orbits. For a better comparison with the traditional EB light-curve fitting codes and, also for better accuracy in several non-dimensional relative quantities (which are not adjusted directly in our method but, indirectly, strongly constrain our solution) we calculate and give, e.g., fractional radii and relative temperatures (e.g., R/a, T_B/T_{Aa}), and some others. Our tables contain dozens of different parameters, which were defined in Rappaport et al. (2023), while the methods of the calculations of the indirectly derived quantities were described or referenced in Borkovits et al. (2015) and Kostov et al. (2021). Here, however, similar to Rappaport et al. (2024), for the sake of completeness, we tabulate the meaning of each parameter (generally noted only with symbols in the results tables) in Table B.1. Finally, note that the system parameters that are derived from the photodynamical analyses are listed in Appendix B, in Tables B.2 through B.6.

6.2. Results for the individual systems

6.2.1. TIC 198581208

The triply eclipsing nature of this formerly known EB (CSS J170425.5+463533) was first reported in Zasche et al. (2022); however, the correct outer orbital period, as well as the first complete analysis of this triple, are given only in this paper. The out-of-eclipse light curve of this EB shows variations whose amplitude is larger than the secondary eclipses themselves. We assumed that this signal had come from chromospheric activity in any of the late-type stars in this triple. Nevertheless, independent of its origin, it was clear that this signal, as it regards the eclipsing light curve analysis, simply caused additional noise. Therefore, we made efforts to remove these distortions with the use of medium-order local smoothing polynomials, separately for each TESS sector, and naturally excluding the eclipsing sections of the TESS light curves. For this process we used 4th to 18th-order polynomials at different sections of the TESS light curve. Such polynomials effectively smooth out the high frequency modulations from the light curve, while better retaining the lower frequency variations which come from the binarity for which the frequencies are nearly equal to or double of the orbital frequency. Despite this, it is clear to us that such polynomials would erase not only those variations which arise from the strongly irregular chromospheric activity, but also they may affect other out-of eclipse variations which may arise from the binarity, such as, e.g., ellipsoidal light variations, reflection effects, Doppler-boosting, etc. Therefore, we selected the order of the fitting polynomials in such a manner that we checked continuously the phase-folded light curve, and retained the shape and structure of the average eclipses, especially close to the first and last contact points.

According to our results, the most massive component of the system is the primary of the inner EB, with $M_{\rm Aa} = 1.04 \pm 0.06\,{\rm M}_\odot$, while the third component has only a slightly lower mass $M_{\rm B} = 0.94 \pm 0.05\,{\rm M}_\odot$. Besides these two sun-like stars, the secondary of the inner EB is a quite low mass with $M_{\rm Aa} = 0.58{\pm}0.03\,{\rm M}_\odot$, which nicely explains the very shallow secondary eclipses. As usual, the mass ratios can be determined with higher accuracies than the individual physical masses, and these are $q_{\rm in} = 0.56 \pm 0.01$ and $q_{\rm out} = 0.576 \pm 0.004$.

The spatial configuration of this old ($\tau = 6.2 \pm 1.7$ Gyr) system was found to be quite flat with $i_{\rm mut} = 0\overset{\circ}{.}2 \pm 0\overset{\circ}{.}1$. This substantial flatness, however, is likely a residual of the formation processes of this triple. Despite the relatively small characteristic size of the inner EB ($a_{\rm in} = 10.0 \pm 0.2\,{\rm R}_\odot$), due to the smaller radii of the EB members, the tidal forces should have remained small during the entire MS lifetime of the system (see, e.g. Correia et al. 2011). In this regard, however, we note that currently the primary star is close to the end of its MS evolution and, therefore, as it evolves, the currently moderate fractional radius of $r_{\rm Aa} = R_{\rm Aa}/a_{\rm in} = 0.127 \pm 0.002$ is expected to grow rapidly, causing more and more significant tidal effects.

The tightness ratio is $P_{\rm out}/P_{\rm in} \simeq 25.3$, and though quite small, is still the third largest in our sample. As the inner orbit is almost circular ($e_{\rm in} = 0.0141 \pm 0.0006$) and the outer one has only moderate eccentricity ($e_{\rm out} = 0.289 \pm 0.001$), this triple looks to be dynamically quite stable.

Finally, we note that for all ten ETV curves (Figs. 2 and D.1), we also plot the best photodynamically modelled ETV curves, as well as the pure geometrical, LTTE, part of this best-fit solution (black curve). Comparing the amplitudes of the entire primary (red) and secondary (blue) ETV curves with the LTTE contribution (black) one can see that the current ETV curve (top left panel of Fig. D.1), as was expected theoretically (see, e. g., Borkovits et al. 2015) for such a tightness ratio (see in the paragraph above), is dominated by the dynamical effects. Note also that the maxima and minima of the black LTTE contribution (which are not necessarily coincident with the extrema of the entire ETV curves) represent the largest and the smallest distances of the EB from the observer, and hence one may expect that the third-body should transit in front of the EB stars (vertical brown lines), and eclipsed by either of the EB stars (vertical green lines) around these LTTE-ETV extrema, respectively.

6.2.2. TIC 265274458

This system was listed as a 2+2 type quadruple system candidate in Kostov et al. (2022) which was based upon only the Year 2 TESS data. Newer observations, however, made it clear that this is an UCHT, exhibiting both kinds of third-body eclipses.

TIC 265274458 has the most extreme inner mass ratio ($q_{\rm in} = 0.229 \pm 0.003$) in our sample. As a consequence, the secondary eclipses are hardly visible and, therefore, this was the only EB in the current sample where we were unable to measure a useful secondary ETV curve. This triple system was found to be quite young ($\tau \approx 270 \pm 30$ Myr), and dominated clearly by the hot primary of the inner EB ($M_{\rm Aa} = 1.90 \pm 0.03\,{\rm M}_\odot$) which emits $\approx 93 \pm 1\%$ of the total flux of the triple, at least in the photometric band used by TESS. The other two late type stars have substantially lower masses: $M_{\rm Ab} = 0.434 \pm 0.007\,{\rm M}_\odot$ and $M_{\rm B} = 0.98 \pm 0.02\,{\rm M}_\odot$. Here we also call attention to the fact that, while the mass of the third star was determined to only ∼5 % fractional error, the relative uncertainty in the much more accurate outer mass ratio is about 1%, which follows from $q_{\rm out} = 0.420 \pm 0.004$. This emphasizes again that the dimensionless relative quantities, such as the mass ratios and the fractional radii (determined themselves mainly by dynamical and light curve effects) have much better accuracies than those of the absolute masses and radii. The latter determinations depend strongly on the PARSEC isochrones which served mainly as proxies for the mass determinations in the absence of any RV data. Regarding the radii, the 1σ statistical uncertainties of the absolute values can exceed even ~2 %, being: $R_{\rm Aa} = 1.70 \pm 0.03\,{\rm R}_\odot$, $R_{\rm Ab} = 1.70 \pm 0.03\,{\rm R}_\odot$ and, $R_{\rm B} = 0.86 \pm 0.02\,{\rm R}_\odot$, while their relative, i.e., dimensionless scaled counterparts were obtained with considerably smaller relative uncertainties: $r_{\rm Aa} = 0.146 \pm 0.001$, $r_{\rm Ab} = 0.0365 \pm 0.0005$ and, $r_{\rm B} = 0.0092 \pm 0.0001$, respectively.

Interestingly, we found both the inner and the outer orbits to be extremely close to circular ($e_{\rm in} = 0.0025 \pm 0.0004$ and, $e_{\rm out} = 0.003 \pm 0.002$). Such a doubly circular, almost flat ($i_{\rm mut} = 0\overset{\circ}{.}7 \pm 0\overset{\circ}{.}3$) configuration would be far from surprising in the case of an UCHT formed by old, and at least partially evolved, stars (see, e.g., the cases of HD 181068 Borkovits et al. 2013; TIC 242132789 Rappaport et al. 2022; and TIC 332521671 Rappaport et al. 2023) where the tidal interactions were strong enough and had time to flatten and circularise the whole systems. In the current situation, however, with young stars having small fractional radii, this is not the case. Therefore, we might argue that the current flat and doubly circular configuration is most likely primordial for this triple.

6.2.3. TIC 283846096

This triple can claim several superlatives amongst our ten sample systems. From a dynamical point of view, this (i) is the tightest triple, having $P_{\rm out}/P_{\rm in} \approx 9.71$, (ii) has the most eccentric inner orbit ($e_{\rm in} = 0.1057 \pm 0.0009$), (iii) is the only one where the outer eccentricity is found to be smaller than the inner one ($e_{\rm out} = 0.068 \pm 0.002$), and (iv) has the second highest outer mass ratio ($q_{\rm out} = 0.880 \pm 0.002$). And, therefore, naturally this triple exhibits the most rapid dynamical AM with $P_{\rm apse}^{\rm obs} \approx 1.8\,{\rm yr}$[3], which means that more than two complete rotations of the orbital ellipse have been completed since the first TESS observations in the summer of 2019. Moreover, from an astrophysical point of view, a further superlative is that this UCHT has both the lowest total mass out of the current ten systems and, also, it contains the smallest mass star in our sample.

The individual masses of the current triple are: $M_{\rm Aa} = 0.59 \pm 0.03\,{\rm M}_\odot$, $M_{\rm Ab} = 0.38 \pm 0.02\,{\rm M}_\odot$ and $M_{\rm B} = 0.86 \pm 0.05\,{\rm M}_\odot$, that is, all three stars are low-mass cool red M and K dwarfs. Here we stress again what we have discussed about the much higher accuracy of the relative, or dimensionless, quantities (as opposed to the absolute, or physical, quantities) such as the mass ratios, which are constrained mainly through the dynamics, i.e., the perturbations. In this triple the mass ratios are orders of magnitude more accurate than the masses themselves, e.g., $q_{\rm in} = 0.636 \pm 0.004$. Turning to the other set of the fundamental parameters and their relative dimensionless counterparts, i.e., the physical and the fractional radii, we find that the relative accuracy difference is less significant, as $R_{\rm Aa} = 0.59 \pm 0.03\,{\rm R}_\odot$, $R_{\rm Ab} = 0.37 \pm 0.03\,{\rm R}_\odot$ and, $R_{\rm B} = 0.83 \pm 0.03\,{\rm R}_\odot$, while the fractional radii are: $r_{\rm Aa} = 0.044 \pm 0.001$, $r_{\rm Ab} = 0.028 \pm 0.001$ and $r_{\rm B} = 0.0113 \pm 0.0003$. Note, in contrast to the two previously discussed triples, here even the uncertainties of the more accurate dimensionless quantities are also a bit higher, especially in the case of the two inner binary members. In our view, these are mainly due to the very shallow regular eclipses, which were insufficient to better constrain the fractional radii. Of course, this shallowness can be well explained by the large outer mass ratio. In this case, the more distant tertiary component is much more massive than the EB members, and therefore it emits more than 86% of the total flux of the triple.

Finally we note another 'superlative' of sorts due to the fact that this is the least observed system in our sample—TESS observed it only during four sectors. Despite this, the outer period ($P_{\rm out} = 55\overset{\rm d}{.}954 \pm 0\overset{\rm d}{.}003$) is quite short, which led to third-body eclipses in all four sectors, and the rapid dynamical AM as well as the large-amplitude $P_{\rm out}$-period ETV-wobbles strongly constrain much of the dynamical parameters. We were thereby able to find a robust and satisfying photo-dynamical solution purely from such a small set of observations.

6.2.4. TIC 337993842

This is the longest outer period triple in our sample with $P_{\rm out} = 101\overset{\rm d}{.}4$ and, therefore, strictly speaking, this already exceeds the formal definition we set for UCHTs with a limit of $P_{\rm out} = 100$ days, but only by $\sim 1.4\%$. Only two third-body events were detected with TESS (though the target was observed in six sectors) and, both of them belong to the superior conjunction of the third star. Despite this, similar to the previous target, due to the well-covered, characteristic ETV pattern, we were able to find a robust photodynamical solution simply from these six sectors of TESS observations.

We found that the distant third component of this triple (with $M_{\rm B} = 2.3 \pm 0.1\,{\rm M}_\odot$) is the most massive object amongst all the thirty stars investigated in the current ten UCHTs. The other two stars of the inner EB are similar to each other, and are also more massive than our Sun ($M_{\rm Aa} = 1.36 \pm 0.04\,{\rm M}_\odot$ and, $M_{\rm Ab} = 1.34 \pm 0.04\,{\rm M}_\odot$). The fractionally more accurate mass ratios are $q_{\rm in} = 0.98 \pm 0.01$ and $q_{\rm out} = 0.85 \pm 0.03$. The physical dimensions as well as the temperatures of the three stars are also larger than that of our Sun, being $R_{\rm Aa} = 1.36 \pm 0.04\,{\rm R}_\odot$, $R_{\rm Ab} = 1.32 \pm 0.04\,{\rm R}_\odot$, $R_{\rm B} = 2.8 \pm 0.2\,{\rm R}_\odot$; and $T_{\rm Aa} = 6650 \pm 100\,{\rm K}$, $T_{\rm Ab} = 6570 \pm 100\,{\rm K}$ and $T_{\rm B} = 8800 \pm 400\,{\rm K}$.

The ETV curve shows evidence of AM and, therefore, some eccentricity of the inner orbit ($e_{\rm in} = 0.0040 \pm 0.0002$). In the absence of any observed third-body events at the inferior conjunction, the amplitude, shape and phase(s) of the $P_{\rm out}$-period ETV wobbles give the chief constraints on the outer eccentricity, which was found to be $e_{\rm out} = 0.214 \pm 0.007$.

Finally, we note that a slightly problematic issue with our solution for this system is that the photodynamically obtained distance ($d_{\rm phot} = 1770 \pm 70\,{\rm pc}$) differs quite significantly from the distance of Bailer-Jones et al. (2021) that was obtained from the normally accurate Gaia DR3 parallaxes ($d_{\rm EDR3} = 2186 \pm 64\,{\rm pc}$). We will discuss the question of the sometimes discrepant parallactic and photometric distances in Sect. 7.

6.2.5. TIC 351404069

This is one of the tightest triples in our sample, with $P_{\rm out}/P_{\rm in} = 10.79$. Moreover, it contains the second most eccentric EB, with $e_{\rm in} = 0.0389 \pm 0.0002$. The rapid, dynamically forced AM is also readily visible. The numerical integrations give its period as

[3] This value, which can be seen directly in the corresponding top right panel of Fig. D.1, differs substantially from the theoretical AM period given in Table B.3, where the tabulated value is $P_{\rm apse} = 4.228 \pm 0.005\,{\rm yr}$. The reason for this discrepancy is due to the fact that the tabulated theoretical values of $P_{\rm apse}$ are calculated from the lowest quadrupole-order perturbation theory, which clearly fails for such a very tight triple system, as was shown in Borkovits & Mitnyan (2023). Corrected formulae for the theoretical AM periods, which take into account higher-order terms (in the perturbation function) and, moreover, non-linear approximations will be presented soon in a separate paper (Deme et al., in prep.).

$P_{\rm aps}^{\rm obs} = 7.4$ yr indicating, again, the insufficiency of the lowest-order, quadrupole-level approximation, which yields a theoretical value of $P_{\rm apse} = 10.92 \pm 0.03$ yrs.

According to our results, the system contains three quite similar stars. The primary of the EB is a slightly evolved F-star, while the secondary EB star, and also the more distant tertiary are two G-type stars. Their masses are radii are $M_{\rm Aa} = 1.16{\pm}0.06\,{\rm M}_\odot$, $M_{\rm Ab} = 0.95{\pm}0.04\,{\rm M}_\odot$, and $M_{\rm B} = 0.97{\pm}0.05\,{\rm M}_\odot$; and $R_{\rm Aa} = 1.99 \pm 0.05\,{\rm R}_\odot$, $R_{\rm Ab} = 0.98 \pm 0.05\,{\rm R}_\odot$, and $R_{\rm B} = 1.01 \pm 0.05\,{\rm R}_\odot$. The more accurate relative quantities are: $q_{\rm in} = 0.826 \pm 0.005$, and $q_{\rm out} = 0.460 \pm 0.002$; and $r_{\rm Aa} = 0.086 \pm 0.001$, $r_{\rm Ab} = 0.042 \pm 0.002$, and $r_{\rm B} = 0.0079 \pm 0.0003$, respectively. Interestingly, despite the fact that the most massive component has a higher mass by $\sim 15 - 17\%$ than the other two stars, due to its slightly evolved nature, the absolute temperatures of all three stars are similar (within their 1σ uncertainties), being $T_{\rm Aa} = 5900 \pm 100$ K, $T_{\rm Ab} = 5865 \pm 85$ K and $T_{\rm B} = 5930 \pm 80$ K, respectively.

Finally, we note that this triple was found to be the second most inclined in our sample with $i_{\rm mut} = 3\overset{\circ}{.}2 \pm 0\overset{\circ}{.}2$.

6.2.6. TIC 378270875

This faint triple system consists of three similarly cool and less massive K dwarfs ($M_{\rm Aa} = 0.83{\pm}0.06\,{\rm M}_\odot$, $M_{\rm Ab} = 0.77{\pm}0.06\,{\rm M}_\odot$, $M_{\rm B} = 0.86 \pm 0.06\,{\rm M}_\odot$, $R_{\rm Aa} = 0.83 \pm 0.02\,{\rm R}_\odot$, $R_{\rm Ab} = 0.76 \pm 0.03\,{\rm R}_\odot$, $R_{\rm B} = 0.88 \pm 0.03\,{\rm R}_\odot$ and $T_{\rm Aa} = 5490 \pm 80$ K, $T_{\rm Ab} = 5210 \pm 80$ K and $T_{\rm B} = 5620 \pm 60$ K). Note, however, that the fractional accuracy of the dimensionless quantities are, again, much better determined as: $q_{\rm in} = 0.936 \pm 0.005$, $q_{\rm out} = 0.533 \pm 0.009$ and $r_{\rm Aa} = 0.090 \pm 0.001$, $r_{\rm Ab} = 0.082 \pm 0.001$ and $r_{\rm B} = 0.0104 \pm 0.0003$, respectively.

As one can see in the top row of Fig. C.2, the TESS-observed third-body eclipses are very shallow and, their depths are usually smaller than the out-of-eclipse light curve variations, the latter of which, irrespective of their origin, we removed with the local fitting of medium-order smoothing polynomials. (The original, that is, unsmoothed, but 1800-sec cadence light curve, is marked with grey in the corresponding panels of the top row of Fig. C.2.)

We note also that this triple was found to be the oldest in our sample with $\tau = 9.4^{+2.0}_{-4.1}$ Gyr, though the uncertainty in its age was found to be quite large and asymmetric.

6.2.7. TIC 403792414

This is another system in our sample where the ETV reveals clear, rapid, dynamically forced AM. However, when we carried out a short timescale numerical integration of the motion, we see that in this dynamically forced AM, substantial higher-order effects are also present. This can be nicely seen on the numerically generated ETV plot, calculated for the current century and shown in Fig. E.1. In Fig. E.2 we illustrate that these interesting extra variations might arise in the AM due to the following reason. The argument of pericentre of the inner orbit ($\omega_{\rm in}$) librates around the argument of pericentre of the outer orbit ($\omega_{\rm out}$), the latter of which revolves in the same direction as that of the orbital motion with a period of $P_{\rm apse,out}^{\rm obs} = 52.4$ yr. (Note, this latter value is very close to the theoretically calculated AM period of the outer orbit, which is $P_{\rm apse,out} = 50.1 \pm 0.2$ yr.) This libration of the inner major axis forces a cyclic variation in the inner eccentricity ($e_{\rm in}$) with the same period (that is, $P_{\rm e-in}^{\rm obs} = P_{\rm lib}^{\rm obs} = 8.6$ yr – see in the right panel of Fig. E.2) and, finally, this latter variation results directly in the extra periodicity in the ETV curve (Fig. E.1). Here we note also, that a very similar behaviour was reported and discussed in the case of another tight, compact triple, KIC 9714358, in Borkovits & Mitnyan (2023).

Regarding the deduced stellar parameters of this triple, this is also formed by three low-mass, cool dwarf stars with masses: $M_{\rm Aa} = 0.84 \pm 0.06\,{\rm M}_\odot$, $M_{\rm Ab} = 0.58 \pm 0.04\,{\rm M}_\odot$, and $M_{\rm B} = 0.80 \pm 0.06\,{\rm M}_\odot$; radii: $R_{\rm Aa} = 0.83 \pm 0.06\,{\rm R}_\odot$, $R_{\rm Ab} = 0.58 \pm 0.04\,{\rm R}_\odot$, and $R_{\rm B} = 0.76 \pm 0.05\,{\rm R}_\odot$; and $T_{\rm eff}$: $T_{\rm Aa} = 5430 \pm 180$ K, $T_{\rm Ab} = 3945 \pm 90$ K, and $T_{\rm B} = 5180 \pm 140$ K, respectively. The more accurate dimensionless quantities are $q_{\rm in} = 0.69 \pm 0.02$ and $q_{\rm out} = 0.56 \pm 0.01$. This is also a flat ($i_{\rm mut} = 0\overset{\circ}{.}7 \pm 0\overset{\circ}{.}4$) and old ($\tau = 6.3^{+3.3}_{-1.5}$ Gyr) triple system.

6.2.8. TIC 403916758

This triple star is very close to the class of objects which are known as 'double twins', as both the inner and outer mass ratios are close to unity. In this system, $q_{\rm in} = 0.98 \pm 0.03$ and $q_{\rm out} = 0.98 \pm 0.02$. Though the enrichment of 'double twins' amongst the population of the triple stars is predicted by some of the multiple star evolution theories (see Offner et al. 2023, for further references), from an observational point of view, it is hard to detect them, at least photometrically. This is so because of the fact that the tertiary's mass is about twice that of the individual masses of the inner components. Therefore, the emitted fluxes of the inner stars and, in the case of an eclipsing configuration, their mutual eclipses may easily disappear in the glare of the much brighter third star.

Direct photometric discovery of such a double twin becomes easier when it is a relatively flat CHT seen nearly edge-on, and the more massive third component leaves the MS and becomes a red giant (RG). The probability of the system then producing extra (third body) eclipses increases as the radius of the tertiary grows. This is exactly what happens in this triple, which is the only one in the present sample which contains a RG tertiary.

This triple system contains the shortest period inner EB ($P_{\rm in} = 1\overset{\rm d}{.}134$). Therefore, despite the fact that $P_{\rm out} = 71\overset{\rm d}{.}060 \pm 0\overset{\rm d}{.}002 < 100$ d, which classifies this triple as a UCHT, it cannot be considered to be tight, as $P_{\rm out}/P_{\rm in} = 62.66 > 50$, which is the largest in our sample. Therefore, not surprisingly, the ETV is dominated by the small amplitude LTTE and hence, it is completely unusable (see the third row, left panel of Fig. D.1).

In this regard it is important to note that the TESS light curve (third row of Fig. C.2) is very reminiscent of that of HD 181068 (Derekas et al. 2011; Borkovits et al. 2013), one of the first triply eclipsing triples (found with *Kepler*). In both systems the outer eclipses reveal directly that the third most distant component must be an RG star, which strongly dominates the total light of the triple. For such kinds of UCHTs, one may expect (nearly) coplanar and circular inner and outer orbits (due to substantial tidal damping), where the dynamical ETV contribution is nearly zero (see Borkovits et al. 2003). Therefore, the ETV reflects only the low amplitude LTTE signal whose amplitude is much lower than the scatter of the individual ETV points.

In this context, however, it is perhaps somewhat surprising, that this is the least flat triple in our sample with $i_{\rm mut} = 4\overset{\circ}{.}1 \pm 0\overset{\circ}{.}8$. In this regard, however, one should note that the inner eclipses are not deeper than $\sim$0.6 %. Therefore, the variations in the eclipse depths, and the corresponding inferred non-alignment of the orbital planes might be strongly affected by other incidental out-of-eclipse light variations. These could include chromospheric activity, different 'extra fluxes' and/or stray light in the different sectors.

As was already mentioned above, this is the only system in the current sample where the most massive star (component B, with $M_\mathrm{B} = 1.74 \pm 0.06\,\mathrm{M}_\odot$) is clearly evolved from the MS, and is now an RG star with $R_\mathrm{B} = 6.9 \pm 0.3\,\mathrm{R}_\odot$. The other two K dwarf-type inner stars, however, are still on the MS ($M_\mathrm{Aa} = 0.90 \pm 0.03\,\mathrm{M}_\odot$, $M_\mathrm{Ab} = 0.87 \pm 0.03\,\mathrm{M}_\odot$ and $R_\mathrm{Aa} = 0.81 \pm 0.03\,\mathrm{R}_\odot$, $R_\mathrm{Ab} = 0.79 \pm 0.03\,\mathrm{R}_\odot$, respectively):

6.2.9. TIC 405789362

This is the most compact triple system in the current sample (that is, it has the shortest outer period with $P_\mathrm{out} = 46\overset{\mathrm{d}}{.}810 \pm 0\overset{\mathrm{d}}{.}003$), and also one of the tightest ($P_\mathrm{out}/P_\mathrm{in} \approx 10.25$). Due to the small mass and, hence, the low temperature and surface brightness of the less massive tertiary star ($M_\mathrm{Aa} = 1.54 \pm 0.08\,\mathrm{M}_\odot$, $M_\mathrm{Ab} = 1.29 \pm 0.07\,\mathrm{M}_\odot$ and, $M_\mathrm{B} = 0.82 \pm 0.05\,\mathrm{M}_\odot$ or, regarding the mass ratios: $q_\mathrm{in} = 0.837 \pm 0.006$ and $q_\mathrm{out} = 0.293 \pm 0.007$) the TESS light curve displays deep regular eclipses, while the third-body events are very shallow and, some of them are almost hidden by the other kinds of light curve variations and distortions.

The inner orbit has a very low, but definitely non-zero, eccentricity $e_\mathrm{in} = 0.0072 \pm 0.0003$. In this regard we note that, in the case of such a tight triple system, an exactly circular inner orbit is impossible, due to the perturbing force of the tertiary, of which the strength, as well as the orientation varies moment by moment. As a consequence of this small, but non-zero, inner eccentricity, a slight and varying displacement occurs continuously at the times of the secondary eclipses. According to the ETV plot (third row, middle panel of Fig. D.1), during the first observing sectors in Year 2019, they were advanced by ∼15 min relative to the primary eclipses (or, more strictly speaking, they occurred about a quarter of an hour before the mid time between two primary eclipses), while for the Year 2024 observations, the primary and secondary ETV curves overlap each other. Specifically, the secondary eclipses occurred practically at the mid-times between consecutive primary eclipses.

Considering other dynamical properties, the outer orbit is found to be moderately eccentric with $e_\mathrm{out} = 0.163 \pm 0.003$, and the entire triple is flat to within 2°, being $i_\mathrm{mut} = 1\overset{\circ}{.}4 \pm 0\overset{\circ}{.}4$.

6.2.10. TIC 461500036

The features of the light curve from this last system in our sample strongly resemble the previous one. That is, the regular inner primary and secondary eclipses are quite deep (with depths greater than 40%) and look rather similar. By contrast, the third-body eclipses are shallow, however they are well observable due to the precise TESS photometry. The similarity to TIC 405789362, naturally arises from the very similar surface brightness ratios for the two systems. Regarding the fact that both the current and the previous system are formed by three MS-stars, the similarities of the surface brightness ratios imply that both the inner and outer mass ratios of the current system are close to the corresponding quantities of the previous triple. In the current system this is $q_\mathrm{in} = 0.962 \pm 0.008$ and $q_\mathrm{out} = 0.309 \pm 0.006$. Interestingly, not only the mass ratios, but the individual stellar masses are also quite similar to the previous triple as $M_\mathrm{Aa} = 1.29 \pm 0.08\,\mathrm{M}_\odot$, $M_\mathrm{Ab} = 1.25 \pm 0.08\,\mathrm{M}_\odot$ and, $M_\mathrm{B} = 0.79 \pm 0.05\,\mathrm{M}_\odot$.

The similarities, however, end there when one considers the dynamical properties. The current triple has a shorter inner and a longer outer period as compared to the previous system and, hence, is much less tight ($P_\mathrm{out}/P_\mathrm{in} = 22.08$). Due to the nearly two-times lesser tightness, the third-body perturbation forces are weaker, and the inner orbit is allowed to be much closer to circular. However, as was discussed above, the osculating eccentricity cannot reach exactly zero, hence $e_\mathrm{in} = 0.0013 \pm 0.0001$. More interesting, however, is that the outer orbit also has a low eccentricity with $e_\mathrm{out} = 0.032 \pm 0.001$. We will return to the question of the relatively small outer eccentricities in Sect. 7.

Finally, note another similarity to the previous system, as we obtained a very similar mutual inclination between the inner and outer orbital planes, as $i_\mathrm{mut} = 1\overset{\circ}{.}4 \pm 0\overset{\circ}{.}2$.

7. Summary, discussion, and conclusions

This work presents 10 new, ultracompact triply eclipsing triples with a full set of stellar and orbital solutions. These systems were discovered as UCHTs by searching through several million TESS photometric light curves for third-body eclipses in what are otherwise seemingly normal binary systems (see e.g., Kristiansen et al. 2022; Rappaport et al. 2022).

The analyses utilized the photometric light curves from TESS, the ETV curves derived from the TESS light curves, SED data found in the archives and, in a few cases, ground-based follow up eclipse photometry. In contrast to our previous works, however, we did not use photometric data from the archives of ASAS-SN and ATLAS, since the frequent TESS observations by themselves were quite satisfactory for the determination of the orbital solutions. Moreover, due to the faintness of the currently investigated triples, no RV observations were available for our targets. All the above mentioned data were analysed jointly with a complex photodynamical code wherein we solve for all the stellar and orbital system parameters, as well as the distance to the source. Typical uncertainties on the masses and radii are of order a couple per cent to about ∼5 per cent. Uncertainties on the angles associated with the orbital planes (e.g., i_out and i_mut) range from a fraction of a degree to about a degree. See Tables B.2 through B.6.

In Fig. 4 we present a set of nine correlation plots among some of the more physically interesting parameters associated with our collection of 44 triply eclipsing triples that we have analysed in a uniform way. To the ten sources studied in this paper, we have added the 22 triples from our previous closely related papers Rappaport et al. (2022, 2023, 2024), as well as 12 triples studied in Borkovits et al. (2019a, 2020b, 2022a,b); Czavalinga et al. (2023); Kostov et al. (2024), and Mitnyan et al. (2020) using essentially the same selection criteria as well as methods of analysis.

In the top row of Fig. 4, the left two panels show correlations between the two masses of the inner binary and between the tertiary star and the primary of the inner binary. The former pair have a correlation coefficient of 0.71 with all the stars and 0.91 if we eliminate the two secondaries that are farthest from the red (equal mass) line[4]. The correlation coefficient for the tertiary with primary of the EB is only 0.64. These also serve to show that most of the stars in our sample have masses between 0.5 and 2.5 $\mathrm{M}_\odot$.

The top right and middle left panels plot the EB period and outer eccentricity vs. the outer orbital period, respectively. Neither set of orbital parameters is particularly correlated. The P_in vs. P_out diagram does nicely show the rough empirical upper stability limit at $P_\mathrm{out} \gtrsim 7P_\mathrm{in}$.

[4] In both cases the correlation coefficient was calculated without including the massive (∼7 $\mathrm{M}_\odot$) stars in TIC 290061485 which are located off the plot.

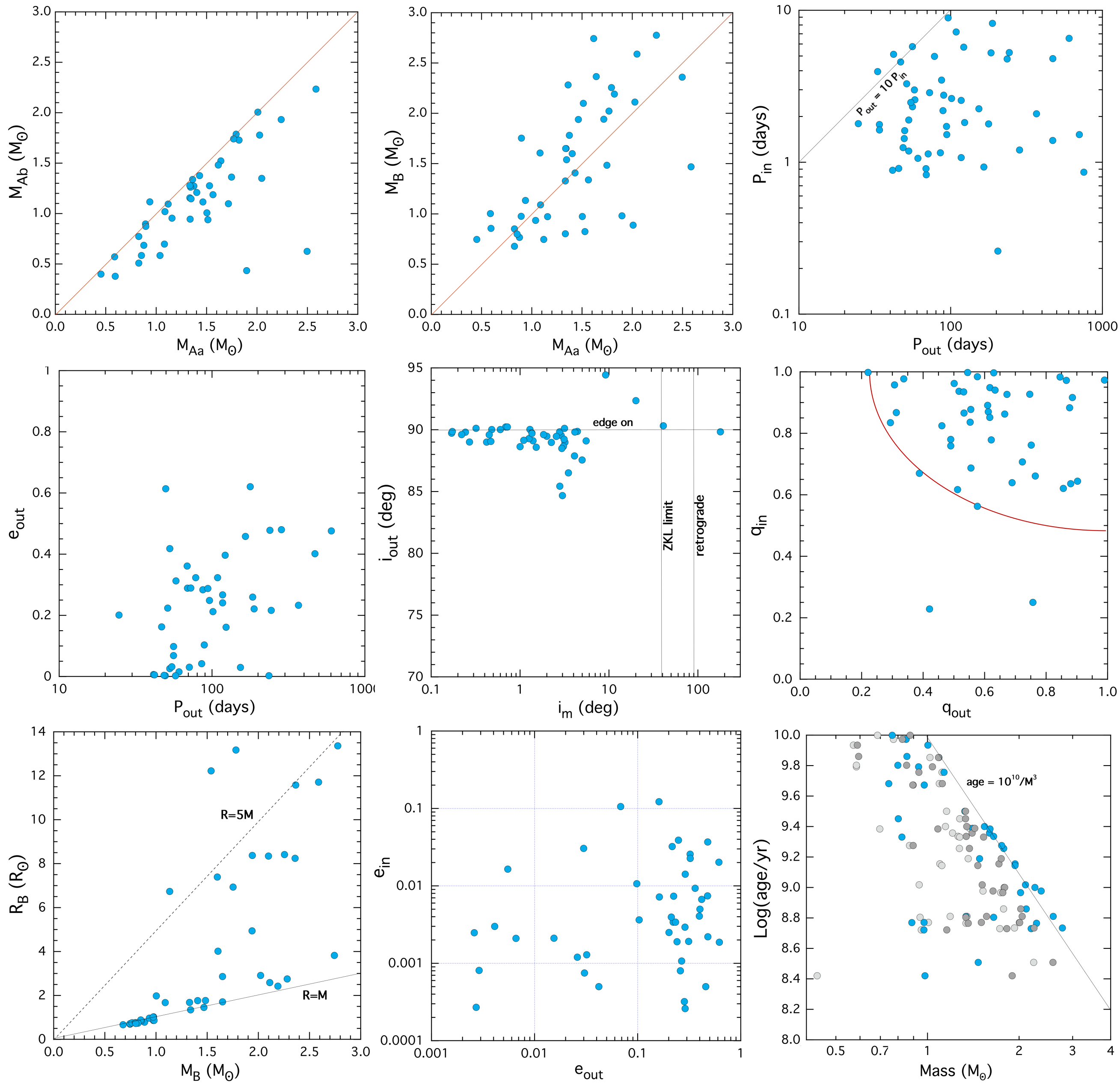

Fig. 4. Statistical plots for properties of 44 triply eclipsing triples uniformly analysed (see text for references). *Top-row panels:* $M_{\rm Ab}$ vs. $M_{\rm Aa}$, $M_{\rm B}$ vs. $M_{\rm Aa}$, and $P_{\rm in}$ vs. $P_{\rm out}$. *Middle-row panels:* $e_{\rm out}$ vs. $P_{\rm out}$, $i_{\rm out}$ vs. $i_{\rm mut}$, and $q_{\rm in}$ vs. $q_{\rm out}$. *Bottom-row panels:* $R_{\rm B}$ vs. $M_{\rm B}$, $e_{\rm in}$ vs. $e_{\rm out}$, and the age of the systems vs. the masses of the tertiary (blue), primary (dark grey) and secondary (light grey) EB stars. In this latter panel as well as the first two panels, the masses of TIC 290061484 are $\sim$7 $M_\odot$ and are off the plots. The red curve in the middle right panel shows how nearly all the systems are confined to $0.2 < q_{\rm out} < 1.0$ and $q_{\rm in} > 0.2$. In the central panel the vertical lines denote the transition to the Von Zeipel-Lidov-Kozai (ZLK) cycles (see Naoz 2016, for a review), and to retrograde orbits, respectively. The sloped dashed lines in the lower left panel are for $R_{\rm B} = 1\,M_{\rm B}$ and $= 5\,M_{\rm B}$ (both expressed in solar units), as rough guides of unevolved and quite evolved stars, respectively.

The middle panel shows the relation between the outer orbital inclination angle and the mutual inclination (i.e., the angle between the inner and outer orbital planes). That most of the values of $i_{\rm out}$ are near 90° is a selection effect since these triples were actually discovered from their third-body eclipses. The same selection also holds, to some extent, for the low values of $i_{\rm mut}$, otherwise third body eclipses would be more difficult to detect. Two of the systems have large enough $i_{\rm mut}$ (20° and 40°) to undergo substantial precession of their orbital planes. Finally, there is one triple (TIC 276162169 = V493 Cygni) in a nearly flat system, but where the outer orbit is likely retrograde with respect to the inner EB; however, as was stated in Rappaport et al. (2023), a verification of that finding will require further observations. These are rare systems.

The middle right panel shows the correlation between the inner mass ratio, $q_{\rm in} = M_{\rm Ab}/M_{\rm Aa} \equiv< 1.0$, and the outer mass ratio $q_{\rm out} \equiv M_{\rm B}/(M_{\rm Aa} + M_{\rm Ab})$. With only two exceptions, $1.0 > q_{\rm in} \gtrsim 0.55$ while $q_{\rm out}$ is typically between 0.3 and 0.9, with no restrictions on it being larger than unity.

The lower left panel gives the relation between the radius of the tertiary star and its mass. Stars lying approximately along the $R = M$ line (both in solar units), indicate largely unevolved stars.

Stars closer to the $R = 5M$ line and above it are progressively more evolved. The tertiary stars in UCHTs generally still have more room to evolve before filling their Roche lobes than do the primary stars of the inner binaries. More evolved, and therefore more luminous, tertiaries make for easier detection; but, on the other hand, if they are too bright they can obscure the third-body eclipses by which these systems are found - at least in this work.

The bottom middle panel shows how the eccentricities of the inner and outer orbits are possibly related. While they both range over about three orders of magnitude, the outer eccentricities span 0.001 to almost 1 while the inner eccentricities span a range that is shifted an order of magnitude lower: 0.0001 to 0.1. They are otherwise uncorrelated.

Finally, in the bottom right corner we show how the ages of the systems that we infer for these compact triples are related to the masses of the tertiaries (blue points) and of the primary (dark grey) and secondary (light grey) stars in the EBs. We omitted one very young (pre-MS) system, as well as TIC 290061484 with an age of 13 Myr and containing ~7 $M_\odot$ stars, and find that the remainder of the systems are modest-to-very old, spanning the range from 300 -1000 Myr. The sloped line is a rough guide to the MS lifetime of stars, going as $10^{10}/M^3$ yr, where the mass is in solar masses.

In Figure 5 we show how the outer eccentricities in the sample of compact triples we have studied vary with the ratio of the tertiary star's radius to the outer semimajor axis. Most of the systems have $e_{\rm out}$ between 0.1 and 0.7. These same systems also have $R_B/a_{\rm out} \lesssim 0.04$. However, there are some 9 systems which have considerably smaller $e_{\rm out}$ and also substantially larger values of $R_B/a_{\rm out}$ ranging from ~0.05-0.15, where we postulate that tidal interactions between the tertiary and the inner binary have tended to circularise the outer orbit. There are three exceptions to this trend where the systems have very small $e_{\rm out}$ and also very low ratios of $R_B/a_{\rm out}$, where tidal circularization should not have played much of a role. In these cases, perhaps the systems were simply born with $e_{\rm out}$ as low as that measured at the current epoch (~0.003).

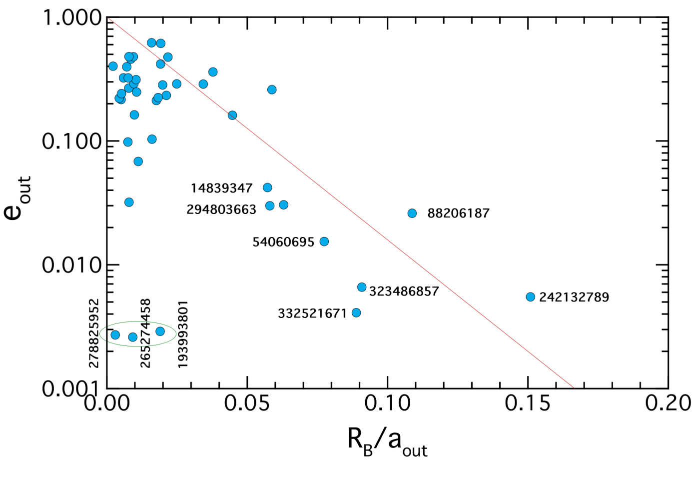

Fig. 5. Eccentricity of the outer orbit of compact triply eclipsing triples vs. the ratio of the tertiary's radius to the outer semimajor axis. With three exceptions (lower left corner), it seems reasonable to infer that tidal circularization of the outer orbit by evolved (i.e., large) tertiaries is responsible for the decaying outer eccentricity with increasing $R_{\rm B}/a_{\rm out}$.

As more and more CHTs become well characterised, a pattern is emerging as to how they populate a tightness-compactness diagram. We show in Fig. 6 the most compact 50 systems that we have collected (most of them from our analysed systems). All the systems are triply eclipsing except for λ Tau (marked in orange) which is sufficiently exceptional that we show it in spite of having no third-body eclipses. They all have $P_{\rm out}/P_{\rm min} > 7$ which seems to be an empirical limit for long-term dynamical stability. The tightest system is KIC 7668648 with $P_{\rm out} = 205$ d, and $P_{\rm out}/P_{\rm in} = 7.36$ (Orosz 2023). The Mardling & Aarseth relations (Mardling & Aarseth 2001) suggests a minimum ratio $P_{\rm out}/P_{\rm min} > 4.7$ for long-term dynamical stability even for coplanar and circular orbits. The most compact triple known to date is TIC 290061484 with an outer period of just 24.5 days (Kostov et al. 2024). There is an intriguing empirical upper envelope shown by the sloped red line in Fig. 6. This line is given mathematically by the condition that $P_{\rm in} \simeq 1$ day. Such a period, of course, is typical of the shorter periods in our sample. Interestingly, this line extrapolates to a minimum outer period for UCHTs of $P_{\rm out,min} \sim 7$ days. Of course, if compact triples can form around contact type binaries, which so far have not been found, then the ultimate theoretical minimum period for UCHT might be as short as just a few days.

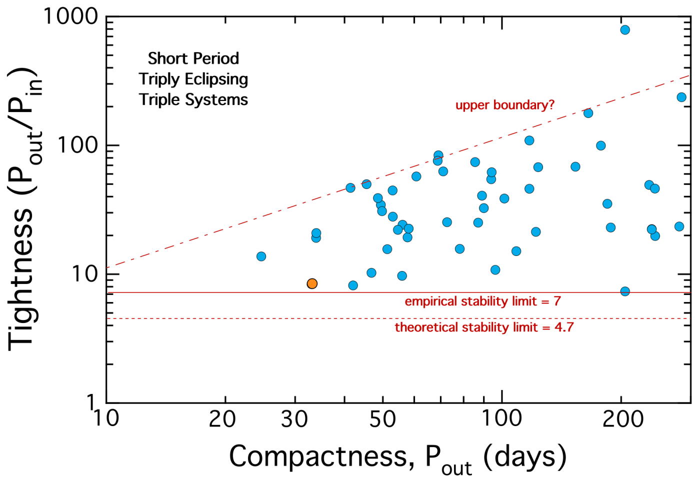

Fig. 6. Tightness of triply eclipsing triple systems ($P_{\rm out}/P_{\rm in}$) as a function of the system compactness. λ Tau (orange circle, Ebbighausen & Struve 1956) is not triply eclipsing, but it is otherwise such a noteworthy benchmark system that we include it for reference. The most compact triple, TIC 290061484, is the leftmost system in the plot. The empirical and theoretical lower limits for dynamical stability are marked with solid and dashed horizontal lines, respectively. A speculative upper boundary is marked with the sloped red dot-dashed line.

Finally, in regard to our statistical-level results, we mention our photometric distance determinations in comparison with the parallactic distances found by Gaia. Fig. 7 shows how our photometric distances stack up against Gaia's distances (Bailer-Jones et al. 2021). These are the same triply eclipsing systems discussed above, and augmented by several other triple systems subjected to the same photodynamical analysis, but ones which are not triply eclipsing. These latter sources are taken from Borkovits et al. (2020a, 2022b); Gaulme et al. (2022), and Borkovits & Mitnyan (2023).

The overall agreement between the our photometric distances and the Gaia results is fairly impressive, and the two sets have broadly comparable error bars. The fitted slope relating them, found from an 'orthogonal distance regression' (ODR) is 0.994 ± 0.0165. The value of χ^2 per degree of freedom reaches unity only after the uncertainties on both data sets have been increased by a factor of 2.8. Despite this general agreement, there

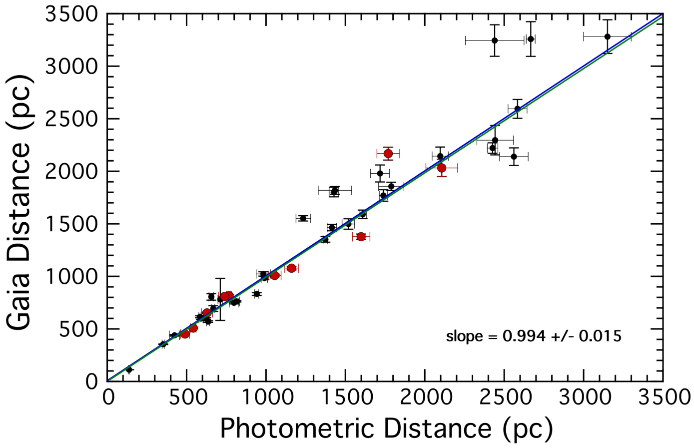

Fig. 7. Comparison of Gaia distances (Bailer-Jones et al. 2021) to 43 triple systems with distances found from our photodynamical fits to the system parameters. The systems marked in red are the 10 from the current work with fitted distances. The blue curve is the line where the Gaia and our photometric distances would match. The green curve results from a formal orthogonal distance regression with a fitted slope of 0.994 ± 0.015. There are three systems not shown. For TIC 388459317 and TIC 52041148, the Gaia points are off the plot and have rather large uncertainties compared to the photometric ones. TIC 280883908 has $d_{\rm Gaia} = 3072 \pm 1000$ pc compared to $d_{\rm photo} = 1183 \pm 40$ pc, where the Gaia point is quite obviously not very good, and its presence on the plot with such a large error bar would be visually distracting.

are a number of points where the two distances differ by more than a few statistical error bars. It is not obvious to us from an inspection of this plot which distance is manifestly more accurate. It is possible that one or both of the distance sets have underestimated their uncertainties. We note that most of the outer orbits, range from about 1/6-1 year, and in some cases may be somewhat distorting Gaia's parallax measurement. For our photometric distances, some of the SED data may have been taken during eclipses, the PARSEC isochrones are based on non-rotating stars, and there are likely to be uncertainties in the wavelength-dependent interstellar extinction that we rely on.

Data availability

Tables F.1–F.10 are only available in electronic form at the CDS via anonymous ftp to cdsarc.u-strasbg.fr (130.79.128.5) or via `http://cdsweb.u-strasbg.fr/cgi-bin/qcat?J/A+A/`.

Acknowledgements. This project has received funding from the HUN-REN Hungarian Research Network. T. B., T. M., I. B. B. and A. P. acknowledge the financial support of the Hungarian National Research, Development and Innovation Office – NKFIH Grants K-147131 and K-138962. V. B. K. is grateful for financial support from NSF grant AST-2206814. Z. G., T. P., and Z. D. acknowledge support from the ESA PRODEX project 'Observation of Exoplanets with the CHEOPS Space Observatory' (PEA 4000137122), and the ESA PRODEX project ?Hungarian Contribution to ESA's Ariel Space Telescope Mission: 'II. High-Precision Photometry with Ariel' between ELTE Eötvös Loránd University and the European Space Agency, as well as from the VEGA grant of the Slovak Academy of Sciences (No. 2/0031/22), the Slovak Research and Development Agency contract (No. APVV-20-0148), and the support of the city of Szombathely. This paper makes extensive use of data collected by the *TESS* mission. Funding for the *TESS* mission is provided by the NASA Science Mission directorate. Some of the data presented in this paper were obtained from the Mikulski Archive for Space Telescopes (MAST). STScI is operated by the Association of Universities for Research in Astronomy, Inc., under NASA contract NAS5-26555. Support for MAST for non-HST data is provided by the NASA Office of Space Science via grant NNX09AF08G and by other grants and contracts. Distances and other astrometric properties for all targets, and outer orbits for two of our sources, were taken from the archives of European Space Agency (ESA) mission *Gaia*[5], processed by the *Gaia* Data Processing and Analysis Consortium (DPAC)[6]. Funding for the DPAC has been provided by national institutions, in particular the institutions participating in the *Gaia* Multilateral Agreement. Some of the SED fluxes and magnitudes were obtained with the Wide-field Infrared Survey Explorer, which is a joint project of the University of California, Los Angeles, and the Jet Propulsion Laboratory/California Institute of Technology, funded by the National Aeronautics and Space Administration. Additionally, some of the SED fluxes and magnitudes were obtained with the Two Micron All Sky Survey, which is a joint project of the University of Massachusetts and the Infrared Processing and Analysis Center/California Institute of Technology, funded by the National Aeronautics and Space Administration and the National Science Foundation. We used the Simbad service operated by the Centre des Données Stellaires (Strasbourg, France). This research has also made use of the VizieR catalogue access tool, CDS, Strasbourg, France (DOI : 10.26093/cds/vizier). The original description of the VizieR service was published in Ochsenbein et al. (2000).

References

Bailer-Jones, C. A. L., Rybizki, J., Fouesneau, M., Demleitner., M., Andrae, R., 2021, AJ, 161, 147
Borkovits, T. 2022, Galaxies, 10, 9
Borkovits, T., & Mitnyan, T. 2023, Universe, 9, 485
Borkovits, T., Érdi, B., Forgács-Dajka, E., Kovács, T. 2003, A&A, 398, 1091
Borkovits, T., Derekas, A., Kiss, L.L., et al. 2013, MNRAS, 428, 1656
Borkovits T., Rappaport S., Hajdu T., Sztakovics J., 2015, MNRAS, 448, 946
Borkovits, T., Hajdu, T., Sztakovics, J., Rappaport, S., Levine, A., Bíró, I. B., Klagyivik, P., 2016, MNRAS, 455, 4136
Borkovits, T., Albrecht, S., Rappaport, S., et al. 2018, MNRAS, 478, 513
Borkovits, T., Rappaport, S., Kaye, T., et al. 2019a, MNRAS, 483, 1934
Borkovits, T., Sperauskas, J., Tokovinin, A., Latham, D. W., Csányi, I., Hajdu, T., Molnár, L., 2019b, MNRAS, 487, 4631
Borkovits, T., Rappaport, S., Hajdu, T., et al. 2020a, MNRAS, 493, 5005
Borkovits, T., Rappaport, S., Tan, T.G., et al. 2020b, MNRAS, 496, 4624
Borkovits, T., Rappaport, S., Maxted, P. F. L., et al. 2021, MNRAS, 503, 3759
Borkovits, T., Mitnyan, T., Rappaport, S., et al. 2022a, MNRAS, 510, 1352
Borkovits, T., Rappaport, S. A., Toonen, S., Moe, M., Mitnyan, T., Csányi, I., 2022b, MNRAS, 515, 3773
Borkovits, T., Rappaport, S. A., Mitnyan, T., et al., 2025, A&A, 695, A209
Borucki W. J. et al., 2010, Science, 327, 977
Bressan, A., Marigo, P., Girardi, L. et al. 2012, MNRAS, 427, 127
Carter, J.A., Fabrycky, D.C., Ragozzine, D., et al. 2011, Sci, 331, 562
Correia, A.C.M, Laskar, J., Farago, F., Boué, G., 2011, CeMDA, 111, 105
Cutri, R.M., Wright, E.L., Conrow, T., et al. 2013, wise.rept, 1C.
Czavalinga, D. R., Borkovits, T., Mitnyan, T., Rappaport, S. A.& Pál, A. 2023, MNRAS, 526, 2830
Derekas, A., Kiss, L. L., Borkovits, T., et al. 2011, Sci, 332, 216
Ebbighausen, E. G., Struve, O. 1956, ApJ, 124, 507
Ford, E. B., 2005, AJ, 129, 1706
Gaia Collaboration, Brown, A. G. A., Vallenari, A., Prusti, T. et al. 2021, A&A, 649, A1
Gaulme, P., Borkovits, T., Appourchaux, T., et al. 2022, A&A, 668, A173
Grishin, E., Perets, H.B., 2022, MNRAS, 512, 4993
Henden, A. A., Levine, S., Terrell, D., Welch, D. 2015, American Astronomical Society, AAS Meeting #225, id.336.16
Kisseleva-Eggleton, L., Eggleton, P. 2010, in *International Conference on Binaries: in celebration of Ron Webbink's 65th Birthday*, eds. Kalogera, V., van der Sluys, M., American Institute of Physics Conference Series, 1314, 128
Kostov et al., 2021, ApJ, 917, 93
Kostov, V.B., Powell, B.P., Rappaport, S.A, et al., 2022, ApJS, 259, 66
Kostov, V.B., Rappaport, S.A., Borkovits, T., et al., 2024, ApJ, 974, 25
Kristiansen, M.H., Rappaport, S., Vanderburg, A., et al. 2022, PASP, 134, 074401
Lightkurve Collaboration, Cardoso, José Vinícius de Miranda, Hedges, C., Gully-Santiago, M., et al. 2018, Astrophysics Source Code Library, record ascl:1812.013, arXiv: 1812.013
Lindegren, L., Bastian, U., Biermann, M., et al. 2021, A&A, 649, 4L
Mardling R. A., & Aarseth S. J., 2001, MNRAS, 321, 398
Mitnyan, T., Borkovits, T., Rappaport, S., Pál, A., Maxted, P. F. L., 2020, MNRAS, 498, 6034
Naoz, S. 2016, ARA&A, 54, 441
Ochsenbein F., Bauer P., Marcout J., 2000, A&AS, 143, 23
Offner, S. S. R., Moe, M., Kratter, K. M., Sadavoy, S. I., Jensen, E. L. N., Tobin, J. J., 2023 ASP Conf. Ser. 534, 275
Orosz, J.A. 2023, Universe, 9, 12, 505

[5] `https://www.cosmos.esa.int/gaia`
[6] `https://www.cosmos.esa.int/web/gaia/dpac/consortium`

Paegert, M. et al, 2021, arXiv:2108.04778
Pál, A., 2012, MNRAS, 421, 1825
Rappaport S., Deck K., Levine A., Borkovits T., Carter J., El Mellah I., Sanchis-Ojeda R., & Kalomeni B., 2013, ApJ, 768, 33
Rappaport, S., Borkovits, T., Gagliano, R., et al. 2022, MNRAS, 513, 4341
Rappaport, S., Borkovits, T., Gagliano, R., et al. 2023, MNRAS, 521, 558
Rappaport, S., Borkovits, T., Mitnyan, T., et al. 2024, A&A, 686, A27
Ricker, G.R., Winn, J.N., Vanderspek, R., et al. 2015, JATIS, 1, 014003
Roemer, O. 1677, Philosophical Transactions (1665-1678), Volume 12, 893
Saglia et al., 2025, A&A, 699, A151
Söderhjelm, S. 1975, A&A, 42, 229.
Skrutskie, M.F., Cutri, R.M., Stiening, R., et al. 2006, AJ, 131, 1163
Tokovinin, A., 2014, AJ, 147, 86
Tokovinin, A., 2021, Universe, 7, 352
Zasche, P., Henzl, Z., & Mašek, M. 2022, A&A, 664, 96

Appendix A: Tabulated system parameters

Coordinates, catalogue passband magnitudes, and some other catalogue parameters of our ten target systems.

Table A.1. Main properties of the first five of the ten triple systems from different catalogues

Parameter	198581208	265274458	283846096	337993842	351404069
RA J2000	17:04:25.48	23:50:46.62	21:03:33.20	22:31:19.72	21:25:46.26
Dec J2000	46:35:33.53	73:09:24.27	21:51:42.01	60:51:25.35	38:59:27.77
T^a	13.76 ± 0.01	12.03 ± 0.01	13.45 ± 0.01	13.07 ± 0.03	12.57 ± 0.01
G^b	14.24 ± 0.00	12.42 ± 0.00	14.07 ± 0.00	13.60 ± 0.00	13.05 ± 0.00
G^b_{BP}	14.62 ± 0.00	12.73 ± 0.03	14.60 ± 0.00	14.07 ± 0.00	13.44 ± 0.00
G^b_{RP}	13.68 ± 0.00	11.93 ± 0.01	13.38 ± 0.00	12.95 ± 0.00	12.49 ± 0.00
B^a	15.28 ± 0.01	13.13 ± 0.52	15.41 ± *NA*	14.69 ± 0.14	13.94 ± 0.05
V^c	14.51 ± 0.02	12.50 ± 0.05	14.35 ± 0.08	13.94 ± 0.14	13.23 ± 0.06
J^d	13.01 ± 0.03	11.34 ± 0.02	12.50 ± 0.03	12.09 ± 0.03	11.93 ± 0.03
H^d	12.61 ± 0.03	11.20 ± 0.03	12.04 ± 0.03	11.87 ± 0.03	11.56 ± 0.03
K^d	12.51 ± 0.03	11.10 ± 0.02	11.93 ± 0.02	11.77 ± 0.03	11.51 ± 0.02
$W1^e$	12.47 ± 0.02	11.02 ± 0.02	11.80 ± 0.02	11.70 ± 0.02	11.38 ± 0.02
$W2^e$	12.49 ± 0.02	11.02 ± 0.02	11.82 ± 0.02	11.69 ± 0.02	11.41 ± 0.02
$W3^e$	11.98 ± 0.19	10.30 ± 0.06	11.91 ± 0.29	12.44 ± 0.43	11.31 ± 0.14
$T_{\rm eff}$ [K]^b	5615 ± 55	9091 ± 296	4975 ± 16	NA	NA
$T_{\rm eff}$ [K]^a	5465 ± 35	7972 ± 153	4923 ± 122	8968 ± 123	5757 ± 125
Radius [$R_\odot$]^a	1.55 ± *NA*	2.29 ± 0.08	1.04 ± *NA*	4.55 ± *NA*	2.50 ± 0.12
Distance [pc]^f	1081 ± 17	816 ± 8	452 ± 6	2186 ± 64	1009 ± 9
$E(B-V)^a$	0.03 ± *NA*	0.43 ± 0.01	0.08 ± 0.01	0.79 ± 0.03	0.10 ± 0.01
μ_α [mas/yr]^b	−8.01 ± 0.02	−1.59 ± 0.01	−6.25 ± 0.02	−2.81 ± 0.01	−7.11 ± 0.01
μ_δ [mas/yr]^b	−6.01 ± 0.02	−2.60 ± 0.01	−13.7 ± 0.02	−1.25 ± 0.01	−9.93 ± 0.01
RUWE^{b,g}	1.05	1.16	1.38	1.00	0.96
astr_ex_noise [mas]^{b,h}	0	0.09	0.10	0	0.03
astr_ex_noise_sig^{b,h}	0	11	5.4	0	1.0
$P_{\rm binary}{}^i$ [d]	2.8769	2.9978	5.8082	2.6272	8.9113
$P_{\rm triple}{}^i$ [d]	72.65	57.72	55.95	101.38	96.24

Notes. General: "NA" and ellipses in this table indicate that the value is not available. (a) *TESS* Input Catalog (TIC v8.2) (Paegert et al. 2021). (b) Gaia EDR3 (Gaia collaboration 2021); the uncertainty in $T_{\rm eff}$ listed here is 1.5 times the geometric mean of the upper and lower error bars of `teff_gspphot`. Magnitude uncertainties listed as 0.00 are $\lesssim$ 0.005. (c) AAVSO Photometric All Sky Survey (APASS) DR9, (Henden et al. 2015), `http://vizier.u-strasbg.fr/viz-bin/VizieR?-source=II/336/apass9`. (d) 2MASS catalogue (Skrutskie et al. 2006). (e) WISE point source catalogue (Cutri et al. 2013). (f) Bailer-Jones et al. (2021), geometric distances. (g) The Gaia renormalized unit weight error (RUWE) is the square root of the normalized χ^2 of the astrometric fit to the along-scan observations. Values in excess of about unity are sometimes taken to be a sign of stellar multiplicity. (h) Abbreviations for `astrometric_excess_noise` and `astrometric_excess_noise_sig` (Lindegren et al. 2021; `https://gea.esac.esa.int/archive/documentation/GDR2/Gaia_archive/chap_datamodel/sec_dm_main_tables/ssec_dm_gaia_source.html`); these are a measure of "the disagreement, expressed as an angle, between the observations of a source and the best-fitting standard astrometric model." Values of `astrometric_excess_noise_sig` $\gtrsim$ 2 are considered significant. (i) Binary and outer orbital periods from this work; given here for reference purposes.

Table A.2. Main properties of the second five of the ten triple systems from different catalogues

Parameter	378270875	403792414	403916758	405789362	461500036
RA J2000	20:13:45.58	19:16:23.08	01:52:48.09	21:37:44.55	22:19:19.64
Dec J2000	47:40:39.86	26:23:02.86	67:21:05.98	64:48:20.15	85:04:13.37
T^a	13.12 ± 0.04	13.78 ± 0.01	11.31 ± 0.04	14.45 ± 0.02	13.78 ± 0.01
G^b	13.79 ± 0.00	14.51 ± 0.00	12.39 ± 0.00	15.19 ± 0.00	14.34 ± 0.00
G_{BP}^b	14.38 ± 0.00	15.16 ± 0.00	13.57 ± 0.00	15.85 ± 0.00	14.79 ± 0.00
G_{RP}^b	13.05 ± 0.00	13.73 ± 0.00	11.33 ± 0.00	14.40 ± 0.00	13.71 ± 0.00
B^a	15.09 ± 0.23	16.15 ± 0.06	15.25 ± *NA*	16.69 ± 0.07	15.60 ± 0.30
V^c	14.00 ± 0.03	14.83 ± 0.07	13.31 ± 0.07	15.65 ± 0.06	14.68 ± 0.03
J^d	12.01 ± 0.02	12.64 ± 0.02	9.73 ± 0.02	13.57 ± 0.03	12.96 ± 0.03
H^d	11.52 ± 0.03	12.10 ± 0.02	9.03 ± 0.03	13.16 ± 0.03	12.59 ± 0.03
K^d	11.37 ± 0.03	11.98 ± 0.03	8.82 ± 0.02	13.01 ± 0.03	12.55 ± 0.03
$W1^e$	11.21 ± 0.02	11.97 ± 0.02	8.65 ± 0.02	12.71 ± 0.03	12.52 ± 0.02
$W2^e$	11.27 ± 0.02	12.01 ± 0.02	8.68 ± 0.02	12.72 ± 0.03	12.52 ± 0.02
$W3^e$	11.79 ± 0.19	11.85 ± 0.25	8.58 ± 0.03	12.70 ± *NA*	12.43 ± 0.31
$T_{\rm eff}$ [K]^b	5015 ± 43	4903 ± 21	4871 ± 12	7194 ± 73	5858 ± 39
$T_{\rm eff}$ [K]^a	4705 ± 122	5018 ± 123	4211 ± 122	6129 ± 124	5561 ± 122
Radius [$R_\odot$]^a	1.38 ± *NA*	1.34 ± *NA*	9.74 ± *NA*	2.91 ± *NA*	2.25 ± *NA*
Distance [pc]^f	509 ± 7	654 ± 7	804 ± 8	2036 ± 187	1355 ± 32
$E(B-V)^a$	0.07 ± 0.06	0.26 ± 0.01	0.51 ± 0.08	0.58 ± 0.02	0.15 ± 0.01
μ_α [mas/yr]^b	3.38 ± 0.03	5.59 ± 0.01	3.25 ± 0.01	−4.49 ± 0.03	−1.18 ± 0.02
μ_δ [mas/yr]^b	2.00 ± 0.03	7.21 ± 0.02	−1.36 ± 0.02	−3.31 ± 0.02	1.12 ± 0.02
RUWE^{b,g}	1.93	1.03	1.33	0.96	0.99
astr_ex_noise [mas]^{b,h}	0.23	0	0.14	0	0
astr_ex_noise_sig^{b,h}	31	0	26	0	0
$P_{\rm binary}{}^i$ [d]	2.5769	4.9949	1.3371	4.5778	2.4712
$P_{\rm triple}{}^i$ [d]	58.12	78.20	71.06	46.81	54.56

Notes. See the notes under Table A.1.

Table A.3. TESS observation sectors for the triples

Object	Sectors observed	Third body events
TIC 198581208	S24–26,51–53,78–80	24,26,51,52,79,80
TIC 265274458[a]	17,19,24–25,52,58–59,78–79,85–86	17,19,24,52,58,59,78,79,85,86
TIC 283846096	15,41,55,82	15,41,55,82
TIC 337993842	16–17,24,57,84–85	17, 84
TIC 351404069	15–16,55–56,75–76,82–83	55, 56, 76, 83
TIC 378270875	14–15,41,55–56,75–76,81–83	14,55,76,82
TIC 403792414	40–41,54,80–81	40,41,54,80–81
TIC 403916758	18,24–25,52,58–59,78–79,85–86	24,25,58,79,85
TIC 405789362	16–18,24,56–58,76–78,83–85	16,17,18,24,56,57,58,76,77,78,83,84,85
TIC 461500036	18,20,25–26,40,52–53.58–60,73,78–79,85–86	20,25,53,59,73,79,85

Notes. None of these sources will be observed in further TESS sectors until the end of Cycle 8 observations; [(a)] T IC 265274458 was also observed with 2-min cadence time in Sectors between 24 and 79.

Appendix B: Tabulated results of the photodynamical analyses

In this appendix we tabulate the results of the joint photodynamical analyses.

Table B.1. Definitions of triple system parameters in Tables B.2 – B.6

Parameter[a]	Definition
t_0	Epoch time for osculating elements
P	Orbital period
a	Orbital semimajor axis
e	Orbital eccentricity
ω	Argument of periastron (of secondary)
i	Orbital inclination angle
$\mathcal{T}_0^{\mathrm{inf/sup}}$	Time of conjunction of the secondary[b]
τ	Time of periastron passage
Ω	Longitude of the node relative to the node of the inner orbit
i_{mut}	Mutual inclination angle[c]
q	Mass ratio (secondary/primary)
K_{pri}	"K" velocity amplitude of primary
K_{sec}	"K" velocity amplitude of secondary
R/a	Stellar radius divided by semimajor axis
$T_{\mathrm{eff}}/T_{\mathrm{eff,Aa}}$	Temperature relative to EB primary
fractional flux	Stellar contribution in the given band
M	Stellar mass
R	Stellar radius
T_{eff}	Stellar effective temperature
L_{bol}	Stellar bolometric luminosity
M_{bol}	Stellar absolute bolometric magnitude
M_V	Stellar absolute visual magnitude
$\log g$	log surface gravity (cgs units)
$[M/H]$	log metallicity abundance to H, by mass
$E(B-V)$	Colour excess in B-V bands
extra light, ℓ_4	Contaminating flux in the given band
$(M_V)_{\mathrm{tot}}$	System absolute visual magnitude
distance	Distance to the source

Notes. (a) The units for the parameters are given in Tables B.2– B.6. (b) The superscript of "inf/sup" indicates inferior vs. superior conjunctions. (By default we give inferior conjunctions. Superior conjunctions are indicated by asteriks.) (c) More explicitly, this is the angle between the orbital planes of the inner binary and the outer triple orbit.

Table B.2. Orbital and astrophysical parameters of TICs 198581208 and 265274458 from the joint photodynamical light curve, ETV, SED and PARSEC isochrone solution.

	TIC 198581208		TIC 265274458	
orbital elements				
	subsystem			
	Aa–Ab	A–B	Aa–Ab	A–B
t_0 [BJD - 2400000]	58955.0		58764.5	
P [days]	$2.869542^{+0.000039}_{-0.000040}$	$72.6507^{+0.0017}_{-0.0019}$	$2.990213^{+0.000067}_{-0.000065}$	$57.7193^{+0.0013}_{-0.0015}$
a [$R_\odot$]	$9.99^{+0.16}_{-0.17}$	$100.2^{+1.6}_{-1.8}$	$11.588^{+0.055}_{-0.083}$	$93.74^{+0.41}_{-0.64}$
e	$0.01413^{+0.00046}_{-0.00062}$	$0.28945^{+0.00098}_{-0.00099}$	$0.00248^{+0.00037}_{-0.00029}$	$0.0026^{+0.0015}_{-0.0014}$
ω [deg]	$97.4^{+1.5}_{-3.0}$	$95.600^{+0.071}_{-0.070}$	302^{+13}_{-10}	58^{+8}_{-18}
i [deg]	$89.50^{+0.14}_{-0.15}$	$89.60^{+0.02}_{-0.02}$	$90.48^{+0.25}_{-0.24}$	$90.22^{+0.06}_{-0.07}$
$\mathcal{T}_0^{\rm inf/sup}$ [BJD - 2400000]	$58957.6102^{+0.0001}_{-0.0001}$	$58975.6080^{+0.0117}_{-0.0131}$	$58766.3499^{+0.0001}_{-0.0001}$	$58781.1864^{+0.0023}_{-0.0024}$
τ [BJD - 2400000]	$58956.236^{+0.013}_{-0.024}$	$58941.243^{+0.013}_{-0.012}$	$58763.627^{+0.112}_{-0.081}$	$58746.8^{+1.3}_{-3.9}$
Ω [deg]	0.0	$-0.06^{+0.18}_{-0.17}$	0.0	$0.60^{+0.33}_{-0.36}$
$i_{\rm mut}$ [deg]	$0.22^{+0.14}_{-0.11}$		$0.72^{+0.36}_{-0.28}$	
$\varpi^{\rm dyn}$ [deg]	$277.4^{+1.5}_{-3.0}$	$275.6^{+0.07}_{-0.07}$	122^{+13}_{-10}	236^{+8}_{-24}
$i^{\rm dyn}$ [deg]	$0.19^{+0.12}_{-0.10}$	$0.03^{+0.02}_{-0.02}$	$0.62^{+0.31}_{-0.25}$	$0.09^{+0.05}_{-0.04}$
$\Omega^{\rm dyn}$ [deg]	326^{+73}_{-71}	146^{+73}_{-71}	114^{+35}_{-24}	294^{+35}_{-24}
$i_{\rm inv}$ [deg]	$89.59^{+0.02}_{-0.03}$		$90.26^{+0.05}_{-0.05}$	
$\Omega_{\rm inv}$ [deg]	$-0.05^{+0.16}_{-0.15}$		$0.52^{+0.29}_{-0.31}$	
mass ratio [$q = M_{\rm sec}/M_{\rm pri}$]	$0.563^{+0.010}_{-0.012}$	$0.576^{+0.004}_{-0.004}$	$0.229^{+0.002}_{-0.003}$	$0.421^{+0.003}_{-0.005}$
$K_{\rm pri}$ [km s^{-1}]	$63.47^{+0.78}_{-0.71}$	$26.67^{+0.56}_{-0.53}$	$36.53^{+0.30}_{-0.36}$	$24.32^{+0.17}_{-0.20}$
$K_{\rm sec}$ [km s^{-1}]	$112.7^{+2.5}_{-2.4}$	$46.29^{+0.76}_{-0.78}$	$159.6^{+1.0}_{-1.2}$	$57.85^{+0.35}_{-0.47}$
Apsidal and nodal motion related parameters				
$P_{\rm apse}$ [year]	$15.63^{+0.07}_{-0.07}$	$97.23^{+0.66}_{-0.50}$	$13.56^{+0.11}_{-0.09}$	$90.93^{+0.63}_{-0.57}$
$P_{\rm apse}^{\rm dyn}$ [year]	$7.33^{+0.03}_{-0.03}$	$12.10^{+0.04}_{-0.04}$	$6.35^{+0.05}_{-0.04}$	$10.55^{+0.07}_{-0.06}$
$P_{\rm node}^{\rm dyn}$ [year]	$13.82^{+0.06}_{-0.06}$		$11.94^{+0.07}_{-0.08}$	
$\Delta\omega_{\rm 3b}$ [arcsec/cycle]	$1368.6^{+6.4}_{-6.1}$	21305^{+72}_{-68}	1661^{+11}_{-12}	19408^{+113}_{-120}
$\Delta\omega_{\rm GR}$ [arcsec/cycle]	$1.343^{+0.042}_{-0.046}$	$0.230^{+0.007}_{-0.008}$	$1.664^{+0.016}_{-0.024}$	$0.292^{+0.003}_{-0.004}$
$\Delta\omega_{\rm tide}$ [arcsec/cycle]	$18.3^{+1.1}_{-1.0}$	$0.035^{+0.002}_{-0.002}$	$8.38^{+0.37}_{-0.39}$	$0.034^{+0.001}_{-0.002}$

	TIC 198581208			TIC 265274458		
stellar parameters						
	Aa	Ab	B	Aa	Ab	B
Relative quantities						
fractional radius [R/a]	$0.1270^{+0.0015}_{-0.0015}$	$0.0581^{+0.0012}_{-0.0012}$	$0.0096^{+0.0003}_{-0.0002}$	$0.1463^{+0.0012}_{-0.0014}$	$0.0365^{+0.0004}_{-0.0005}$	$0.0092^{+0.0001}_{-0.0001}$
temperature relative to $(T_{\rm eff})_{\rm Aa}$	1	$0.6502^{+0.0057}_{-0.0056}$	$0.9531^{+0.0042}_{-0.0042}$	1	$0.3923^{+0.0056}_{-0.0042}$	$0.6463^{+0.0064}_{-0.0074}$
fractional flux [in *TESS*-band]	$0.6487^{+0.0154}_{-0.0219}$	$0.0245^{+0.0009}_{-0.0009}$	$0.3194^{+0.0136}_{-0.030}$	$0.9261^{+0.0058}_{-0.0108}$	$0.0019^{+0.0001}_{-0.0001}$	$0.0643^{+0.0019}_{-0.0020}$
Physical quantities						
M [$M_\odot$]	$1.038^{+0.054}_{-0.057}$	$0.584^{+0.026}_{-0.026}$	$0.935^{+0.048}_{-0.050}$	$1.898^{+0.029}_{-0.043}$	$0.434^{+0.007}_{-0.007}$	$0.981^{+0.012}_{-0.019}$
R [$R_\odot$]	$1.270^{+0.033}_{-0.032}$	$0.581^{+0.020}_{-0.021}$	$0.965^{+0.044}_{-0.040}$	$1.698^{+0.017}_{-0.028}$	$0.424^{+0.006}_{-0.009}$	$0.863^{+0.013}_{-0.019}$
$T_{\rm eff}$ [K]	6095^{+99}_{-64}	3956^{+72}_{-52}	5801^{+99}_{-65}	8537^{+165}_{-147}	3345^{+42}_{-20}	5516^{+64}_{-63}
$L_{\rm bol}$ [$L_\odot$]	$1.99^{+0.23}_{-0.17}$	$0.074^{+0.012}_{-0.008}$	$0.95^{+0.16}_{-0.12}$	$13.8^{+1.0}_{-1.3}$	$0.020^{+0.001}_{-0.001}$	$0.618^{+0.046}_{-0.048}$
$M_{\rm bol}$	$4.02^{+0.10}_{-0.12}$	$7.60^{+0.12}_{-0.17}$	$4.83^{+0.14}_{-0.17}$	$1.92^{+0.11}_{-0.08}$	$9.00^{+0.06}_{-0.06}$	$5.29^{+0.09}_{-0.08}$
M_V	$4.05^{+0.11}_{-0.13}$	$8.68^{+0.15}_{-0.23}$	$4.88^{+0.15}_{-0.19}$	$1.91^{+0.09}_{-0.06}$	$11.03^{+0.11}_{-0.14}$	$5.40^{+0.10}_{-0.09}$
$\log g$ [dex]	$4.247^{+0.014}_{-0.012}$	$4.675^{+0.013}_{-0.012}$	$4.439^{+0.014}_{-0.016}$	$4.257^{+0.007}_{-0.007}$	$4.820^{+0.010}_{-0.007}$	$4.556^{+0.010}_{-0.007}$
Global system parameters						
log(age) [dex]	$9.792^{+0.103}_{-0.134}$			$8.420^{+0.054}_{-0.042}$		
$[M/H]$ [dex]	$-0.105^{+0.110}_{-0.058}$			$0.131^{+0.029}_{-0.070}$		
$E(B-V)$ [mag]	$0.200^{+0.026}_{-0.018}$			$0.473^{+0.018}_{-0.019}$		
extra light ℓ_4 [in *TESS*-band]	$0.006^{+0.014}_{-0.004}$			$0.008^{+0.011}_{-0.006}$		
$(M_V)_{\rm tot}$	$3.62^{+0.12}_{-0.15}$			$1.86^{+0.09}_{-0.06}$		
distance [pc]	1161^{+43}_{-44}			767^{+11}_{-17}		

Table B.3. Orbital and astrophysical parameters of TICs 283846096 and 337993842 from the joint photodynamical light curve, ETV, SED and PARSEC isochrone solution.

	TIC 283846096		TIC 337993842	
orbital elements				
	subsystem			
	Aa–Ab	A–B	Aa–Ab	A–B
t_0 [BJD - 2400000]	58711.0		58738.5	
P [days]	$5.76474^{+0.00096}_{-0.00077}$	$55.9539^{+0.0023}_{-0.0034}$	$2.626577^{+0.000042}_{-0.000046}$	$101.3859^{+0.0030}_{-0.0028}$
a [$R_\odot$]	$13.41^{+0.26}_{-0.23}$	$75.3^{+1.4}_{-1.3}$	$11.16^{+0.09}_{-0.12}$	$156.4^{+1.9}_{-1.8}$
e	$0.10579^{+0.00080}_{-0.00099}$	$0.0684^{+0.0021}_{-0.0020}$	$0.00395^{+0.00024}_{-0.00018}$	$0.2122^{+0.0046}_{-0.0093}$
ω [deg]	$241.4^{+1.4}_{-0.9}$	$263.9^{+1.0}_{-1.0}$	$8.8^{+4.0}_{-4.2}$	$166.2^{+2.5}_{-2.5}$
i [deg]	$89.66^{+0.06}_{-0.06}$	$89.59^{+0.02}_{-0.03}$	$88.90^{+0.30}_{-0.33}$	$89.14^{+0.04}_{-0.04}$
$\mathcal{T}_0^{\mathrm{inf/sup}}$ [BJD - 2400000]	$58712.4342^{+0.0041}_{-0.0022}$	$58722.9417^{+0.0027*}_{-0.0027}$	$58740.6730^{+0.0003}_{-0.0002}$	$58790.0973^{+0.0226*}_{-0.0193}$
τ [BJD - 2400000]	$58712.064^{+0.021}_{-0.015}$	$58693.88^{+0.19}_{-0.19}$	$58738.765^{+0.029}_{-0.031}$	$58703.86^{+0.68}_{-0.65}$
Ω [deg]	0.0	$-0.44^{+0.06}_{-0.07}$	0.0	$-1.02^{+0.41}_{-0.51}$
i_{mut} [deg]	$0.45^{+0.07}_{-0.06}$		$1.10^{+0.46}_{-0.32}$	
ϖ^{dyn} [deg]	$61.5^{+1.4}_{-0.9}$	$83.9^{+1.0}_{-1.0}$	$188.8^{+3.9}_{-4.2}$	$346.2^{+2.5}_{-2.5}$
i^{dyn} [deg]	$0.39^{+0.06}_{-0.05}$	$0.06^{+0.02}_{-0.01}$	$0.99^{+0.41}_{-0.29}$	$0.11^{+0.05}_{-0.03}$
Ω^{dyn} [deg]	$260.4^{+7.5}_{-7.6}$	$80.4^{+7.5}_{-7.6}$	283^{+24}_{-16}	103^{+24}_{-16}
i_{inv} [deg]	$89.60^{+0.02}_{-0.03}$		$89.11^{+0.05}_{-0.03}$	
Ω_{inv} [deg]	$-0.38^{+0.05}_{-0.06}$		$-0.92^{+0.37}_{-0.46}$	
mass ratio [$q = M_{\mathrm{sec}}/M_{\mathrm{pri}}$]	$0.636^{+0.004}_{-0.004}$	$0.880^{+0.002}_{-0.002}$	$0.983^{+0.012}_{-0.012}$	$0.849^{+0.032}_{-0.014}$
K_{pri} [km s^{-1}]	$46.05^{+0.87}_{-0.80}$	$31.95^{+0.62}_{-0.55}$	$106.58^{+1.00}_{-1.20}$	$36.62^{+1.15}_{-0.63}$
K_{sec} [km s^{-1}]	$72.30^{+1.48}_{-1.29}$	$36.29^{+0.70}_{-0.62}$	$108.44^{+1.23}_{-1.46}$	$43.10^{+0.39}_{-0.37}$
Apsidal and nodal motion related parameters				
P_{apse} [year]	$4.228^{+0.005}_{-0.005}$	$26.41^{+0.05}_{-0.05}$	$25.43^{+0.42}_{-0.54}$	$265.3^{+4.3}_{-1.3}$
$P_{\mathrm{apse}}^{\mathrm{dyn}}$ [year]	$1.955^{+0.005}_{-0.006}$	$3.20^{+0.01}_{-0.02}$	$12.90^{+0.15}_{-0.21}$	$23.81^{+0.21}_{-0.22}$
$P_{\mathrm{node}}^{\mathrm{dyn}}$ [year]	$3.64^{+0.02}_{-0.01}$		$26.17^{+0.30}_{-0.25}$	
$\Delta\omega_{3\mathrm{b}}$ [arcsec/cycle]	10461^{+31}_{-24}	62095^{+293}_{-212}	$676.7^{+9.2}_{-6.9}$	15107^{+141}_{-130}
$\Delta\omega_{\mathrm{GR}}$ [arcsec/cycle]	$0.61^{+0.02}_{-0.02}$	$0.202^{+0.008}_{-0.007}$	$2.00^{+0.03}_{-0.04}$	$0.276^{+0.006}_{-0.007}$
$\Delta\omega_{\mathrm{tide}}$ [arcsec/cycle]	$0.14^{+0.02}_{-0.02}$	$0.0010^{+0.0002}_{-0.0001}$	$44.1^{+4.7}_{-4.3}$	$0.031^{+0.003}_{-0.003}$

stellar parameters	TIC 283846096			TIC 337993842		
	Aa	Ab	B	Aa	Ab	B
Relative quantities						
fractional radius [R/a]	$0.0441^{+0.0013}_{-0.0011}$	$0.0279^{+0.0010}_{-0.0008}$	$0.0112^{+0.0004}_{-0.0002}$	$0.1214^{+0.0026}_{-0.0027}$	$0.1186^{+0.0025}_{-0.0025}$	$0.0176^{+0.0011}_{-0.0010}$
temperature relative to $(T_{\mathrm{eff}})_{\mathrm{Aa}}$	1	$0.8422^{+0.0153}_{-0.0210}$	$1.3699^{+0.0085}_{-0.0092}$	1	$0.9907^{+0.0067}_{-0.0066}$	$1.3141^{+0.0705}_{-0.0466}$
fractional flux [in TESS-band]	$0.1095^{+0.0053}_{-0.0043}$	$0.0197^{+0.0010}_{-0.0016}$	$0.8311^{+0.0214}_{-0.0428}$	$0.0906^{+0.0029}_{-0.0027}$	$0.0838^{+0.0030}_{-0.0026}$	$0.8010^{+0.0147}_{-0.0315}$
Physical quantities						
M [$M_\odot$]	$0.594^{+0.035}_{-0.031}$	$0.378^{+0.022}_{-0.019}$	$0.856^{+0.050}_{-0.044}$	$1.361^{+0.037}_{-0.045}$	$1.338^{+0.034}_{-0.042}$	$2.282^{+0.133}_{-0.084}$
R [$R_\odot$]	$0.591^{+0.028}_{-0.024}$	$0.374^{+0.021}_{-0.016}$	$0.840^{+0.047}_{-0.027}$	$1.355^{+0.040}_{-0.043}$	$1.324^{+0.039}_{-0.039}$	$2.752^{+0.163}_{-0.147}$
T_{eff} [K]	3947^{+69}_{-72}	3315^{+16}_{-22}	5410^{+60}_{-71}	6649^{+111}_{-99}	6578^{+116}_{-80}	8736^{+544}_{-342}
L_{bol} [$L_\odot$]	$0.076^{+0.014}_{-0.011}$	$0.015^{+0.001}_{-0.001}$	$0.544^{+0.083}_{-0.062}$	$3.23^{+0.34}_{-0.32}$	$2.96^{+0.30}_{-0.25}$	$40.11^{+7.67}_{-4.71}$
M_{bol}	$7.57^{+0.17}_{-0.18}$	$9.31^{+0.10}_{-0.09}$	$5.43^{+0.13}_{-0.15}$	$3.50^{+0.11}_{-0.11}$	$3.59^{+0.10}_{-0.10}$	$0.76^{+0.14}_{-0.19}$
M_V	$8.66^{+0.23}_{-0.21}$	$11.34^{+0.05}_{-0.06}$	$5.57^{+0.15}_{-0.17}$	$3.47^{+0.12}_{-0.11}$	$3.56^{+0.10}_{-0.11}$	$0.76^{+0.11}_{-0.12}$
$\log g$ [dex]	$4.666^{+0.014}_{-0.017}$	$4.867^{+0.017}_{-0.021}$	$4.519^{+0.014}_{-0.022}$	$4.307^{+0.014}_{-0.015}$	$4.320^{+0.014}_{-0.015}$	$3.916^{+0.059}_{-0.055}$

Global system parameters	TIC 283846096	TIC 337993842
log(age) [dex]	$9.860^{+0.130}_{-0.113}$	$8.765^{+0.062}_{-0.102}$
$[M/H]$ [dex]	$-0.052^{+0.111}_{-0.053}$	$0.154^{+0.066}_{-0.121}$
$E(B-V)$ [mag]	$0.158^{+0.021}_{-0.021}$	$0.764^{+0.043}_{-0.038}$
extra light ℓ_4 [in TESS-band]	$0.038^{+0.050}_{-0.023}$	$0.024^{+0.033}_{-0.016}$
$(M_V)_{\mathrm{tot}}$	$5.50^{+0.16}_{-0.17}$	$0.61^{+0.11}_{-0.12}$
distance [pc]	490^{+31}_{-21}	1770^{+70}_{-74}

Table B.4. Orbital and astrophysical parameters of TICs 351404069 and 378270875 from the joint photodynamical light curve, ETV, SED and PARSEC isochrone solution.

	TIC 351404069			TIC 378270875		
orbital elements						
	subsystem					
	Aa–Ab		A–B	Aa–Ab		A–B
t_0 [BJD - 2400000]	59814.0			58683.0		
P [days]	$8.91637^{+0.00024}_{-0.00023}$		$96.2431^{+0.0033}_{-0.0029}$	$2.573263^{+0.000048}_{-0.000042}$		$58.1195^{+0.0018}_{-0.0015}$
a [$R_\odot$]	$23.23^{+0.34}_{-0.40}$		$128.72^{+1.86}_{-2.23}$	$9.25^{+0.24}_{-0.19}$		$85.25^{+2.17}_{-1.86}$
e	$0.03890^{+0.00019}_{-0.00022}$		$0.24879^{+0.00029}_{-0.00028}$	$0.00192^{+0.00026}_{-0.00021}$		$0.3125^{+0.0050}_{-0.0021}$
ω [deg]	$207.93^{+0.24}_{-0.19}$		$183.74^{+0.53}_{-0.54}$	$295.3^{+6.5}_{-6.9}$		$314.21^{+0.51}_{-0.66}$
i [deg]	$87.24^{+0.15}_{-0.14}$		$90.11^{+0.05}_{-0.05}$	$88.93^{+0.10}_{-0.10}$		$89.00^{+0.05}_{-0.05}$
$\mathcal{T}_0^{\mathrm{inf/sup}}$ [BJD - 2400000]	$59823.2857^{+0.0006}_{-0.0006}$		$59815.7901^{+0.0102*}_{-0.0119}$	$58684.2847^{+0.0002}_{-0.0002}$		$58704.2085^{+0.0264}_{-0.0200}$
τ [BJD - 2400000]	$59821.8437^{+0.0061}_{-0.0048}$		$59736.988^{+0.126}_{-0.128}$	$58681.891^{+0.047}_{-0.049}$		$58649.808^{+0.060}_{-0.081}$
Ω [deg]	0.0		$1.30^{+0.22}_{-0.17}$	0.0		$-0.15^{+0.26}_{-0.29}$
i_{mut} [deg]	$3.16^{+0.17}_{-0.19}$			$0.27^{+0.19}_{-0.14}$		
ϖ^{dyn} [deg]	$27.90^{+0.24}_{-0.19}$		$3.74^{+0.53}_{-0.54}$	$115.3^{+6.5}_{-6.9}$		$134.21^{+0.51}_{-0.66}$
i^{dyn} [deg]	$2.46^{+0.13}_{-0.15}$		$0.70^{+0.04}_{-0.04}$	$0.23^{+0.16}_{-0.12}$		$0.05^{+0.03}_{-0.02}$
Ω^{dyn} [deg]	$24.4^{+3.3}_{-2.9}$		$204.4^{+3.3}_{-2.9}$	290^{+101}_{-37}		110^{+101}_{-37}
i_{inv} [deg]	$89.47^{+0.05}_{-0.05}$			$88.98^{+0.04}_{-0.04}$		
Ω_{inv} [deg]	$1.01^{+0.17}_{-0.13}$			$-0.12^{+0.22}_{-0.24}$		
mass ratio [$q = M_{\mathrm{sec}}/M_{\mathrm{pri}}$]	$0.826^{+0.005}_{-0.005}$		$0.460^{+0.002}_{-0.002}$	$0.936^{+0.005}_{-0.005}$		$0.533^{+0.009}_{-0.008}$
K_{pri} [km s^{-1}]	$59.55^{+0.92}_{-1.03}$		$22.03^{+0.33}_{-0.40}$	$87.90^{+2.16}_{-1.61}$		$26.98^{+1.05}_{-0.40}$
K_{sec} [km s^{-1}]	$72.20^{+1.13}_{-1.26}$		$47.84^{+0.71}_{-0.81}$	$93.94^{+2.48}_{-2.04}$		$50.93^{+1.25}_{-0.89}$
Apsidal and nodal motion related parameters						
P_{apse} [year]	$10.92^{+0.03}_{-0.03}$		$38.41^{+0.05}_{-0.05}$	$11.66^{+0.10}_{-0.15}$		$58.67^{+0.27}_{-0.40}$
$P_{\mathrm{apse}}^{\mathrm{dyn}}$ [year]	$4.78^{+0.01}_{-0.01}$		$6.98^{+0.01}_{-0.01}$	$5.32^{+0.04}_{-0.06}$		$8.42^{+0.05}_{-0.08}$
$P_{\mathrm{node}}^{\mathrm{dyn}}$ [year]	$8.53^{+0.02}_{-0.02}$			$9.83^{+0.11}_{-0.07}$		
$\Delta\omega_{3\mathrm{b}}$ [arcsec/cycle]	6608^{+16}_{-16}		48935^{+70}_{-74}	1702^{+20}_{-13}		24498^{+235}_{-140}
$\Delta\omega_{\mathrm{GR}}$ [arcsec/cycle]	$0.753^{+0.022}_{-0.026}$		$0.211^{+0.006}_{-0.007}$	$1.431^{+0.074}_{-0.059}$		$0.264^{+0.014}_{-0.011}$
$\Delta\omega_{\mathrm{tide}}$ [arcsec/cycle]	$3.69^{+0.25}_{-0.23}$		$0.021^{+0.001}_{-0.001}$	$8.35^{+0.53}_{-0.51}$		$0.015^{+0.001}_{-0.001}$
stellar parameters						
	Aa	Ab	B	Aa	Ab	B
Relative quantities						
fractional radius [R/a]	$0.0859^{+0.0012}_{-0.0011}$	$0.0421^{+0.0014}_{-0.0016}$	$0.0079^{+0.0002}_{-0.0003}$	$0.0901^{+0.0012}_{-0.0013}$	$0.0818^{+0.0010}_{-0.0012}$	$0.0104^{+0.0003}_{-0.0003}$
temperature relative to $(T_{\mathrm{eff}})_{\mathrm{Aa}}$	1	$0.9942^{+0.0071}_{-0.0069}$	$1.0045^{+0.0068}_{-0.0067}$	1	$0.9486^{+0.0036}_{-0.0039}$	$1.0242^{+0.0104}_{-0.0109}$
fractional flux [in *TESS*-band]	$0.4718^{+0.0274}_{-0.0260}$	$0.1103^{+0.0034}_{-0.0030}$	$0.1230^{+0.0041}_{-0.0044}$	$0.3263^{+0.0068}_{-0.0062}$	$0.2198^{+0.0051}_{-0.0053}$	$0.4040^{+0.0288}_{-0.0340}$
Physical quantities						
M [$M_\odot$]	$1.157^{+0.052}_{-0.058}$	$0.954^{+0.042}_{-0.048}$	$0.973^{+0.043}_{-0.051}$	$0.827^{+0.066}_{-0.052}$	$0.773^{+0.060}_{-0.046}$	$0.851^{+0.076}_{-0.050}$
R [$R_\odot$]	$1.993^{+0.045}_{-0.051}$	$0.977^{+0.045}_{-0.052}$	$1.018^{+0.042}_{-0.060}$	$0.834^{+0.022}_{-0.020}$	$0.756^{+0.026}_{-0.025}$	$0.884^{+0.031}_{-0.034}$
T_{eff} [K]	5902^{+91}_{-100}	5863^{+75}_{-78}	5929^{+67}_{-79}	5487^{+82}_{-72}	5205^{+82}_{-65}	5621^{+58}_{-51}
L_{bol} [$L_\odot$]	$4.34^{+0.38}_{-0.46}$	$1.02^{+0.14}_{-0.15}$	$1.14^{+0.14}_{-0.18}$	$0.571^{+0.046}_{-0.044}$	$0.379^{+0.031}_{-0.025}$	$0.696^{+0.066}_{-0.055}$
M_{bol}	$3.18^{+0.12}_{-0.09}$	$4.75^{+0.18}_{-0.14}$	$4.62^{+0.19}_{-0.12}$	$5.38^{+0.09}_{-0.08}$	$5.82^{+0.08}_{-0.09}$	$5.16^{+0.09}_{-0.10}$
M_V	$3.22^{+0.14}_{-0.10}$	$4.80^{+0.19}_{-0.15}$	$4.66^{+0.20}_{-0.13}$	$5.50^{+0.10}_{-0.10}$	$6.02^{+0.10}_{-0.09}$	$5.25^{+0.20}_{-0.11}$
$\log g$ [dex]	$3.900^{+0.012}_{-0.012}$	$4.437^{+0.026}_{-0.021}$	$4.410^{+0.029}_{-0.018}$	$4.516^{+0.012}_{-0.017}$	$4.570^{+0.008}_{-0.007}$	$4.477^{+0.021}_{-0.020}$
Global system parameters						
log(age) [dex]		$9.721^{+0.083}_{-0.044}$			$9.972^{+0.084}_{-0.269}$	
$[M/H]$ [dex]		$-0.129^{+0.132}_{-0.073}$			$-0.166^{+0.166}_{-0.149}$	
$E(B-V)$ [mag]		$0.132^{+0.024}_{-0.026}$			$0.402^{+0.018}_{-0.018}$	
extra light ℓ_4 [in *TESS*-band]		$0.294^{+0.028}_{-0.027}$			$0.051^{+0.035}_{-0.030}$	
$(M_V)_{\mathrm{tot}}$		$2.78^{+0.16}_{-0.11}$			$4.35^{+0.08}_{-0.09}$	
distance [pc]		1055^{+33}_{-44}			542^{+18}_{-15}	

Table B.5. Orbital and astrophysical parameters of TICs 403792414 and 403916758 from the joint photodynamical light curve, ETV, SED and PARSEC isochrone solution.

	TIC 403792414		TIC 403916758	
orbital elements				
	subsystem			
	Aa–Ab	A–B	Aa–Ab	A–B
t_0 [BJD - 2400000]	59388.0		58790.5	
P [days]	$4.97416^{+0.00026}_{-0.00027}$	$78.197^{+0.012}_{-0.012}$	$1.1337956^{+0.0000087}_{-0.0000079}$	$71.0600^{+0.0020}_{-0.0018}$
a [R$_\odot$]	$13.83^{+0.26}_{-0.38}$	$100.6^{+2.1}_{-2.7}$	$5.531^{+0.067}_{-0.057}$	$110.07^{+0.77}_{-1.60}$
e	$0.02263^{+0.00081}_{-0.00055}$	$0.3232^{+0.0026}_{-0.0026}$	$0.00075^{+0.00087}_{-0.00035}$	$0.0305^{+0.0067}_{-0.0155}$
ω [deg]	$80.90^{+0.54}_{-0.56}$	$82.364^{+0.058}_{-0.057}$	173^{+69}_{-41}	$270.1^{+1.9}_{-1.4}$
i [deg]	$90.14^{+0.27}_{-0.34}$	$90.01^{+0.07}_{-0.06}$	$86.57^{+1.16}_{-0.57}$	$87.88^{+0.19}_{-0.22}$
$\mathcal{T}_0^{\rm inf/sup}$ [BJD - 2400000]	$59391.3367^{+0.0004}_{-0.0005}$	$59390.340^{+0.016}_{-0.018}*$	$58792.1781^{+0.0002}_{-0.0003}$	$58967.071^{+0.034}_{-0.036}$
τ [BJD - 2400000]	$59388.7175^{+0.0073}_{-0.0076}$	$59389.536^{+0.017}_{-0.017}$	$58791.86^{+0.18}_{-0.18}$	$58897.50^{+1.54}_{-1.36}$
Ω [deg]	0.0	$-0.40^{+0.56}_{-0.63}$	0.0	$3.76^{+1.00}_{-0.69}$
$i_{\rm mut}$ [deg]	$0.60^{+0.50}_{-0.28}$		$4.09^{+0.77}_{-0.76}$	
$\varpi^{\rm dyn}$ [deg]	$260.89^{+0.54}_{-0.56}$	$262.36^{+0.06}_{-0.06}$	359^{+74}_{-37}	$90.1^{+1.9}_{-1.4}$
$i^{\rm dyn}$ [deg]	$0.49^{+0.41}_{-0.23}$	$0.10^{+0.09}_{-0.05}$	$3.78^{+0.72}_{-0.70}$	$0.30^{+0.06}_{-0.06}$
$\Omega^{\rm dyn}$ [deg]	248^{+34}_{-79}	68^{+34}_{-79}	69^{+17}_{-5}	249^{+17}_{-5}
$i_{\rm inv}$ [deg]	$90.04^{+0.06}_{-0.07}$		$87.79^{+0.21}_{-0.25}$	
$\Omega_{\rm inv}$ [deg]	$-0.33^{+0.46}_{-0.52}$		$3.48^{+0.92}_{-0.63}$	
mass ratio [$q = M_{\rm sec}/M_{\rm pri}$]	$0.689^{+0.015}_{-0.016}$	$0.558^{+0.010}_{-0.011}$	$0.982^{+0.022}_{-0.028}$	$0.983^{+0.022}_{-0.021}$
$K_{\rm pri}$ [km s^{-1}]	$57.3^{+1.8}_{-1.6}$	$24.65^{+0.68}_{-0.72}$	$122.1^{+1.9}_{-1.9}$	$38.65^{+0.69}_{-0.48}$
$K_{\rm sec}$ [km s^{-1}]	$83.8^{+1.1}_{-2.5}$	$44.28^{+0.69}_{-1.26}$	$124.6^{+2.3}_{-2.3}$	$39.37^{+0.62}_{-0.68}$
Apsidal and nodal motion related parameters				
$P_{\rm apse}$ [year]	$10.61^{+0.13}_{-0.12}$	$50.14^{+0.19}_{-0.19}$	$17.30^{+0.79}_{-0.95}$	$409.6^{+3.7}_{-2.9}$
$P_{\rm apse}^{\rm dyn}$ [year]	$4.80^{+0.05}_{-0.05}$	$7.46^{+0.06}_{-0.05}$	$10.97^{+0.37}_{-0.32}$	$28.31^{+0.24}_{-0.26}$
$P_{\rm node}^{\rm dyn}$ [year]	$8.759^{+0.073}_{-0.082}$		$30.41^{+0.31}_{-0.30}$	
$\Delta\omega_{\rm 3b}$ [arcsec/cycle]	3677^{+35}_{-39}	37209^{+257}_{-277}	$253.7^{+3.3}_{-2.8}$	8906^{+82}_{-75}
$\Delta\omega_{\rm GR}$ [arcsec/cycle]	$0.857^{+0.033}_{-0.047}$	$0.205^{+0.008}_{-0.011}$	$2.637^{+0.064}_{-0.054}$	$0.266^{+0.004}_{-0.008}$
$\Delta\omega_{\rm tide}$ [arcsec/cycle]	$0.67^{+0.07}_{-0.12}$	$0.0024^{+0.0003}_{-0.0004}$	107^{+15}_{-10}	$0.94^{+0.21}_{-0.14}$

	Aa	Ab	B	Aa	Ab	B
stellar parameters						
Relative quantities						
fractional radius [R/a]	$0.0599^{+0.0019}_{-0.0022}$	$0.0421^{+0.0015}_{-0.0020}$	$0.0076^{+0.0003}_{-0.0003}$	$0.1456^{+0.0039}_{-0.0044}$	$0.1421^{+0.0037}_{-0.0030}$	$0.0631^{+0.0026}_{-0.0021}$
temperature relative to $(T_{\rm eff})_{\rm Aa}$	1	$0.7276^{+0.0151}_{-0.0123}$	$0.9542^{+0.0189}_{-0.0192}$	1	$0.9870^{+0.0155}_{-0.0202}$	$1.0349^{+0.0165}_{-0.0183}$
fractional flux [in *TESS*-band]	$0.5117^{+0.0333}_{-0.0300}$	$0.0678^{+0.0074}_{-0.0050}$	$0.3647^{+0.0335}_{-0.0320}$	$0.0107^{+0.0009}_{-0.0008}$	$0.0097^{+0.0006}_{-0.0008}$	$0.9308^{+0.0290}_{-0.0493}$
Physical quantities						
M [M$_\odot$]	$0.854^{+0.042}_{-0.072}$	$0.584^{+0.040}_{-0.044}$	$0.799^{+0.059}_{-0.061}$	$0.897^{+0.030}_{-0.039}$	$0.873^{+0.032}_{-0.026}$	$1.753^{+0.053}_{-0.068}$
R [R$_\odot$]	$0.835^{+0.026}_{-0.055}$	$0.582^{+0.032}_{-0.041}$	$0.763^{+0.041}_{-0.042}$	$0.807^{+0.028}_{-0.033}$	$0.786^{+0.029}_{-0.023}$	$6.932^{+0.340}_{-0.293}$
$T_{\rm eff}$ [K]	5440^{+157}_{-191}	3945^{+87}_{-84}	5169^{+147}_{-119}	5185^{+110}_{-111}	5115^{+100}_{-114}	5372^{+111}_{-149}
$L_{\rm bol}$ [L$_\odot$]	$0.546^{+0.100}_{-0.114}$	$0.073^{+0.011}_{-0.013}$	$0.373^{+0.077}_{-0.064}$	$0.422^{+0.070}_{-0.065}$	$0.379^{+0.061}_{-0.53}$	$35.6^{+6.6}_{-5.2}$
$M_{\rm bol}$	$5.43^{+0.26}_{-0.18}$	$7.61^{+0.21}_{-0.16}$	$5.84^{+0.20}_{-0.20}$	$5.71^{+0.18}_{-0.17}$	$5.82^{+0.16}_{-0.16}$	$0.89^{+0.17}_{-0.19}$
M_V	$5.56^{+0.31}_{-0.22}$	$8.72^{+0.26}_{-0.23}$	$6.06^{+0.25}_{-0.25}$	$5.92^{+0.23}_{-0.21}$	$6.06^{+0.22}_{-0.20}$	$1.19^{+0.17}_{-0.13}$
$\log g$ [dex]	$4.533^{+0.021}_{-0.024}$	$4.673^{+0.029}_{-0.016}$	$4.576^{+0.018}_{-0.018}$	$4.576^{+0.017}_{-0.016}$	$4.587^{+0.013}_{-0.015}$	$2.998^{+0.025}_{-0.034}$

	TIC 403792414	TIC 403916758
Global system parameters		
log(age) [dex]	$9.802^{+0.182}_{-0.113}$	$9.275^{+0.033}_{-0.036}$
$[M/H]$ [dex]	$-0.072^{+0.122}_{-0.169}$	$0.174^{+0.023}_{-0.067}$
$E(B-V)$ [mag]	$0.334^{+0.048}_{-0.060}$	$0.977^{+0.029}_{-0.023}$
extra light ℓ_4 [in *TESS*-band]	$0.054^{+0.020}_{-0.022}$	$0.049^{+0.050}_{-0.029}$
$(M_V)_{\rm tot}$	$4.96^{+0.29}_{-0.17}$	$1.17^{+0.17}_{-0.13}$
distance [pc]	629^{+26}_{-48}	740^{+41}_{-34}

Table B.6. Orbital and astrophysical parameters of TICs 405789362 and 461500036 from the joint photodynamical light curve, ETV, SED and PARSEC isochrone solution.

	TIC 405789362			TIC 461500036		
	orbital elements					
	subsystem					
	Aa–Ab		A–B	Aa–Ab		A–B
t_0 [BJD - 2400000]		58738.0			58790.5	
P [days]	$4.56619^{+0.00025}_{-0.00021}$		$46.8103^{+0.0032}_{-0.0025}$	$2.469953^{+0.000019}_{-0.000022}$		$54.56390^{+0.00070}_{-0.00068}$
a [$R_\odot$]	$16.34^{+0.35}_{-0.23}$		$84.0^{+1.8}_{-1.2}$	$10.59^{+0.10}_{-0.30}$		$91.21^{+0.85}_{-2.53}$
e	$0.00719^{+0.00022}_{-0.00027}$		$0.1623^{+0.0029}_{-0.0021}$	$0.00129^{+0.00014}_{-0.00012}$		$0.0320^{+0.0011}_{-0.0009}$
ω [deg]	$329.8^{+2.3}_{-2.7}$		$351.24^{+0.78}_{-0.84}$	139^{+14}_{-15}		$188.00^{+0.31}_{-0.26}$
i [deg]	$89.60^{+0.57}_{-0.56}$		$89.72^{+0.13}_{-0.10}$	$88.71^{+0.11}_{-0.11}$		$89.70^{+0.07}_{-0.07}$
$\mathcal{T}_0^{\mathrm{inf/sup}}$ [BJD - 2400000]	$58741.1492^{+0.0004}_{-0.0005}$		$58753.797^{+0.023}_{-0.035}$	$58791.3937^{+0.0002}_{-0.0002}$		$58842.8333^{+0.0081}_{-0.0086}$
τ [BJD - 2400000]	$58737.333^{+0.029}_{-0.034}$		$58715.211^{+0.084}_{-0.102}$	$58790.49^{+0.10}_{-0.11}$		$58835.647^{+0.051}_{-0.042}$
Ω [deg]	0.0		$-1.26^{+0.55}_{-0.40}$	0.0		$0.92^{+0.15}_{-0.20}$
i_{mut} [deg]		$1.36^{+0.43}_{-0.37}$			$1.36^{+0.16}_{-0.17}$	
ϖ^{dyn} [deg]	$149.8^{+2.3}_{-2.7}$		$171.23^{+0.78}_{-0.84}$	319^{+14}_{-15}		$8.00^{+0.31}_{-0.26}$
i^{dyn} [deg]	$0.95^{+0.30}_{-0.26}$		$0.41^{+0.13}_{-0.11}$	$1.02^{+0.12}_{-0.13}$		$0.34^{+0.04}_{-0.04}$
Ω^{dyn} [deg]	276^{+28}_{-28}		96^{+28}_{-28}	$42.7^{+6.3}_{-7.1}$		$222.7^{+6.3}_{-7.1}$
i_{inv} [deg]		$89.72^{+0.14}_{-0.22}$			$89.45^{+0.05}_{-0.05}$	
Ω_{inv} [deg]		$-0.88^{+0.39}_{-0.28}$			$0.69^{+0.11}_{-0.15}$	
mass ratio [$q = M_{\mathrm{sec}}/M_{\mathrm{pri}}$]	$0.837^{+0.006}_{-0.006}$		$0.293^{+0.007}_{-0.007}$	$0.962^{+0.008}_{-0.007}$		$0.309^{+0.006}_{-0.005}$
K_{pri} [km s^{-1}]	$82.5^{+1.8}_{-1.4}$		$20.90^{+0.61}_{-0.58}$	$106.1^{+1.2}_{-2.4}$		$20.97^{+0.33}_{-0.29}$
K_{sec} [km s^{-1}]	$98.7^{+1.8}_{-1.6}$		$71.25^{+1.36}_{-1.09}$	$110.9^{+1.1}_{-4.0}$		$68.28^{+0.79}_{-2.20}$
	Apsidal and nodal motion related parameters					
P_{apse} [year]	$7.34^{+0.14}_{-0.14}$		$17.28^{+0.07}_{-0.07}$	$13.12^{+0.15}_{-0.16}$		$47.64^{+0.16}_{-0.15}$
$P_{\mathrm{apse}}^{\mathrm{dyn}}$ [year]	$3.04^{+0.05}_{-0.05}$		$3.99^{+0.04}_{-0.04}$	$6.24^{+0.06}_{-0.07}$		$9.51^{+0.06}_{-0.07}$
$P_{\mathrm{node}}^{\mathrm{dyn}}$ [year]		$5.20^{+0.06}_{-0.07}$			$11.89^{+0.12}_{-0.11}$	
$\Delta\omega_{\mathrm{3b}}$ [arcsec/cycle]	5296^{+82}_{-80}		$^{+}_{-}$	1289^{+16}_{-14}		8906^{+82}_{-75}
$\Delta\omega_{\mathrm{GR}}$ [arcsec/cycle]	$1.419^{+0.061}_{-0.039}$		$0.366^{+0.016}_{-0.010}$	$2.038^{+0.040}_{-0.116}$		$0.345^{+0.006}_{-0.019}$
$\Delta\omega_{\mathrm{tide}}$ [arcsec/cycle]	$29.1^{+3.3}_{-2.7}$		$0.154^{+0.017}_{-0.014}$	$113.7^{+2.1}_{-2.1}$		$0.228^{+0.004}_{-0.004}$
	stellar parameters					
	Aa	Ab	B	Aa	Ab	B
	Relative quantities					
fractional radius [R/a]	$0.1269^{+0.0025}_{-0.0024}$	$0.0841^{+0.0039}_{-0.0032}$	$0.00881^{+0.00036}_{-0.00032}$	$0.1520^{+0.0010}_{-0.0012}$	$0.1372^{+0.0016}_{-0.0014}$	$0.00794^{+0.00017}_{-0.00014}$
temperature relative to $(T_{\mathrm{eff}})_{\mathrm{Aa}}$	1	$0.9776^{+0.0104}_{-0.0137}$	$0.7522^{+0.0137}_{-0.0134}$	1	$0.9942^{+0.0026}_{-0.0027}$	$0.7624^{+0.0085}_{-0.0099}$
fractional flux [in *TESS*-band]	$0.6505^{+0.0331}_{-0.0286}$	$0.2667^{+0.0060}_{-0.0056}$	$0.0289^{+0.0041}_{-0.0038}$	$0.5326^{+0.0080}_{-0.0098}$	$0.4262^{+0.0065}_{-0.0052}$	$0.0380^{+0.0036}_{-0.0034}$
fractional flux [in Sloan r'-band]	$0.6604^{0.0231}_{-0.0227}$	$0.2693^{0.0084}_{-0.0094}$	$0.0254^{+0.0042}_{-0.0039}$	$0.5107^{+0.0154}_{-0.0135}$	$0.4078^{+0.0176}_{-0.0116}$	$0.0319^{+0.0035}_{-0.0032}$
	Physical Quantities					
M [$M_\odot$]	$1.529^{+0.094}_{-0.068}$	$1.276^{+0.086}_{-0.054}$	$0.824^{+0.051}_{-0.046}$	$1.334^{+0.039}_{-0.120}$	$1.277^{+0.039}_{-0.100}$	$0.802^{+0.028}_{-0.056}$
R [$R_\odot$]	$2.074^{+0.072}_{-0.060}$	$1.373^{+0.094}_{-0.069}$	$0.740^{+0.042}_{-0.037}$	$1.609^{+0.016}_{-0.044}$	$1.453^{+0.028}_{-0.056}$	$0.724^{+0.022}_{-0.035}$
T_{eff} [K]	6292^{+235}_{-103}	6151^{+134}_{-51}	4755^{+177}_{-138}	6148^{+75}_{-39}	6114^{+64}_{-37}	4693^{+79}_{-80}
L_{bol} [$L_\odot$]	$5.99^{+0.25}_{-0.55}$	$2.40^{+0.58}_{-0.26}$	$0.251^{+0.074}_{-0.048}$	$3.30^{+0.20}_{-0.20}$	$2.63^{+0.20}_{-0.22}$	$0.227^{+0.032}_{-0.031}$
M_{bol}	$2.83^{+0.11}_{-0.21}$	$3.82^{+0.12}_{-0.24}$	$6.27^{+0.23}_{-0.28}$	$3.47^{+0.07}_{-0.06}$	$3.72^{+0.09}_{-0.08}$	$6.38^{+0.16}_{-0.14}$
M_V	$2.79^{+0.12}_{-0.23}$	$3.80^{+0.13}_{-0.26}$	$6.71^{+0.33}_{-0.38}$	$3.46^{+0.08}_{-0.08}$	$3.71^{+0.11}_{-0.09}$	$6.86^{+0.21}_{-0.19}$
$\log g$ [dex]	$3.988^{+0.014}_{-0.014}$	$4.267^{+0.026}_{-0.030}$	$4.614^{+0.019}_{-0.022}$	$4.148^{+0.009}_{-0.019}$	$4.216^{+0.005}_{-0.005}$	$4.621^{+0.010}_{-0.011}$
	Global system parameters					
log(age) [dex]		$9.331^{+0.078}_{-0.170}$			$9.451^{+0.168}_{-0.087}$	
$[M/H]$ [dex]		$0.356^{+0.123}_{-0.116}$			$0.332^{+0.104}_{-0.230}$	
$E(B-V)$ [mag]		$0.573^{+0.052}_{-0.028}$			$0.294^{+0.021}_{-0.013}$	
extra light ℓ_4 [in *TESS*-band]		$0.0539^{+0.0282}_{-0.355}$			$0.0025^{+0.0034}_{-0.0018}$	
extra light ℓ_4 [in Sloan r'-band]		$0.0437^{+0.0244}_{-0.0237}$			$0.050^{+0.022}_{-0.034}$	
$(M_V)_{\mathrm{tot}}$		$2.42^{+0.12}_{-0.24}$			$2.80^{+0.09}_{-0.08}$	
distance [pc]		2107^{+112}_{-86}			1599^{+27}_{-63}	

Appendix C: Light curve sections around the third-body eclipses

In this appendix we plot characteristic light curve sections of nine of the ten investigated systems.

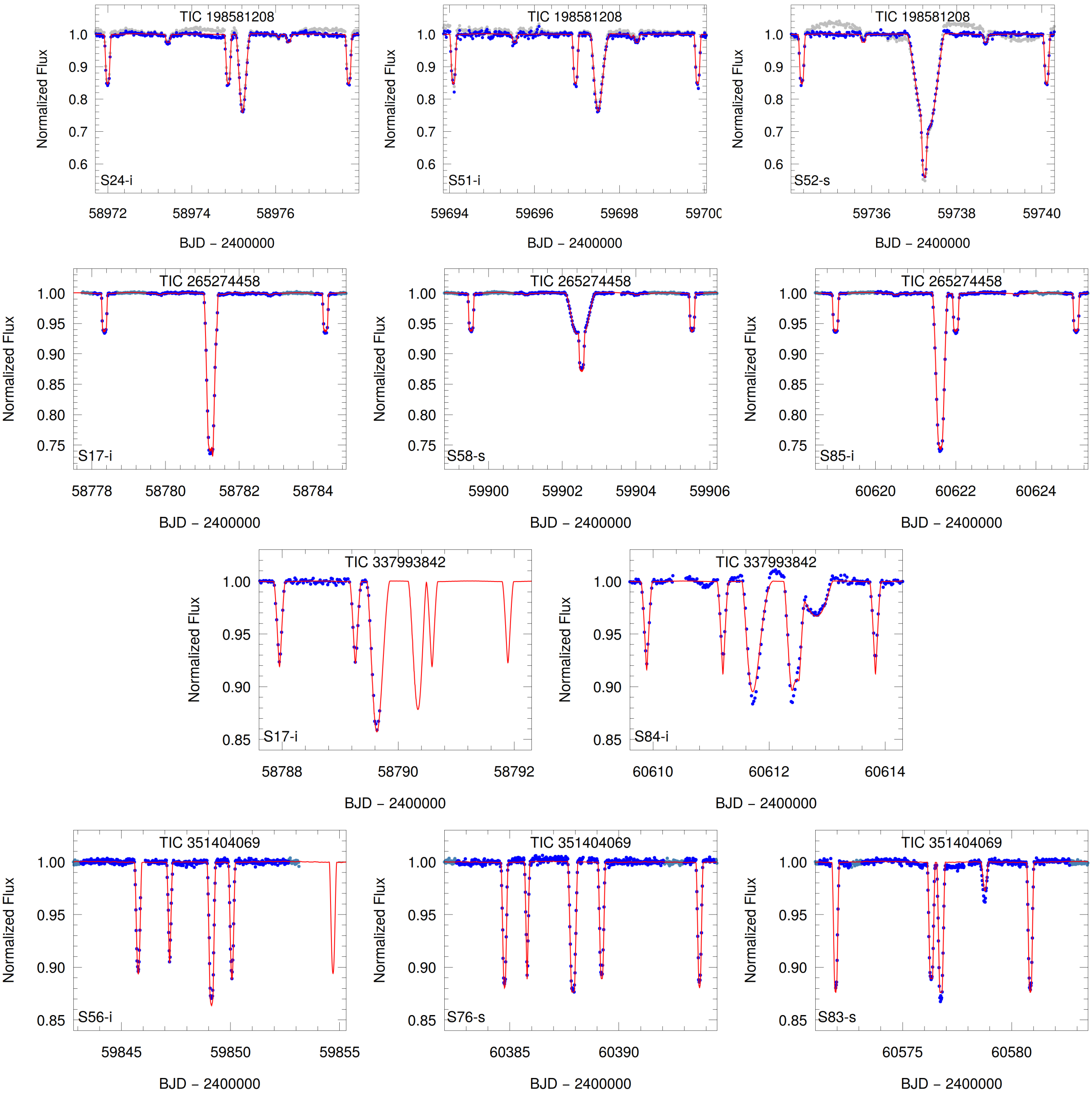

Fig. C.1. Light curves (blue points) and model fits (smooth red curves) near the third-body eclipses of four targets. *From top to bottom panels:* 198581208, 265274458, 337993842, 351404069. The grey points represent original, unsmoothed, but 1800-sec-binned TESS light curves. Dark/pale blue points are for those light curve sections which were used/not-used for the photodynamical solution, after the removal of the likely effects of stellar activity. The sector numbers are indicated in the lower left corner of each panel. Letters 'i' or 's' after the sector numbers refer to the inferior or superior conjunction of the third star, respectively.

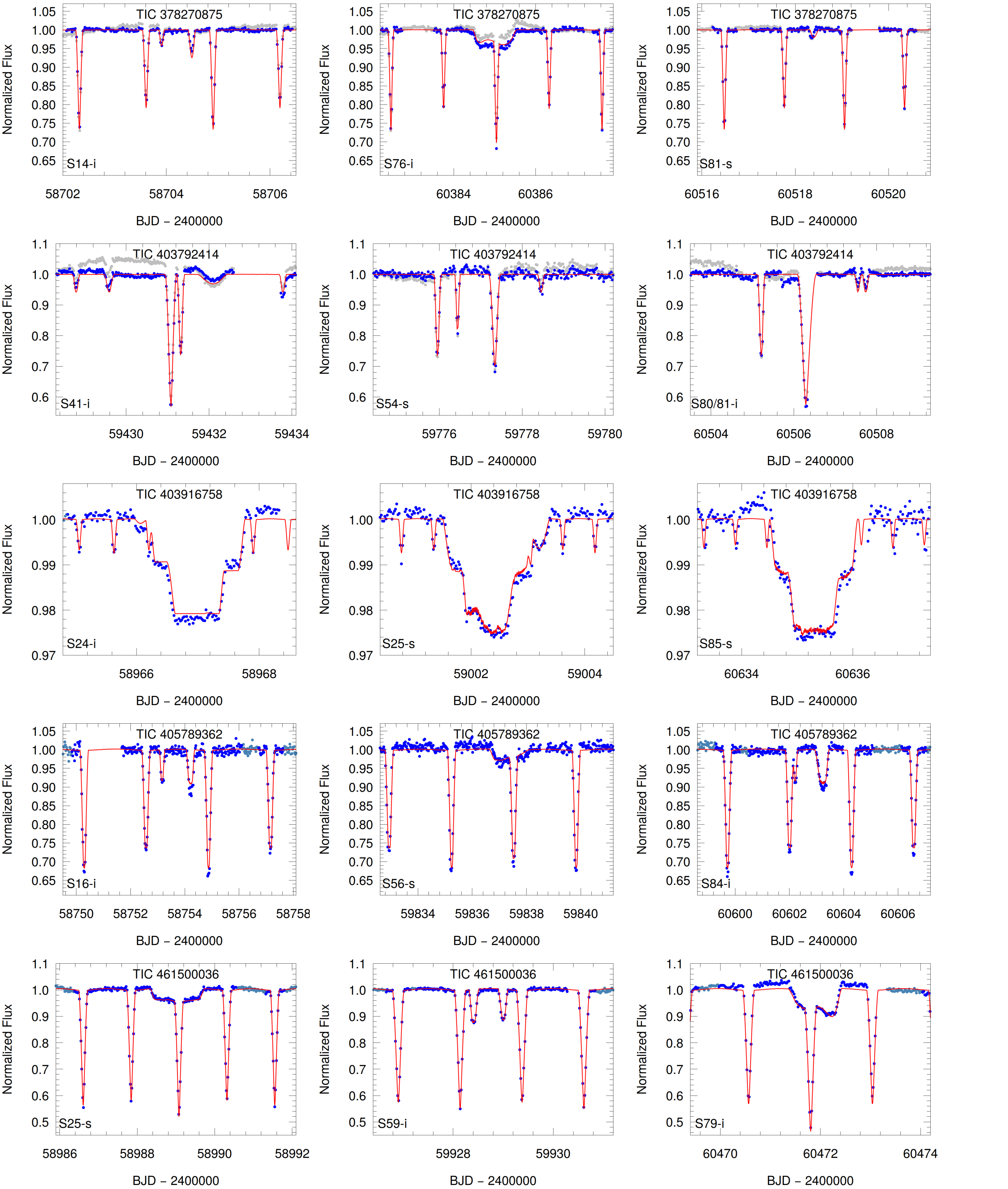

Fig. C.2. Light curves (blue points) and model fits (smooth red curves) near to the third-body eclipses of the second five targets. *From top to bottom panels:* TICs 378270875, 403792414, 403916758, 405789362, 461500036. See Fig. C.1 for details.

Appendix D: Eclipse Timing Variations curves

In this appendix we plot the ETV curves of nine of the ten investigated triple systems.

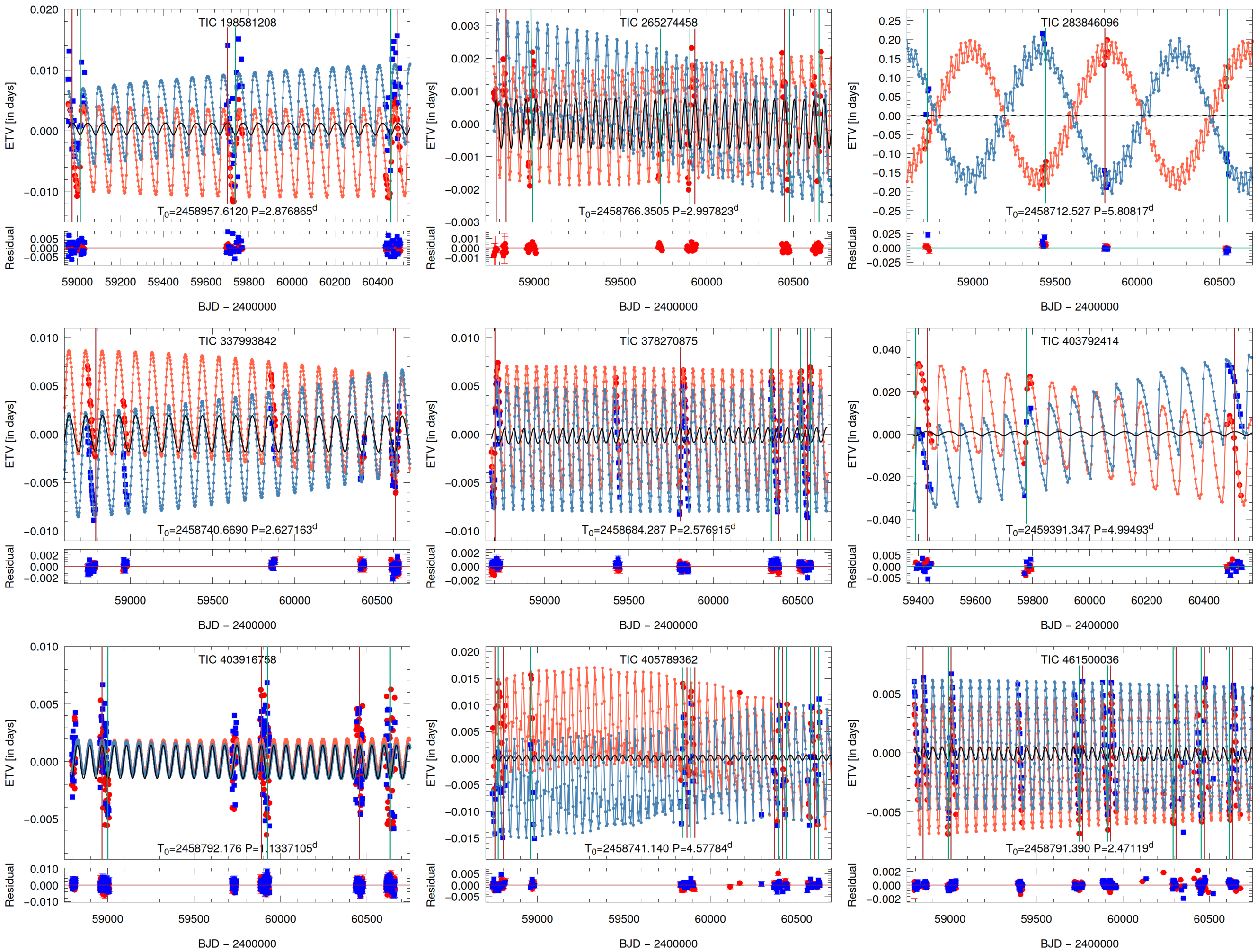

Fig. D.1. Primary and secondary ETV curves (red and blue circles, respectively) formed from the TESS observations with the best-fit photodynamical solution for nine targets. The horizontally centred black curve represents the pure LTTE contribution. Vertical lines mark the times of the observed outer eclipses (green – the binary occulting the tertiary star and, brown – vica versa).

Appendix E: Dynamics of TIC 403792414

In this appendix we plot some auxiliary figures about the irregular AM of TIC 403792414. This effect is discussed in Sect. 6.2.7.

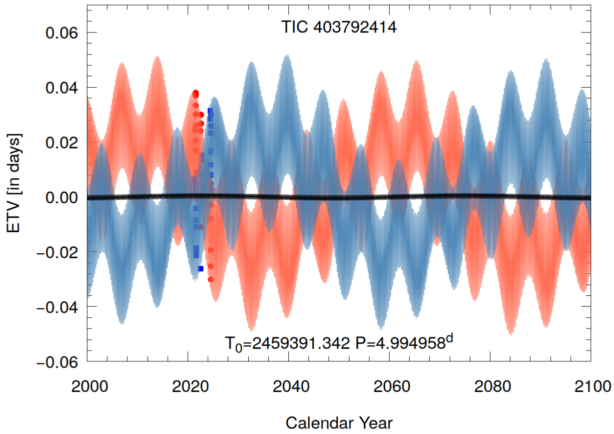

Fig. E.1. Numerically generated ETV curves for TIC 403792414 spanning the current century. The red and blue curves represent the numerically calculated ETV curves. The ETV points derived from the TESS eclipse observations are plotted with red circles and blue squares. The black curve around the zero ETV level indicates the pure LTTE contribution. The hugely uneven nature of the apsidal motion is clearly visible. See the text for further details.

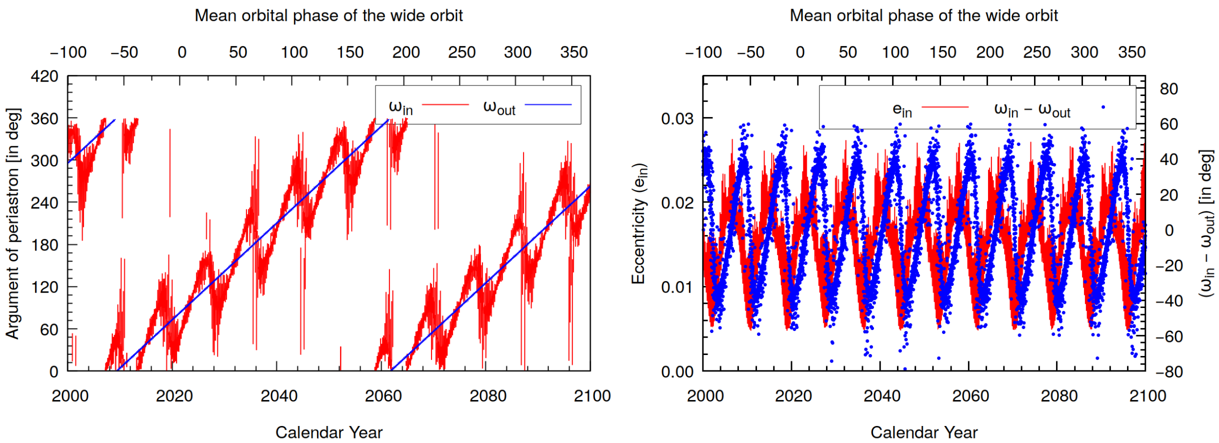

Fig. E.2. The evolution of some of the orbital elements of TIC 403792414 over the current century. *Left panel:* The variations of the observable arguments of periastrons of the inner and the outer orbits (ω_{in} – red; ω_{out} – blue, respectively). As one can see nicely, the major axis of the inner ellipse librates around the direction of the rotating major axis of the outer orbit. *Right panel:* The cyclic variations of the inner eccentricity (red) and the difference of the inner and outer arguments of pericenters (blue). See the text for further details.

Appendix F: Eclipse times of the inner EBs of the ten triples

In this appendix we tabulate the times of the individual primary and secondary eclipses of the inner EBs of the triples considered in this study. These naturally include mostly eclipses from *TESS*, plus a few that were observed from the ground (Tables F.1–F.10). In the final, A&A version, we present only the list of times of minima for TIC 198581208. The other nine tables, together with this sample table, are available at the CDS, in machine readable form. Here, in the arXiv version, however, all the ten tables are published.

Table F.1. Times of minima of TIC 198581208

BJD −2 400 000	Cycle no.	std. dev. (*d*)	BJD −2 400 000	Cycle no.	std. dev. (*d*)	BJD −2 400 000	Cycle no.	std. dev. (*d*)	BJD −2 400 000	Cycle no.	std. dev. (*d*)
58956.18207	-0.5	0.00296	59012.26646	19.0	0.00026	59728.60025	268.0	0.00017	60457.89061	521.5	0.00137
58957.61645	0.0	0.00027	59016.58859	20.5	0.00230	59730.04626	268.5	0.00135	60462.20733	523.0	0.00015
58959.05198	0.5	0.00211	59018.02947	21.0	0.00023	59732.91804	269.5	0.00112	60463.65632	523.5	0.00060
58960.49317	1.0	0.00031	59019.47592	21.5	0.00108	59734.35654	270.0	0.00034	60465.08735	524.0	0.00012
58961.94039	1.5	0.09870	59020.90715	22.0	0.00028	59740.11718	272.0	0.00043	60466.53950	524.5	0.00089
58963.37010	2.0	0.00048	59023.78392	23.0	0.00031	59741.56735	272.5	0.00106	60467.96765	525.0	0.00010
58964.81266	2.5	0.00145	59025.22410	23.5	0.00097	59742.99488	273.0	0.00019	60469.41809	525.5	0.00075
58966.24601	3.0	0.00033	59026.66007	24.0	0.00033	59744.44178	273.5	0.00128	60470.84533	526.0	0.00015
58967.68449	3.5	0.00175	59028.09927	24.5	0.00136	59745.87509	274.0	0.00028	60472.28946	526.5	0.00103
58970.55895	4.5	0.00592	59029.53776	25.0	0.00071	59747.30385	274.5	0.00783	60473.72383	527.0	0.00014
58971.99729	5.0	0.00041	59030.97662	25.5	0.00377	59748.75260	275.0	0.00016	60475.17296	527.5	0.00090
58973.43174	5.5	0.00221	59032.41379	26.0	0.00072	59750.20342	275.5	0.00093	60476.60225	528.0	0.00014
58976.31281	6.5	0.00196	59033.85857	26.5	0.00340	59751.63191	276.0	0.00016	60478.04116	528.5	0.00082
58977.74723	7.0	0.00058	59694.09049	256.0	0.00047	59753.07267	276.5	0.00078	60479.47831	529.0	0.00012
58979.19340	7.5	0.00212	59695.53211	256.5	0.08725	59754.50694	277.0	0.00019	60480.91934	529.5	0.00155
58980.62419	8.0	0.00068	59696.96759	257.0	0.00023	59764.58442	280.5	0.00141	60482.35428	530.0	0.00015
58982.06356	8.5	0.00172	59699.84349	258.0	0.00017	59766.01130	281.0	0.00042	60483.80173	530.5	0.00071
58984.94391	9.5	0.00304	59701.29567	258.5	0.00066	59767.45685	281.5	0.00134	60485.23157	531.0	0.00013
58986.37457	10.0	0.00029	59702.71954	259.0	0.00021	59768.88752	282.0	0.00021	60488.10621	532.0	0.00010
58987.81495	10.5	0.01842	59704.16330	259.5	0.00077	60434.88656	513.5	0.00066	60489.55828	532.5	0.00066
58989.25017	11.0	0.00138	59708.46988	261.0	0.00021	60436.31327	514.0	0.00012	60490.98283	533.0	0.00012
58992.12627	12.0	0.00153	59709.91422	261.5	0.00115	60439.18952	515.0	0.00009	60492.41824	533.5	0.00073
58993.56967	12.5	0.00164	59711.34453	262.0	0.00034	60440.63982	515.5	0.00102	60493.85830	534.0	0.00055
58995.00205	13.0	0.00085	59712.78723	262.5	0.00099	60442.06558	516.0	0.00014	60495.30100	534.5	0.00078
58997.87740	14.0	0.00020	59714.21995	263.0	0.00017	60443.50953	516.5	0.00107	60496.73403	535.0	0.00010
58999.32373	14.5	0.00102	59715.66605	263.5	0.00105	60444.94033	517.0	0.00017	60498.18087	535.5	0.00070
59000.75499	15.0	0.00057	59717.09550	264.0	0.00022	60446.38870	517.5	0.00084	60499.60903	536.0	0.00011
59003.63316	16.0	0.00036	59719.97248	265.0	0.00048	60447.81835	518.0	0.00012	60501.06038	536.5	0.00062
59005.07827	16.5	0.01652	59722.84688	266.0	0.00038	60449.27196	518.5	0.00092	60502.48586	537.0	0.00016
59006.50930	17.0	0.00032	59724.30188	266.5	0.00199	60453.57077	520.0	0.00010	60503.93412	537.5	0.00133
59007.95503	17.5	0.00086	59725.72336	267.0	0.00023	60455.02008	520.5	0.00071	60505.35892	538.0	0.00014
59010.83469	18.5	0.10628	59727.16805	267.5	0.00144	60456.44837	521.0	0.00014			

Notes. Integer and half-integer cycle numbers (here and the following tables) denote primary and secondary eclipses, respectively.

Table F.2. Times of minima of TIC 265274458

BJD −2 400 000	Cycle no.	std. dev. (*d*)	BJD −2 400 000	Cycle no.	std. dev. (*d*)	BJD −2 400 000	Cycle no.	std. dev. (*d*)	BJD −2 400 000	Cycle no.	std. dev. (*d*)
58766.35145	0.0	0.00015	58979.19474	71.0	0.00007	59896.52796	377.0	0.00006	60463.11771	566.0	0.00008
58769.34910	1.0	0.00118	58985.19242	73.0	0.00010	59899.52642	378.0	0.00008	60466.11444	567.0	0.00007
58772.34703	2.0	0.00042	58988.19042	74.0	0.00007	59905.52382	380.0	0.00005	60469.11194	568.0	0.00011
58775.34469	3.0	0.00164	58991.18941	75.0	0.00008	59908.52218	381.0	0.00007	60472.11061	569.0	0.00006
58778.34285	4.0	0.00052	58994.18680	76.0	0.00006	59911.52121	382.0	0.00012	60475.10866	570.0	0.00009
58787.33588	7.0	0.00030	58997.18479	77.0	0.00007	59914.51848	383.0	0.00007	60478.10704	571.0	0.00009
58817.31450	17.0	0.00024	59000.18223	78.0	0.00008	59917.51588	384.0	0.00008	60613.01066	616.0	0.00007
58820.31329	18.0	0.00008	59003.17951	79.0	0.00010	59920.51406	385.0	0.00009	60616.00847	617.0	0.00006
58823.31003	19.0	0.00023	59006.17718	80.0	0.00006	59926.50911	387.0	0.00007	60619.00629	618.0	0.00007
58826.30817	20.0	0.00061	59009.17460	81.0	0.00007	59929.50667	388.0	0.00008	60622.00437	619.0	0.00063
58829.30601	21.0	0.00158	59719.65654	318.0	0.00011	59932.50474	389.0	0.00006	60625.00169	620.0	0.00009
58832.30413	22.0	0.00078	59722.65447	319.0	0.00007	59935.50279	390.0	0.00007	60627.99892	621.0	0.00008
58835.30145	23.0	0.00051	59725.65292	320.0	0.00009	60436.14008	557.0	0.00007	60630.99698	622.0	0.00008
58838.29883	24.0	0.00155	59728.65126	321.0	0.00007	60439.13690	558.0	0.00008	60633.99379	623.0	0.00013
58958.21192	64.0	0.00007	59734.64830	323.0	0.00010	60442.13437	559.0	0.00008	60636.99147	624.0	0.00005
58961.20942	65.0	0.00008	59737.64641	324.0	0.00007	60445.13268	560.0	0.00007	60639.98812	625.0	0.00012
58964.20688	66.0	0.00009	59740.64444	325.0	0.00006	60448.13002	561.0	0.00008	60645.98485	627.0	0.00004
58967.20336	67.0	0.00009	59884.53823	373.0	0.00008	60451.12828	562.0	0.00006	60648.98250	628.0	0.00007
58970.20128	68.0	0.00008	59887.53568	374.0	0.00007	60454.12605	563.0	0.00006	60651.98147	629.0	0.00006
58973.19866	69.0	0.00008	59890.53248	375.0	0.00007	60457.12327	564.0	0.00010	60654.97984	630.0	0.00013
58976.19622	70.0	0.00007	59893.52993	376.0	0.00006	60460.12092	565.0	0.00007	60660.97683	632.0	0.00007

Table F.3. Times of minima of TIC 283846096

BJD −2 400 000	Cycle no.	std. dev. (*d*)	BJD −2 400 000	Cycle no.	std. dev. (*d*)	BJD −2 400 000	Cycle no.	std. dev. (*d*)	BJD −2 400 000	Cycle no.	std. dev. (*d*)
58712.43950	0.0	0.00224	59424.24473	122.5	0.00626	59801.41518	187.5	0.00226	60536.39001	314.0	0.00061
58715.43348	0.5	0.05156	59426.74948	123.0	0.00123	59804.61672	188.0	0.00116	60539.08722	314.5	0.00155
58718.26642	1.0	0.00390	59430.04019	123.5	0.00295	59807.21333	188.5	0.00471	60542.17732	315.0	0.00066
58727.11261	2.5	0.00694	59432.57505	124.0	0.00116	59812.98631	189.5	0.00161	60544.90293	315.5	0.00144
58729.93548	3.0	0.00296	59435.83245	124.5	0.10680	59816.27810	190.0	0.00137	60550.69154	316.5	0.00164
58732.92584	3.5	0.02686	59438.41518	125.0	0.00137	59818.80318	190.5	0.00361	60553.84582	317.0	0.00061
58735.72082	4.0	0.16640	59444.23570	126.0	0.00163	59822.05533	191.0	0.00194	60556.46774	317.5	0.00154
59420.97900	122.0	0.00231	59798.78826	187.0	0.00099						

Table F.4. Times of minima of TIC 337993842

BJD −2 400 000	Cycle no.	std. dev. (*d*)	BJD −2 400 000	Cycle no.	std. dev. (*d*)	BJD −2 400 000	Cycle no.	std. dev. (*d*)	BJD −2 400 000	Cycle no.	std. dev. (*d*)
58739.35602	-0.5	0.00041	58784.00912	16.5	0.00034	59870.35209	430.0	0.00025	60595.44314	706.0	0.00035
58740.67607	0.0	0.00036	58785.32858	17.0	0.00034	59871.66113	430.5	0.00028	60596.75439	706.5	0.00036
58741.98179	0.5	0.00038	58786.63613	17.5	0.00039	59872.97875	431.0	0.00025	60598.06902	707.0	0.00031
58743.30286	1.0	0.00039	58787.95562	18.0	0.00038	59874.28862	431.5	0.00033	60599.38213	707.5	0.00031
58744.60963	1.5	0.00045	58789.26379	18.5	0.00053	59875.60508	432.0	0.00026	60600.69647	708.0	0.00032
58745.92898	2.0	0.00043	58956.09981	82.0	0.00058	59876.91544	432.5	0.00030	60602.01027	708.5	0.00034
58747.23483	2.5	0.00039	58957.40760	82.5	0.00068	59878.23202	433.0	0.00031	60603.32255	709.0	0.00030
58748.55568	3.0	0.00052	58958.72686	83.0	0.00056	59879.54166	433.5	0.00030	60604.63640	709.5	0.00032
58749.86242	3.5	0.00041	58960.03512	83.5	0.00062	59880.85859	434.0	0.00027	60605.95003	710.0	0.00031
58752.49031	4.5	0.00040	58961.35364	84.0	0.00053	60395.77941	630.0	0.00028	60607.26458	710.5	0.00034
58753.80812	5.0	0.00041	58962.66069	84.5	0.00051	60397.09066	630.5	0.00026	60608.57692	711.0	0.00032
58755.11449	5.5	0.00043	58963.97953	85.0	0.00059	60398.40604	631.0	0.00026	60609.89003	711.5	0.00034
58756.43542	6.0	0.00053	58965.28713	85.5	0.00050	60399.71776	631.5	0.00030	60611.20298	712.0	0.00045
58757.74111	6.5	0.00050	58966.60628	86.0	0.00052	60401.03152	632.0	0.00026	60613.83023	713.0	0.00051
58759.06210	7.0	0.00037	58967.91271	86.5	0.00052	60403.66027	633.0	0.00031	60615.14629	713.5	0.00045
58760.36818	7.5	0.00039	58970.54056	87.5	0.00059	60404.97224	633.5	0.00026	60616.46038	714.0	0.00056
58761.68761	8.0	0.00050	58974.48655	89.0	0.00050	60406.28647	634.0	0.00029	60617.77462	714.5	0.00049
58762.99459	8.5	0.00054	58975.79375	89.5	0.00059	60418.11054	638.5	0.00025	60619.08674	715.0	0.00041
58765.62121	9.5	0.00036	58977.11264	90.0	0.00071	60419.42378	639.0	0.00027	60620.40181	715.5	0.00039
58766.94214	10.0	0.00039	58978.42073	90.5	0.00050	60420.73890	639.5	0.00027	60621.71535	716.0	0.00044
58768.24796	10.5	0.00037	58979.73955	91.0	0.00050	60422.05310	640.0	0.00025	60623.03173	716.5	0.00042
58769.56815	11.0	0.00038	58981.04716	91.5	0.00053	60423.36641	640.5	0.00024	60624.34209	717.0	0.00046
58770.87464	11.5	0.00034	59854.59211	424.0	0.00028	60584.93790	702.0	0.00032	60625.65742	717.5	0.00050
58772.19468	12.0	0.00038	59855.90233	424.5	0.00026	60586.25020	702.5	0.00031	60626.97071	718.0	0.00057
58773.50137	12.5	0.00036	59857.21946	425.0	0.00030	60587.56306	703.0	0.00028	60628.28522	718.5	0.00048
58774.82082	13.0	0.00049	59858.52951	425.5	0.00028	60588.87648	703.5	0.00024	60629.60082	719.0	0.00046
58776.12786	13.5	0.00050	59859.84603	426.0	0.00027	60590.18929	704.0	0.00031	60630.91386	719.5	0.00044
58778.75396	14.5	0.00037	59861.15517	426.5	0.00026	60591.50333	704.5	0.00035	60632.22668	720.0	0.00036
58780.07453	15.0	0.00036	59862.47257	427.0	0.00025	60592.81650	705.0	0.00029	60633.54286	720.5	0.00052
58781.38181	15.5	0.00039	59867.72469	429.0	0.00029	60594.12944	705.5	0.00035	60634.85573	721.0	0.00040
58782.70227	16.0	0.00033	59869.03596	429.5	0.00029						

Table F.5. Times of minima of TIC 351404069

BJD −2 400 000	Cycle no.	std. dev. (*d*)	BJD −2 400 000	Cycle no.	std. dev. (*d*)	BJD −2 400 000	Cycle no.	std. dev. (*d*)	BJD −2 400 000	Cycle no.	std. dev. (*d*)
58713.90919	-0.5	0.00051	59818.99070	123.5	0.00051	60349.16412	183.0	0.00039	60393.69644	188.0	0.00035
58718.45552	0.0	0.00045	59823.27403	124.0	0.00041	60353.62223	183.5	0.00069	60536.35144	204.0	0.00026
58722.81104	0.5	0.00095	59827.94418	124.5	0.00038	60358.05710	184.0	0.00043	60540.71828	204.5	0.00035
58727.35608	1.0	0.00051	59832.17404	125.0	0.00040	60362.51292	184.5	0.00042	60545.24445	205.0	0.00034
58731.70573	1.5	0.00078	59836.84659	125.5	0.00037	60366.95099	185.0	0.00038	60549.61684	205.5	0.00033
58736.25469	2.0	0.00057	59841.11189	126.0	0.00040	60371.41166	185.5	0.00050	60554.13773	206.0	0.00029
58740.59707	2.5	0.00049	59845.77213	126.5	0.00045	60375.84931	186.0	0.00039	60558.51710	206.5	0.00036
58745.15324	3.0	0.00050	59850.06540	127.0	0.00036	60380.30850	186.5	0.00045	60563.03258	207.0	0.00033
58754.05127	4.0	0.00044	60340.26817	182.0	0.00029	60384.75992	187.0	0.00039	60567.41565	207.5	0.00039
58762.95196	5.0	0.00069	60344.71478	182.5	0.00051	60389.21318	187.5	0.00037	60580.85536	209.0	0.00036
59801.18277	121.5	0.00042									

Table F.6. Times of minima of TIC 378270875

BJD −2 400 000	Cycle no.	std. dev. (*d*)	BJD −2 400 000	Cycle no.	std. dev. (*d*)	BJD −2 400 000	Cycle no.	std. dev. (*d*)	BJD −2 400 000	Cycle no.	std. dev. (*d*)
58684.28515	0.0	0.00040	59438.03168	292.5	0.00026	60341.24879	643.0	0.00023	60517.76692	711.5	0.00024
58685.57149	0.5	0.00067	59439.32149	293.0	0.00019	60342.53697	643.5	0.00028	60519.05678	712.0	0.00018
58686.86054	1.0	0.00035	59440.60712	293.5	0.00029	60343.82678	644.0	0.00021	60520.34404	712.5	0.00017
58688.14767	1.5	0.00057	59441.89717	294.0	0.00019	60345.11412	644.5	0.00025	60521.63392	713.0	0.00015
58689.43640	2.0	0.00051	59443.18297	294.5	0.00027	60346.40308	645.0	0.00052	60522.92041	713.5	0.00015
58690.72320	2.5	0.00062	59444.47278	295.0	0.00018	60347.69054	645.5	0.00030	60524.20997	714.0	0.00013
58692.01233	3.0	0.00039	59445.75886	295.5	0.00020	60348.97987	646.0	0.00020	60525.49610	714.5	0.00020
58693.29975	3.5	0.00053	59797.50904	432.0	0.00042	60350.26670	646.5	0.00025	60526.78560	715.0	0.00013
58694.58879	4.0	0.00036	59798.79447	432.5	0.00052	60351.55626	647.0	0.00017	60528.07190	715.5	0.00018
58695.87620	4.5	0.00040	59800.08594	433.0	0.00038	60352.84191	647.5	0.00023	60529.36147	716.0	0.00016
58698.45255	5.5	0.00061	59801.37160	433.5	0.00047	60354.13256	648.0	0.00020	60530.64816	716.5	0.00023
58699.74188	6.0	0.00052	59802.66327	434.0	0.00039	60355.41817	648.5	0.00029	60531.93754	717.0	0.00013
58701.02988	6.5	0.00069	59803.94949	434.5	0.00047	60356.70731	649.0	0.00022	60534.51276	718.0	0.00012
58702.31978	7.0	0.00043	59805.24125	435.0	0.00037	60357.99353	649.5	0.00027	60535.79908	718.5	0.00016
58703.60912	7.5	0.00068	59806.52800	435.5	0.00054	60359.28330	650.0	0.00024	60537.08883	719.0	0.00014
58704.90036	8.0	0.00045	59807.82062	436.0	0.00037	60360.56983	650.5	0.00031	60538.37453	719.5	0.00016
58706.18972	8.5	0.00054	59809.10814	436.5	0.00057	60361.85907	651.0	0.00028	60539.66474	720.0	0.00014
58707.48190	9.0	0.00036	59811.68813	437.5	0.00018	60363.14599	651.5	0.00036	60540.95025	720.5	0.00017
58708.76999	9.5	0.00070	59812.97893	438.0	0.00015	60364.43480	652.0	0.00022	60542.24056	721.0	0.00015
58710.06133	10.0	0.00034	59814.26613	438.5	0.00023	60365.72128	652.5	0.00028	60543.52633	721.5	0.00017
58712.63898	11.0	0.00039	59815.55732	439.0	0.00021	60367.01068	653.0	0.00018	60544.81619	722.0	0.00013
58713.92678	11.5	0.00053	59816.84437	439.5	0.00025	60368.29706	653.5	0.00024	60546.10199	722.5	0.00017
58715.21655	12.0	0.00041	59818.13498	440.0	0.00021	60369.58684	654.0	0.00020	60547.39221	723.0	0.00012
58716.50398	12.5	0.00058	59819.42252	440.5	0.00034	60370.87304	654.5	0.00027	60548.67792	723.5	0.00017
58717.79367	13.0	0.00046	59820.71278	441.0	0.00030	60372.16258	655.0	0.00023	60549.96841	724.0	0.00014
58719.08003	13.5	0.00079	59821.99988	441.5	0.00039	60373.44949	655.5	0.00024	60551.25460	724.5	0.00018
58720.37088	14.0	0.00048	59823.29006	442.0	0.00036	60374.73848	656.0	0.00017	60552.54456	725.0	0.00013
58721.65746	14.5	0.00079	59825.86611	443.0	0.00049	60376.02484	656.5	0.00026	60553.83045	725.5	0.00018
58722.94812	15.0	0.00067	59827.15239	443.5	0.00056	60377.31473	657.0	0.00018	60555.12134	726.0	0.00013
58725.52332	16.0	0.00017	59828.44249	444.0	0.00037	60378.60088	657.5	0.00019	60556.40753	726.5	0.00015
58726.80951	16.5	0.00040	59829.72867	444.5	0.00044	60379.89093	658.0	0.00014	60557.69825	727.0	0.00013
58728.09899	17.0	0.00029	59831.01901	445.0	0.00034	60381.17753	658.5	0.00022	60558.98404	727.5	0.00016
58729.38503	17.5	0.00049	59832.30396	445.5	0.00042	60382.46751	659.0	0.00015	60560.27697	728.0	0.00012
58730.67474	18.0	0.00040	59833.59457	446.0	0.00023	60383.75541	659.5	0.00025	60561.56491	728.5	0.00015
58731.96103	18.5	0.00053	59834.88022	446.5	0.00029	60385.04501	660.0	0.00020	60562.85714	729.0	0.00012
58733.25074	19.0	0.00057	59836.17079	447.0	0.00022	60386.33436	660.5	0.00030	60564.14502	729.5	0.00017
58734.53643	19.5	0.00093	59837.45593	447.5	0.00028	60387.62520	661.0	0.00024	60565.43678	730.0	0.00013
58735.82654	20.0	0.00073	59838.74651	448.0	0.00049	60388.91365	661.5	0.00027	60566.72298	730.5	0.00016
58737.11275	20.5	0.00140	59840.03165	448.5	0.00021	60390.20515	662.0	0.00019	60568.01471	731.0	0.00013
59421.29054	286.0	0.00020	59841.32202	449.0	0.00014	60391.49306	662.5	0.00027	60569.30110	731.5	0.00014
59422.57645	286.5	0.00023	59842.60710	449.5	0.00020	60392.78302	663.0	0.00021	60570.59329	732.0	0.00012
59423.86691	287.0	0.00017	59843.89787	450.0	0.00015	60394.07071	663.5	0.00028	60573.17165	733.0	0.00012
59425.15231	287.5	0.00023	59845.18308	450.5	0.00027	60507.45423	707.5	0.00018	60574.45909	733.5	0.00015
59426.44249	288.0	0.00018	59846.47387	451.0	0.00024	60508.74474	708.0	0.00013	60575.74959	734.0	0.00014
59427.72837	288.5	0.00022	59847.75852	451.5	0.00034	60510.03246	708.5	0.00016	60577.03566	734.5	0.00017
59429.01818	289.0	0.00021	59849.04956	452.0	0.00025	60511.32325	709.0	0.00014	60578.32616	735.0	0.00013
59430.30411	289.5	0.00021	59850.33437	452.5	0.00034	60512.61092	709.5	0.00019	60579.61230	735.5	0.00015
59431.59362	290.0	0.00015	59851.62520	453.0	0.00030	60513.90194	710.0	0.00015	60580.90291	736.0	0.00011
59434.16946	291.0	0.00027	59852.91051	453.5	0.00038	60515.18959	710.5	0.00020	60582.18842	736.5	0.00014
59435.45638	291.5	0.00031	60339.95849	642.5	0.00022	60516.47934	711.0	0.00014	60583.47854	737.0	0.00013
59436.74508	292.0	0.00024									

Table F.7. Times of minima of TIC 403792414

BJD −2 400 000	Cycle no.	std. dev. (*d*)	BJD −2 400 000	Cycle no.	std. dev. (*d*)	BJD −2 400 000	Cycle no.	std. dev. (*d*)	BJD −2 400 000	Cycle no.	std. dev. (*d*)
59391.36642	0.0	0.00084	59423.80076	6.5	0.00176	59778.45988	77.5	0.00391	60500.22737	222.0	0.00095
59393.84551	0.5	0.00464	59426.32710	7.0	0.00063	59780.97284	78.0	0.00124	60502.74607	222.5	0.00158
59396.37449	1.0	0.00130	59428.79336	7.5	0.00154	59785.97024	79.0	0.00059	60505.21473	223.0	0.00039
59398.84138	1.5	0.00417	59431.31860	8.0	0.00041	59788.45458	79.5	0.00363	60507.73852	223.5	0.00093
59401.36991	2.0	0.00096	59433.77914	8.5	0.01752	59790.96860	80.0	0.00121	60510.20456	224.0	0.00022
59403.83489	2.5	0.00193	59436.30569	9.0	0.00079	59793.45113	80.5	0.00722	60512.72659	224.5	0.00083
59406.36374	3.0	0.00141	59438.77536	9.5	0.01035	59795.96028	81.0	0.00089	60517.72173	225.5	0.00128
59408.82709	3.5	0.01201	59441.29652	10.0	0.00102	60480.24627	218.0	0.00022	60520.18312	226.0	0.00026
59411.35519	4.0	0.00156	59443.76775	10.5	0.00575	60482.77173	218.5	0.00114	60522.71174	226.5	0.00072
59413.82382	4.5	0.04310	59446.28806	11.0	0.00099	60490.24036	220.0	0.00043	60525.17223	227.0	0.00022
59416.34687	5.0	0.00130	59770.94788	76.0	0.00042	60492.75854	220.5	0.00094	60527.70313	227.5	0.00106
59418.81010	5.5	0.01119	59773.43011	76.5	0.00208	60495.23270	221.0	0.00022	60530.16230	228.0	0.00026
59421.33779	6.0	0.00042	59775.95283	77.0	0.00063	60497.75526	221.5	0.00080	60532.69232	228.5	0.00103

Table F.8. Times of minima of TIC 403916758

BJD −2 400 000	Cycle no.	std. dev. (*d*)	BJD −2 400 000	Cycle no.	std. dev. (*d*)	BJD −2 400 000	Cycle no.	std. dev. (*d*)	BJD −2 400 000	Cycle no.	std. dev. (*d*)
58791.04022	-1.0	0.00303	58991.71010	176.0	0.00139	59900.39543	977.5	0.00098	60461.58223	1472.5	0.00190
58791.60976	-0.5	0.00451	58992.28190	176.5	0.00259	59900.95764	978.0	0.00095	60462.14926	1473.0	0.00213
58792.17603	0.0	0.00251	58992.84495	177.0	0.00224	59901.52962	978.5	0.00099	60463.28434	1474.0	0.00093
58792.74172	0.5	0.00710	58993.41207	177.5	0.00293	59902.09476	979.0	0.00106	60463.85343	1474.5	0.00184
58793.30940	1.0	0.00148	58993.97480	178.0	0.00141	59902.66247	979.5	0.00113	60464.41731	1475.0	0.00206
58793.87868	1.5	0.00208	58994.54858	178.5	0.00577	59903.22643	980.0	0.00105	60466.11977	1476.5	0.00128
58794.44339	2.0	0.00198	58995.11384	179.0	0.00216	59903.79554	980.5	0.00118	60466.68878	1477.0	0.00230
58795.00722	2.5	0.00205	58997.37476	181.0	0.00830	59904.36509	981.0	0.00097	60467.25332	1477.5	0.00176
58795.57709	3.0	0.00263	58997.94324	181.5	0.00375	59904.93050	981.5	0.00090	60467.81998	1478.0	0.00089
58796.14246	3.5	0.00360	58998.51339	182.0	0.00822	59905.49202	982.0	0.00105	60468.38769	1478.5	0.00179
58796.70889	4.0	0.00501	58999.08247	182.5	0.00374	59906.06582	982.5	0.00096	60468.95879	1479.0	0.00209
58797.27788	4.5	0.00161	58999.64410	183.0	0.00277	59906.62950	983.0	0.00135	60469.52523	1479.5	0.00156
58797.84526	5.0	0.00139	59000.21001	183.5	0.00507	59907.19856	983.5	0.00116	60470.08819	1480.0	0.00093
58798.98043	6.0	0.00164	59000.77819	184.0	0.01704	59907.76767	984.0	0.00124	60470.65861	1480.5	0.00168
58799.54787	6.5	0.00144	59001.34787	184.5	0.00315	59908.33018	984.5	0.00101	60471.22586	1481.0	0.00107
58800.11128	7.0	0.00167	59003.61174	186.5	0.00539	59908.89265	985.0	0.00121	60471.79080	1481.5	0.00171
58803.51318	10.0	0.02232	59004.18107	187.0	0.00223	59909.46123	985.5	0.00117	60472.35947	1482.0	0.00101
58804.08049	10.5	0.00368	59004.75116	187.5	0.00118	59910.59104	986.5	0.05691	60472.92035	1482.5	0.00167
58804.64630	11.0	0.00129	59005.31440	188.0	0.00160	59911.16643	987.0	0.08659	60473.49100	1483.0	0.00130
58805.21213	11.5	0.00284	59006.44958	189.0	0.00248	59911.73486	987.5	0.06630	60474.05622	1483.5	0.00210
58805.77971	12.0	0.00168	59007.01863	189.5	0.00235	59912.29634	988.0	0.02874	60474.62383	1484.0	17.23120
58806.34933	12.5	0.00188	59007.57895	190.0	0.00167	59912.86012	988.5	0.07287	60475.19222	1484.5	0.00144
58806.91420	13.0	0.00084	59008.14644	190.5	0.00186	59913.43349	989.0	0.08579	60475.76319	1485.0	0.00252
58807.48232	13.5	0.00143	59008.71467	191.0	0.01936	59913.99605	989.5	0.06127	60476.32201	1485.5	0.00158
58808.04581	14.0	0.00118	59718.99759	817.5	0.00300	59914.55962	990.0	0.07533	60477.45861	1486.5	0.00111
58808.61635	14.5	0.00165	59719.55944	818.0	0.00327	59915.13010	990.5	0.04083	60478.02796	1487.0	0.00205
58809.18572	15.0	0.00157	59720.13132	818.5	0.34983	59915.69993	991.0	0.09531	60478.59231	1487.5	0.00126
58809.75078	15.5	0.00283	59720.69784	819.0	0.00455	59916.26634	991.5	0.13087	60479.16135	1488.0	0.00181
58810.31706	16.0	0.00110	59721.26164	819.5	0.00223	59917.96510	993.0	0.03070	60610.67126	1604.0	0.00163
58810.88241	16.5	0.00138	59721.83041	820.0	0.00345	59918.52908	993.5	0.09838	60611.24073	1604.5	0.00235

Table F.8. Times of minima of TIC 403916758 (continued)

BJD −2 400 000	Cycle no.	std. dev. (*d*)	BJD −2 400 000	Cycle no.	std. dev. (*d*)	BJD −2 400 000	Cycle no.	std. dev. (*d*)	BJD −2 400 000	Cycle no.	std. dev. (*d*)
58811.45291	17.0	0.00140	59722.39655	820.5	0.00174	59919.09275	994.0	0.12269	60611.80608	1605.0	0.00098
58812.02046	17.5	0.00164	59722.96294	821.0	0.00229	59919.66919	994.5	0.06085	60612.37421	1605.5	0.00154
58812.58289	18.0	0.00122	59723.53152	821.5	0.00125	59920.23332	995.0	0.05982	60612.94109	1606.0	0.00119
58813.15199	18.5	0.00315	59724.09955	822.0	0.00134	59920.79877	995.5	0.07230	60613.50401	1606.5	0.00222
58813.71698	19.0	0.00111	59724.66526	822.5	0.00194	59921.36212	996.0	0.03137	60614.07488	1607.0	0.00232
58814.28690	19.5	0.00854	59725.23054	823.0	0.00143	59921.94030	996.5	0.30148	60614.64179	1607.5	0.00129
58956.00095	144.5	0.00171	59725.80161	823.5	0.00132	59922.49720	997.0	5.08376	60615.21227	1608.0	0.00107
58956.56460	145.0	0.00153	59726.36693	824.0	0.00131	59923.06306	997.5	11.22033	60615.77550	1608.5	0.00252
58957.13080	145.5	0.00228	59726.93168	824.5	0.00170	59923.63885	998.0	0.09612	60616.34391	1609.0	0.00155
58957.70208	146.0	0.00181	59727.50016	825.0	0.00144	59926.47257	1000.5	0.05885	60616.90941	1609.5	0.00280
58958.26665	146.5	0.00450	59728.06641	825.5	0.00112	59927.03164	1001.0	0.10370	60617.47367	1610.0	0.00114
58958.83897	147.0	0.00554	59728.63508	826.0	0.00143	59927.60477	1001.5	0.04014	60618.04539	1610.5	0.00202
58959.40207	147.5	0.00308	59729.20045	826.5	0.00080	59928.17192	1002.0	0.02430	60618.60238	1611.0	0.00183
58959.96742	148.0	0.01125	59729.76820	827.0	0.00142	59928.73759	1002.5	0.16595	60619.17794	1611.5	0.00148
58960.53615	148.5	0.00163	59731.46617	828.5	0.03619	59929.29778	1003.0	0.07405	60619.73740	1612.0	0.00184
58961.10300	149.0	0.00185	59732.03029	829.0	0.00290	59929.86870	1003.5	0.35554	60620.30867	1612.5	0.00106
58961.66803	149.5	0.00163	59732.59925	829.5	0.02918	59931.00286	1004.5	0.72601	60620.87550	1613.0	0.00133
58962.23483	150.0	0.00320	59733.17047	830.0	0.01378	59931.56846	1005.0	0.05043	60621.44087	1613.5	0.00232
58962.80556	150.5	0.00366	59733.73902	830.5	0.00389	59932.13652	1005.5	0.05836	60622.00666	1614.0	0.00222
58963.37247	151.0	0.00151	59734.30213	831.0	0.00196	59932.70632	1006.0	0.02232	60622.57780	1614.5	0.00134
58963.93583	151.5	0.00148	59734.86745	831.5	0.00205	59933.27224	1006.5	0.45953	60623.13916	1615.0	0.00166
58964.50137	152.0	0.00714	59735.43766	832.0	0.00170	59933.83944	1007.0	0.04401	60623.71163	1615.5	0.00120
58965.07272	152.5	0.00236	59736.00380	832.5	0.00191	59934.40533	1007.5	0.23692	60624.27093	1616.0	0.00172
58965.63562	153.0	0.00280	59736.57123	833.0	0.00178	59934.96770	1008.0	0.17964	60624.84783	1616.5	0.00219
58967.90178	155.0	0.01454	59737.70285	834.0	0.00156	59935.54030	1008.5	0.08855	60625.40497	1617.0	0.00160
58969.60332	156.5	0.00224	59738.26615	834.5	0.00223	59936.66628	1009.5	0.09679	60625.97667	1617.5	0.00131
58970.17345	157.0	0.01160	59738.83931	835.0	0.00135	60434.37639	1448.5	0.00112	60630.51326	1621.5	0.00114
58970.74442	157.5	0.00554	59739.40656	835.5	0.00177	60434.94464	1449.0	0.00166	60631.08098	1622.0	0.00113
58971.30696	158.0	0.00280	59739.97036	836.0	0.00261	60435.50780	1449.5	0.00214	60631.65012	1622.5	0.00149
58971.87607	158.5	0.00281	59740.53738	836.5	0.00180	60436.07600	1450.0	0.00235	60632.20785	1623.0	0.00113
58972.44125	159.0	0.00284	59741.10621	837.0	0.00135	60436.64386	1450.5	0.00139	60632.77857	1623.5	0.00221
58973.00507	159.5	0.00267	59741.67352	837.5	0.00126	60437.21446	1451.0	0.00169	60633.34822	1624.0	0.00113
58973.56805	160.0	0.03552	59742.23838	838.0	0.00196	60438.34426	1452.0	0.00154	60633.91004	1624.5	0.00106
58974.13943	160.5	0.00347	59742.80822	838.5	0.00161	60438.91240	1452.5	0.00109	60636.74787	1627.0	0.00237
58974.70518	161.0	0.00169	59882.82355	962.0	0.00159	60439.47775	1453.0	0.00148	60637.31404	1627.5	0.00242
58975.27439	161.5	0.00219	59883.38649	962.5	0.00111	60440.04610	1453.5	0.00115	60638.44808	1628.5	0.00452
58975.84059	162.0	0.00234	59883.95377	963.0	0.00154	60440.61370	1454.0	0.00156	60639.01552	1629.0	0.00529
58976.40785	162.5	0.00920	59884.52024	963.5	0.00107	60441.18319	1454.5	0.00148	60639.58460	1629.5	0.01030
58976.97351	163.0	0.00121	59885.08944	964.0	0.00126	60442.31166	1455.5	0.00142	60640.15482	1630.0	0.00754
58977.53915	163.5	0.00198	59885.65606	964.5	0.00081	60442.88489	1456.0	0.00194	60640.71532	1630.5	0.01488
58978.10775	164.0	0.00523	59886.22734	965.0	0.00087	60443.44805	1456.5	0.00145	60641.27644	1631.0	0.00197
58978.67306	164.5	0.00219	59886.79170	965.5	0.00092	60444.01633	1457.0	0.00164	60643.54506	1633.0	0.00187
58979.24094	165.0	0.00120	59887.35376	966.0	0.00129	60444.57732	1457.5	0.00137	60644.11215	1633.5	0.00166
58979.80895	165.5	0.00502	59887.92104	966.5	0.00102	60445.15093	1458.0	0.00169	60644.68723	1634.0	0.00196
58980.37576	166.0	0.00551	59888.48716	967.0	0.00097	60445.71538	1458.5	0.00128	60645.25080	1634.5	0.00194
58980.94088	166.5	0.00125	59890.75782	969.0	0.00089	60446.28503	1459.0	0.00120	60646.38495	1635.5	0.00192
58981.50641	167.0	0.00150	59891.32610	969.5	0.00113	60446.84681	1459.5	0.00188	60646.95006	1636.0	0.00265
58982.08009	167.5	0.00182	59891.89546	970.0	0.00100	60447.41860	1460.0	0.00144	60647.51318	1636.5	0.00269
58983.77708	169.0	0.01122	59892.46094	970.5	0.00107	60447.98262	1460.5	0.00152	60648.08210	1637.0	0.00261
58984.34561	169.5	0.01005	59893.02460	971.0	0.00109	60448.55334	1461.0	0.00230	60649.21263	1638.0	0.00404
58984.90380	170.0	0.05017	59893.59126	971.5	0.00097	60449.11997	1461.5	0.00181	60650.35479	1639.0	0.00316
58985.47845	170.5	0.00502	59894.15858	972.0	0.00116	60453.08270	1465.0	0.00175	60651.48057	1640.0	0.00465
58986.04237	171.0	0.00261	59894.72592	972.5	0.00151	60453.65494	1465.5	0.00084	60652.61394	1641.0	0.00230
58986.61117	171.5	0.04506	59895.29159	973.0	0.00096	60454.22123	1466.0	0.00220	60653.75678	1642.0	0.00510
58987.17431	172.0	0.00203	59895.85920	973.5	0.00094	60454.78903	1466.5	0.00135	60656.58174	1644.5	0.00219
58987.74519	172.5	0.01713	59896.42322	974.0	0.00119	60455.35136	1467.0	0.00236	60659.42245	1647.0	0.00191
58988.30850	173.0	0.00127	59896.98864	974.5	0.00114	60455.92274	1467.5	0.00161	60659.98398	1647.5	1.35208
58988.87373	173.5	0.00142	59897.55935	975.0	0.00108	60456.48778	1468.0	0.00193	60660.56116	1648.0	0.00359
58989.44281	174.0	0.00288	59898.12762	975.5	0.00081	60458.75136	1470.0	0.00132	60661.12289	1648.5	0.00167
58990.01410	174.5	0.00181	59898.69021	976.0	0.00090	60459.88501	1471.0	0.00923	60661.68868	1649.0	0.00243
58990.57456	175.0	0.01592	59899.25980	976.5	0.00188	60460.45088	1471.5	0.00130	60662.25962	1649.5	0.00193
58991.14521	175.5	0.00416	59899.82633	977.0	0.00091	60461.02278	1472.0	0.00284			

Table F.9. Times of minima of TIC 405789362

BJD −2 400 000	Cycle no.	std. dev. (*d*)	BJD −2 400 000	Cycle no.	std. dev. (*d*)	BJD −2 400 000	Cycle no.	std. dev. (*d*)	BJD −2 400 000	Cycle no.	std. dev. (*d*)
58738.84443	-0.5	0.00041	58963.16388	48.5	0.00030	59892.45421	251.5	0.00020	60444.08244	372.0	0.00014
58741.14567	0.0	0.00019	58965.46590	49.0	0.00014	59894.74946	252.0	0.00020	60446.36875	372.5	0.00013
58743.41839	0.5	0.00034	58967.73967	49.5	0.00029	59897.02859	252.5	0.00026	60448.65848	373.0	0.00024
58745.71622	1.0	0.00025	58970.03628	50.0	0.00014	59899.32453	253.0	0.00017	60560.80125	397.5	0.00027
58747.99476	1.5	0.00043	58972.31123	50.5	0.00026	59901.60165	253.5	0.00019	60563.09047	398.0	0.00015
58750.28976	2.0	0.00059	58974.60963	51.0	0.00022	59903.89744	254.0	0.00013	60565.37913	398.5	0.00018
58752.57021	2.5	0.00030	58976.88288	51.5	0.00027	59908.46977	255.0	0.00015	60567.66359	399.0	0.00017
58754.87358	3.0	0.00045	58979.18515	52.0	0.00045	60114.47159[a]	300.0	0.00006	60572.23910	400.0	0.00016
58757.15447	3.5	0.00027	58981.45807	52.5	0.00024	60169.41811[a]	312.0	0.00004	60574.52627	400.5	0.00018
58759.46051	4.0	0.00036	59826.07245	237.0	0.00017	60295.28396[a]	339.5	0.00006	60576.81664	401.0	0.00013
58761.73494	4.5	0.00043	59828.35344	237.5	0.00018	60368.53672	355.5	0.00020	60579.11696	401.5	0.00022
58766.31205	5.5	0.00018	59830.64640	238.0	0.00018	60370.82813	356.0	0.00031	60581.41208	402.0	0.00015
58768.61639	6.0	0.00015	59832.92701	238.5	0.00027	60373.11405	356.5	0.00022	60583.70410	402.5	0.00016
58770.89670	6.5	0.00025	59835.22609	239.0	0.00019	60375.40265	357.0	0.00024	60585.99280	403.0	0.00014
58773.19849	7.0	0.00050	59837.51888	239.5	0.00026	60377.69013	357.5	0.00019	60588.27752	403.5	0.00017
58775.47418	7.5	0.00043	59839.82003	240.0	0.00018	60379.97775	358.0	0.00021	60590.56688	404.0	0.00015
58777.77464	8.0	0.00037	59842.10262	240.5	0.00020	60382.26482	358.5	0.00023	60592.85399	404.5	0.00016
58780.05095	8.5	0.00019	59844.39709	241.0	0.00020	60386.83742	359.5	0.00026	60595.14210	405.0	0.00013
58782.35156	9.0	0.00028	59846.67684	241.5	0.00025	60389.12713	360.0	0.00019	60599.71712	406.0	0.00016
58784.62246	9.5	0.00021	59848.96969	242.0	0.00020	60391.41946	360.5	0.00021	60602.00566	406.5	0.00015
58786.92436	10.0	0.00022	59851.24772	242.5	0.00028	60393.72193	361.0	0.00019	60604.29240	407.0	0.00017
58789.20092	10.5	0.00089	59853.54580	243.0	0.00022	60396.01280	361.5	0.00023	60606.58190	407.5	0.00020
58791.49841	11.0	0.00034	59855.82330	243.5	0.00024	60398.30463	362.0	0.00023	60608.86730	408.0	0.00012
58793.77077	11.5	0.00029	59858.12006	244.0	0.00021	60400.59337	362.5	0.00025	60611.15684	408.5	0.00019
58796.06961	12.0	0.00028	59862.69321	245.0	0.00019	60402.87984	363.0	0.00025	60613.44299	409.0	0.00024
58798.34724	12.5	0.00054	59869.55246	246.5	0.00021	60405.16455	363.5	0.00031	60618.01551	410.0	0.00014
58800.64864	13.0	0.00028	59871.84812	247.0	0.00017	60418.88932	366.5	0.00031	60620.30480	410.5	0.00015
58805.23663	14.0	0.00023	59874.13286	247.5	0.00022	60421.18132	367.0	0.00015	60622.59304	411.0	0.00015
58807.51610	14.5	0.00036	59876.42491	248.0	0.00017	60423.46824	367.5	0.00022	60624.89134	411.5	0.00034
58809.81266	15.0	0.00017	59881.00351	249.0	0.00023	60434.90713	370.0	0.00017	60627.18735	412.0	0.00024
58812.09039	15.5	0.00036	59883.29430	249.5	0.00023	60437.19507	370.5	0.00019	60629.48332	412.5	0.00017
58814.39426	16.0	0.00019	59885.59524	250.0	0.00013	60439.49026	371.0	0.00012	60631.76981	413.0	0.00013
58958.58683	47.5	0.00034	59887.88295	250.5	0.00018	60441.78950	371.5	0.00017	60634.05668	413.5	0.00014
58960.88886	48.0	0.00017	59890.17405	251.0	0.00016						

Notes. [a]: These eclipses observed with the GAO80 instrument.

Table F.10. Times of minima of TIC 461500036

BJD −2 400 000	Cycle no.	std. dev. (*d*)	BJD −2 400 000	Cycle no.	std. dev. (*d*)	BJD −2 400 000	Cycle no.	std. dev. (*d*)	BJD −2 400 000	Cycle no.	std. dev. (*d*)
58791.39329	0.0	0.00119	59032.32894	97.5	0.00015	59894.77700	446.5	0.00006	60412.48899[a]	656.0	0.00002
58792.63164	0.5	0.00009	59033.56140	98.0	0.00009	59896.01066	447.0	0.00008	60434.73454	665.0	0.00008
58793.86528	1.0	0.00013	59034.79978	98.5	0.00007	59897.24718	447.5	0.00008	60435.96862	665.5	0.00007
58795.10193	1.5	0.00011	59391.89327	243.0	0.00009	59898.48121	448.0	0.00006	60437.20269	666.0	0.00009
58796.33557	2.0	0.00011	59393.13059	243.5	0.00010	59899.71715	448.5	0.00007	60438.43897	666.5	0.00007
58797.57278	2.5	0.00008	59394.36417	244.0	0.00012	59900.95129	449.0	0.00007	60439.67264	667.0	0.00007
58798.80596	3.0	0.00012	59395.60086	244.5	0.00010	59902.18760	449.5	0.00005	60440.90937	667.5	0.00008
58800.04291	3.5	0.00019	59396.83412	245.0	0.00012	59904.65772	450.5	0.00007	60442.14261	668.0	0.00008
58801.27639	4.0	0.00014	59398.07052	245.5	0.00008	59905.89231	451.0	0.00006	60443.37897	668.5	0.00009
58803.74615	5.0	0.00011	59399.30478	246.0	0.00008	59907.12833	451.5	0.00007	60444.61348	669.0	0.00010
58804.98322	5.5	0.00014	59400.54155	246.5	0.00006	59908.36261	452.0	0.00006	60445.84932	669.5	0.00008
58806.21609	6.0	0.00009	59401.77402	247.0	0.00007	59909.59884	452.5	0.00006	60447.08356	670.0	0.00007
58807.45303	6.5	0.00013	59403.01114	247.5	0.00005	59912.06949	453.5	0.00007	60448.31849	670.5	0.00010
58808.68666	7.0	0.00009	59404.24430	248.0	0.00007	59913.30372	454.0	0.00006	60449.55473	671.0	0.00007
58809.92352	7.5	0.00012	59405.48074	248.5	0.00013	59914.54089	454.5	0.00006	60453.26004	672.5	0.00007

Notes. Eclipses observed with the [a]: GAO80 and [b]: BAO80 instruments.

Table F.10. Times of minima of TIC 461500036 (continued)

BJD −2 400 000	Cycle no.	std. dev. (*d*)	BJD −2 400 000	Cycle no.	std. dev. (*d*)	BJD −2 400 000	Cycle no.	std. dev. (*d*)	BJD −2 400 000	Cycle no.	std. dev. (*d*)
58811.15678	8.0	0.00011	59406.71345	249.0	0.00008	59915.77580	455.0	0.00007	60454.49516	673.0	0.00007
58812.39444	8.5	0.00007	59407.95227	249.5	0.00008	59917.01332	455.5	0.00005	60455.73104	673.5	0.00007
58813.62674	9.0	0.00014	59409.18421	250.0	0.00008	59918.24803	456.0	0.00005	60456.96625	674.0	0.00007
58814.86397	9.5	0.00029	59410.42204	250.5	0.00010	59919.48518	456.5	0.00006	60458.20215	674.5	0.00007
58843.28889	21.0	0.00012	59411.65479	251.0	0.00009	59920.72062	457.0	0.00007	60459.43821	675.0	0.00010
58844.52677	21.5	0.00014	59412.89216	251.5	0.00011	59921.95768	457.5	0.00007	60460.67433	675.5	0.00009
58845.75995	22.0	0.00007	59414.12502	252.0	0.00007	59923.19281	458.0	0.00006	60461.90891	676.0	0.00008
58846.99814	22.5	0.00009	59415.36247	252.5	0.00007	59924.43116	458.5	0.00009	60463.14656	676.5	0.00010
58848.23092	23.0	0.00016	59416.59517	253.0	0.00010	59925.66519	459.0	0.00007	60464.38166	677.0	0.00007
58849.46855	23.5	0.00006	59417.83283	253.5	0.00008	59926.90532	459.5	0.00006	60466.85341	678.0	0.00008
58850.70140	24.0	0.00010	59719.32676	375.5	0.00010	59928.14106	460.0	0.00006	60468.09182	678.5	0.00007
58851.93929	24.5	0.00010	59720.56147	376.0	0.00009	59930.61358	461.0	0.00005	60469.32800	679.0	0.00007
58853.17183	25.0	0.00015	59721.79774	376.5	0.00009	59931.85014	461.5	0.00006	60470.56631	679.5	0.00009
58854.40974	25.5	0.00006	59723.03181	377.0	0.00009	59933.08462	462.0	0.00006	60473.04068	680.5	0.00009
58856.88006	26.5	0.00014	59724.26781	377.5	0.00006	59934.32127	462.5	0.00006	60474.27469	681.0	0.00008
58858.11195	27.0	0.00011	59725.50131	378.0	0.00009	59935.55514	463.0	0.00005	60475.51197	681.5	0.00008
58859.34959	27.5	0.00010	59726.73836	378.5	0.00008	59938.02575	464.0	0.00024	60476.74713	682.0	0.00009
58860.58220	28.0	0.00018	59727.97147	379.0	0.00010	59939.26250	464.5	0.00009	60477.98341	682.5	0.00008
58861.81955	28.5	0.00012	59729.20814	379.5	0.00007	59940.49574	465.0	0.00007	60479.21672	683.0	0.00007
58863.05270	29.0	0.00011	59731.67795	380.5	0.00008	59941.73234	465.5	0.00006	60496.50821[b]	690.0	0.00002
58864.29012	29.5	0.00010	59732.91253	381.0	0.00008	59942.96643	466.0	0.00004	60522.45641[b]	700.5	0.00004
58865.52306	30.0	0.00014	59734.14833	381.5	0.00008	59944.20284	466.5	0.00005	60611.41878	736.5	0.00005
58866.75977	30.5	0.00008	59735.38266	382.0	0.00011	59945.43627	467.0	0.00005	60612.65289	737.0	0.00006
58867.99290	31.0	0.00009	59736.61878	382.5	0.00009	59946.67285	467.5	0.00006	60613.88911	737.5	0.00005
58984.13655	78.0	0.00019	59737.85275	383.0	0.00007	59947.90657	468.0	0.00005	60615.12330	738.0	0.00007
58985.37368	78.5	0.00013	59739.08906	383.5	0.00006	59949.14318	468.5	0.00006	60616.36009	738.5	0.00013
58986.60717	79.0	0.00009	59740.32262	384.0	0.00009	59955.31709	471.0	0.00006	60617.59413	739.0	0.00005
58987.84406	79.5	0.00007	59741.55902	384.5	0.00008	59956.55372	471.5	0.00006	60618.83050	739.5	0.00007
58989.07830	80.0	0.00008	59742.79304	385.0	0.00008	59957.78739	472.0	0.00005	60620.06491	740.0	0.00005
58990.31589	80.5	0.00007	59744.02948	385.5	0.00018	59959.02381	472.5	0.00007	60621.30130	740.5	0.00006
58991.55019	81.0	0.00011	59745.26364	386.0	0.00007	59960.25792	473.0	0.00005	60622.53619	741.0	0.00007
58992.78800	81.5	0.00007	59746.50008	386.5	0.00008	59961.49416	473.5	0.00006	60623.77263	741.5	0.00006
58994.02254	82.0	0.00008	59747.73370	387.0	0.00018	60113.47613[a]	535.0	0.00002	60625.00824	742.0	0.00007
58995.26133	82.5	0.00007	59748.97116	387.5	0.00007	60134.47855[a]	543.5	0.00002	60626.24520	742.5	0.00008
58997.73337	83.5	0.00009	59750.20489	388.0	0.00009	60234.56155[a]	584.0	0.00007	60627.48087	743.0	0.00006
58998.96788	84.0	0.00004	59751.44240	388.5	0.00008	60286.45554	605.0	0.00009	60628.71756	743.5	0.00006
59000.20681	84.5	0.00012	59752.67738	389.0	0.00007	60287.69106	605.5	0.00015	60631.18964	744.5	0.00005
59001.44179	85.0	0.00014	59753.91440	389.5	0.00005	60288.92553	606.0	0.00009	60632.42675	745.0	0.00004
59002.68044	85.5	0.00011	59755.14972	390.0	0.00008	60290.16296	606.5	0.00007	60633.66435	745.5	0.00004
59003.91512	86.0	0.00013	59757.62218	391.0	0.00007	60291.39646	607.0	0.00006	60637.37368	747.0	0.00006
59006.38715	87.0	0.00010	59758.85977	391.5	0.00009	60292.63348	607.5	0.00006	60638.61009	747.5	0.00006
59007.62579	87.5	0.00012	59760.09474	392.0	0.00008	60293.86756	608.0	0.00006	60639.84518	748.0	0.00006
59008.85931	88.0	0.00006	59761.33217	392.5	0.00006	60295.10463	608.5	0.00006	60641.08146	748.5	0.00006
59011.33008	89.0	0.00005	59762.56816	393.0	0.00005	60296.33886	609.0	0.00006	60643.55214	749.5	0.00006
59012.56703	89.5	0.00011	59763.80596	393.5	0.00006	60297.57640	609.5	0.00006	60644.78618	750.0	0.00005
59013.79954	90.0	0.00013	59765.04190	394.0	0.00010	60298.81100	610.0	0.00005	60646.02282	750.5	0.00005
59015.03739	90.5	0.00012	59767.51440	395.0	0.00007	60300.04902	610.5	0.00009	60647.25686	751.0	0.00004
59016.27051	91.0	0.00030	59768.75169	395.5	0.00004	60301.28309	611.0	0.00010	60648.49303	751.5	0.00005
59017.50761	91.5	0.00004	59882.42633	441.5	0.00008	60302.52047	611.5	0.00007	60650.96273	752.5	0.00006
59018.74091	92.0	0.00018	59883.65995	442.0	0.00006	60306.22919	613.0	0.00009	60652.19700	753.0	0.00007
59019.97744	92.5	0.00005	59884.89643	442.5	0.00005	60307.46772	613.5	0.00007	60653.43368	753.5	0.00007
59021.21086	93.0	0.00014	59886.13015	443.0	0.00005	60309.94107	614.5	0.00005	60654.66656	754.0	0.00006
59023.68083	94.0	0.00011	59887.36653	443.5	0.00006	60311.17582	615.0	0.00004	60657.13398	755.0	0.00012
59024.91839	94.5	0.00015	59888.60045	444.0	0.00005	60333.41141[a]	624.0	0.00002	60658.37400	755.5	0.00006
59026.15143	95.0	0.00009	59889.83734	444.5	0.00006	60338.35098[a]	626.0	0.00002	60659.60717	756.0	0.00005
59027.38862	95.5	0.00010	59891.07024	445.0	0.00006	60339.58666[a]	626.5	0.00002	60660.84378	756.5	0.00005
59028.62165	96.0	0.00012	59892.30669	445.5	0.00007	60349.46857[b]	630.5	0.00003	60662.07776	757.0	0.00006
59029.85868	96.5	0.00007	59893.54047	446.0	0.00006	60359.35922[b]	634.5	0.00003	60679.37394[a]	764.0	0.00002
59031.09186	97.0	0.00010									

Notes. Eclipses observed with the [a]: GAO80 and [b]: BAO80 instruments.